Title

PENETRATION OF HIGH-ENERGY HEAVY IONS, WITH THE INCLUSION OF COULOMB, NUCLEAR AND OTHER STOCHASTIC PROCESSES

Authors

Litton, Gerald M.
Lyman, John
Tobias, C.A.

Publication Date

1968-05-01

UCRL-17392 Rev

University of California

Ernest O. Lawrence Radiation Laboratory

PENETRATION OF HIGH-ENERGY HEAVY IONS, WITH THE INCLUSION OF COULOMB, NUCLEAR, AND OTHER STOCHASTIC PROCESSES

Gerald M. Litton, John Lyman, and C. A. Tobias

May 1968

Berkeley, California

DISCLAIMER

UCRL-17392 Rev
UC-34 Physics
TID-4500 (52nd Ed.)

UNIVERSITY OF CALIFORNIA

Lawrence Radiation Laboratory
Berkeley, California

AEC Contract No. W-7405-eng-48

PENETRATION OF HIGH-ENERGY HEAVY IONS, WITH THE INCLUSION OF COULOMB, NUCLEAR, AND OTHER STOCHASTIC PROCESSES

Gerald M. Litton, John Lyman, and C. A. Tobias

May 1968

Printed in the United States of America
Available from
Clearinghouse for Federal Scientific and Technical Information
National Bureau of Standards, U. S. Department of Commerce
Springfield, Virginia 22151
Price: Printed Copy $3.00; Microfiche $0.65

PENETRATION OF HIGH-ENERGY HEAVY IONS, WITH THE INCLUSION OF COULOMB, NUCLEAR, AND OTHER STOCHASTIC PROCESSES

Contents

PENETRATION OF HIGH-ENERGY HEAVY IONS WITH THE INCLUSION OF COULOMB, NUCLEAR, AND OTHER STOCHASTIC PROCESSES*

Gerald M. Litton, John Lyman, and C. A. Tobias

Lawrence Radiation Laboratory
University of California
Berkeley, California

May 1968

ABSTRACT

A general method has been developed for calculating Bragg curves, flux curves, and energy spectra resulting from the transport of high-energy heavy-ion beams in arbitrary media. The method takes into account the processes of energy loss from both electronic and nuclear elastic collisions, nuclear attenuation, small-angle multiple scattering, and straggling, as well as effects due to initial energy and angular spreads of the beam. Contributions from secondary particles are not included.

Calculations are made for ions of various atomic numbers and energies incident on different targets. It is found that for a given range in a particular target, the peak-to-plateau dose ratio goes through a maximum as the atomic number of incident ions increases. Similarly, the Bragg peak full width at half-maximum goes through a minimum.

Another significant result is that for a given particle range, the average energy per atomic mass unit at the Bragg peak is nearly independent of the bombarding ion, and also of the target material.

The calculated results agree very well with experimental data for those cases in which secondary-particle production is of minor importance. In addition, even when secondaries are a large contributing factor, the method yields valuable information regarding the variation in energy deposition by the primary particles.

The calculated results are found to be quite sensitive to the degree of angular and energy spreading of the initial beam.

I. INTRODUCTION

In this paper we consider a beam of monoenergetic particles incident on a slab of material whose transverse dimensions are large compared with the beam dimensions and with the depth of penetration of the beam. As these particles traverse the medium they lose energy through a variety of processes, the predominant ones being ionization energy loss, nuclear interactions, and small-angle multiple scattering. Other processes, including large-angle Coulomb scattering and elastic nuclear scattering, are usually of secondary importance when the initial energy of the beam particles is significantly greater than a few MeV per amu.

A. Energy Loss

The energy loss of a beam of ions results primarily from many collisions between the beam ions and the electrons of the medium, causing a net transfer of energy to the medium. This process is referred to as ionization energy loss.

There are many facets to the highly complex process of charge exchange and ionization energy loss, but a wealth of experimental evidence backs up a great deal of theoretical work. Consequently, very good estimates are available for the rate of ionization energy loss of many ions in many different materials. The state of knowledge with regard to heavy-ion ionization energy loss has been summarized by Northcliffe.[1]

B. Nuclear Interactions

At very high particle energies, nuclear reactions can play an important role in the energy-loss process. A great many different reactions occur, and the total process is exceedingly complex. In some of the collision processes, many different secondary particles can be produced, and each of these gives up energy to the medium by the processes of ionization loss (charged particles only) and nuclear interaction (all particles).

The total cross section for nuclear interactions is known reasonably well over most energies of interest in this work. From this, attenuation factors can be calculated for the beam particles at all penetration distances.

Although the effect of nuclear attenuation on the flux, dose, and spectral curves is taken into account, the additional terms due to the secondary particles produced by the nuclear interactions are neglected in this work.

Elastic scattering of the beam ions by the nuclei of the target causes a small fraction of the total energy deposition in certain regions of the ion energy, in the form of kinetic energy of the recoil target nuclei. This effect is included as a correction term in the calculation of the total stopping power.

In addition to this elastic process, both the incident ion and the target nucleus can be raised to an excited state during an interaction in which the two bodies do not actually merge to produce a single compound nucleus. This effect is commonly referred to as Coulomb excitation, and as a result of such an interaction, each of the two bodies may be raised as high as an MeV or two above its respective ground state. For the energies of interest in this work, the contribution from Coulomb excitation to the total stopping power is negligible (see Appendix D).

C. Multiple Scattering

The process of small-angle multiple scattering leads to a divergence of the beam. As a result, the mean range of the particles decreases somewhat, and the range distribution is broadened. The basic scattering law is well known, so that it is possible to make reasonably accurate estimates of the multiple-scattering effects.[1]

D. Straggling

The process of ionization-energy loss occurs in discrete steps, rather than being continuous. This process leads to the general concept of straggling, whereby a given particle energy does not correspond to a unique distance of travel. Instead, for a given distance of travel, there is a distribution of particle energies, and for a given particle energy, there is a distribution of distances of travel. This distance distribution is of paramount importance in calculating Bragg curves.

E. Other Processes

Various other process (most of them not significant from the standpoint of energy deposition[2]) influence the passage of charged particles through matter; they include large-angle Rutherford scattering, energy transport via fast secondary electrons (δ rays), and Cerenkov radiation.

F. Previous Work

The classical method of calculating Bragg curves is described by Evans.[3] This simple method is based on the assumption that the processes of nuclear attenuation and multiple scattering can be neglected, and that only range

straggling need be considered. Although useful for low-energy beams, this method is of little utility for the work described here; for the beams of interest here, both nuclear interactions and multiple scattering must be considered.

Other authors[4,5] have gone one step further by including the effects of multiple scattering along with range straggling. These methods are not adequate for this work for two reasons. First they do not treat nuclear interactions; in this work, we are concerned with beams of particles that are much heavier than protons, and that often have sufficient energy to cause a significant number of nuclear interactions. Second, these methods are not applicable to very heavy ions, because of various assumptions made with respect to the multiple-scattering process.

II. BASIC EQUATIONS

A. Particle Number Density

We first consider the problem of deriving an expression which describes the attenuation of a beam of particles as they traverse a medium. The beam particles are all assumed to have an initial energy E_o, to be perfectly collimated, and to strike the surface of the medium in a direction parallel to the surface normal. The medium is assumed to be homogeneous, with transverse dimensions large compared both with the beam dimensions and with the depth of penetration of the beam particles.

The medium is assumed to be characterized by a total nuclear-reaction macroscopic cross section $\Sigma(E)$ (in cm^{-1}) and by a stopping power, or specific energy loss, $f(E)$ (in MeV-cm^2/g). The reaction cross section represents any and all nuclear reactions that remove particles from the beam. The function $f(E)$ is the total energy given up to the medium due to interactions between the beam particles and the medium; E is the energy of the particles, in MeV per atomic mass unit.

The path of the beam particles is characterized by the dimension $\bar{s}(E)$, which is defined as the mean distance traveled by particles which have gone from an initial energy E_o to an energy E. Consider those particles that have reached an energy E, denoted by the function $N_e(E)$. In traversing an incremental distance Δs, these particles lose on the average an energy (per amu!) ΔE. Since $f(E)$ is the total energy lost by each particle in a unit distance of travel, then the relation between ΔE and Δs is

$$\Delta E/\Delta s = f(E)/A_p , \tag{1}$$

where A_p is the atomic weight of the beam particles.

For this group of particles, the fractional decrease in their numbers in going from E to E-ΔE is given by the macroscopic reaction cross section multiplied by the mean distance traveled in losing this energy. Thus, we have

$$\frac{\Delta N_e}{N_e}(E) \approx -\Sigma(E)\cdot\Delta s . \tag{2}$$

Using Eqs. 1 and 2 we obtain

$$\frac{dN_e}{N_e}(E) = A_p \cdot \frac{\Sigma(E)}{f(E)}\, dE, \tag{3}$$

where we have taken the limit as ΔE tends to zero.

Equation 3 thus gives the fractional decrease in the number of

particles in losing the increment of energy dE. Note that Eq. 3 is actually an operational definition of the total reaction cross section that is slightly different from the usual definition given by Eq. 2. That is, $\Sigma(E)$ may be considered to be defined in terms of the stopping-power function $f(E)$ rather than in terms of a distance s. This subtle difference is due to the fact that statistical fluctuations, strictly speaking, invalidate the use of a relation of the type given by Eq. 2. In any event, we may regard Eq. 3 as the definition of $\Sigma(E)$ if we wish; in practice Eqs. 2 and 3 are equivalent, because cross-section values are known only approximately.

Integration of Eq. 3 yields the number density of a given energy within the slab,

$$N_e(E) = N_o(E_o)\cdot\exp\{-A_p\int_E^{E_o} [\Sigma(E'/f(E')]dE'\}, \qquad (4)$$

where $N_o(E_o)$ is the number of incident particles, all of which have an energy E_o.

Note that this expression for the number of particles surviving down to an energy E is independent of any particular distance, but is instead a function of only the cross section and stopping power between the initial energy and the energy in question.

The energy loss process is not a continuous one; that is, particles lose energy in discrete steps, rather than continuously. Because of these fluctuations, and because of other processes to be discussed later, a particular energy corresponds to a distribution of path lengths, rather than to a unique value.

1. Mean Path Length of Travel

A very good approximation to the mean path length traveled by particles that have gone from energy E_o to energy E is obtained by direct integration of Eq. 1:

$$\bar{s}(E) = A_p\int_E^{E_o}[1/f(E')]dE'. \qquad (5)$$

2. A Limiting Case

If the reaction cross section is energy-independent, it may be removed from under the integral sign in Eq. 4. Then, we have

$$N_e(E) = N_o(E_o)\cdot\exp\{-A_p\Sigma\int_E^{E_o}[1/f(E')]dE'\}.$$

By using Eq. 5, this becomes simply

$$N_e(E) = N_o(E_o) \cdot \exp\{-\Sigma \cdot \bar{s}(E)\},$$

which is a well-known result.

B. Path-Length Distribution

Equation 4 gives the number of particles reaching energy E. To obtain an expression for the energy deposition and for the flux at a particular distance of travel s, we must relate the energy of an ion to its position. This is done by defining a path-length distribution function as follows.

For a group of particles, each with energy E, $M(s,\bar{s})ds$ is the fraction of these particles that have traveled a distance s, where $\bar{s}$ is the mean distance traveled by particles of energy E_o and is given by Eq. 5.

Lewis[6] has shown that if the path-length distribution is a result of statistical fluctuations in the energy-loss process, then the distribution function should be well represented by a Gaussian. Berger and Seltzer[7] have extended the study of the problem and show that the deviations from a Gaussian are negligible for nearly all cases of interest.

It should be pointed out that the distribution function M should not be affected by the occurrence of nuclear interactions, provided that one is concerned only with the initial beam particles as opposed to nuclear secondaries. This can be argued by considering that the fractional decrease in the number of particles of a given energy, as given by Eq. 4, is a function of the energy only, not of the position of the particles. Another way of stating this is that if at some energy the path-length distribution is Gaussian, then the fractional decrease in particles lying in any given distance increment is constant. Therefore, the attenuation does not affect the shape of the path-length distribution.

Processes other than energy-loss fluctuations also contribute to the path-length distribution, the principal ones being multiple scattering and the energy spread, and imperfect collimation of the initial beam. We assume that these effects are such that the path-length distribution is still well represented by a Gaussian. The validity of this assumption is discussed later, when each of these processes is examined.

Therefore, the path-length distribution function is written in the form

$$M(s,\bar{s}) = \frac{1}{\sqrt{2\pi}\ \sigma(E,E_o)} \cdot \exp\left\{ -\left[\frac{s - \bar{s}}{\sqrt{2}\ \sigma(E,E_o)} \right]^2 \right\} ds. \qquad (6)$$

The quantity $[\sigma(E,E_o)]^2$ is the variance in the path-length distribution for particles slowing down from energy E_o to energy E. In general, this variance is the sum of several terms, each of which represents the variance due to a particular effect. Calculation of the variance is discussed fully in later sections.

Note that there may be a small range of energies near E_o for which Eq. 6 does not hold. Thus, consider an energy E near E_o. If $\sigma(E,E_o)$ is not sufficiently large, then the distribution function cannot be symmetric, because s can never be less than zero (no path length).

Thus, for Eq. 6 to be valid, we require that E be small enough so that the inequality

$$\bar{s}(E) \gg \sqrt{2}\ \sigma(E,E_o)$$

is satisfied.

This requirement usually imposes no practical limitations, since for energies near E_o, the quantities of interest -- such as dose and flux -- are independent of the form of the distribution function (see Appendix B).

Many authors have adopted the convention of using the quantity called the straggling parameter, equal to $\sqrt{2}\ \sigma(E,E_o)$, rather than the standard deviation $\sigma(E,E_o)$. However, inasmuch as the term "straggle" carries particular implications with respect to energy-loss fluctuations, we shall adhere to the use of the variance itself.

We now transform the distribution $M(s,\bar{s})$ as follows. Defining the variable U as

$$U(E) = \frac{s - \bar{s}(E)}{\sqrt{2}\ \sigma(E,E_o)}, \qquad (7)$$

we can write

$$M(s,\bar{s})ds = M(U)\ dU = \frac{1}{\sqrt{\pi}}\ e^{-U^2}\ dU. \qquad (8)$$

The distribution $M(U)dU$ may now be interpreted as the fraction of particles of energy E that have traveled a distance s such that the normalized difference between s and the mean distance of travel $\bar{s}(E)$ is

within an increment dU of U, and U is the normalized difference given by Eq. 7. Therefore, given the total number of particles $N_e(E)$, as calculated from Eq. 4, the number of those having traveled a distance s is given as

$$dN(s,E) = N_e(E)\cdot M(U)dU, \tag{9}$$

where U is an implicit function of E and is given by Eq. 7.

C. Flux and Dose Distributions

The total flux at a distance s is now obtained by integration of Eq. 9 from $U(E_o)$ to U(0). Using Eqs. 4 and 8 and changing the variable of integration from U to E, we obtain the total flux at a distance s:

$$N(s) = N_o(E_o)\int_o^{E_o} \exp\left\{-A_p\int_E^{E_o} \frac{\Sigma(E')}{f(E')}\,dE'\right\}\left[\frac{e^{-U^2}}{\sqrt{\pi}}\right]\left(\frac{dU}{dE}\right)dE \ . \tag{10}$$

The mean range of the particles, $R(E_o)$, is given by Eq. 5 with E = 0. The quantity $\sigma^2(E_o)$ is the variance for particles having come to rest. It is equivalent to $\sigma^2(E,E_o)$ with E = 0; that is

$$\sigma^2(E_o) \equiv \sigma^2(0,E_o).$$

We also wish to calculate the total dose at s. If dN(s) represents a certain number of particles of energy E, as given by Eq. 9, then dN(s)f(E) is the dose per unit distance of travel of these particles at s. Thus, the total dose is

$$D(s) = \int_{\text{All E}} dN(s,E)\, f(E).$$

Using Eqs. 4, 8 and 9 we then have

$$D(s) = N_o(E_o)\int_o^{E_o} \exp\left\{-A_p\int_E^{E_o} \frac{\Sigma(E')}{f(E')}\,dE'\right\}\left[e^{-U^2}\right]\frac{f(E)}{\sqrt{\pi}}\,(dU/dE)dE \tag{11}$$

It should be noted that in Eqs. 10 and 11 the independent variable E appears, as well as the variable U. In order to perform the integration, one of these must be expressed in terms of the other. This is easily done, inasmuch as the unique relationship between them is given by Eq. 7.

D. Energy Spectrum

At any given position s, the total flux may be written as

$$N(s) = \int_{\text{All E}} N(E,s)\,dE,$$

where $N(E,s)dE$ is the number of particles having energies within dE of E. Comparing this expression with that given by Eq. 10, we deduce that the spectrum at any position is given as

$$N(E,s) = N_o(E_o) \exp\left\{-A_p \int_E^{E_o} \frac{\Sigma(E')}{f(E')}\, dE'\right\} e^{-U^2} \cdot \frac{1}{\sqrt{\pi}} (dU/dE),$$

with U given by Eq. 7.

E. Some Simplifying Cases

Suppose that the cross section is independent of energy. Then, as before, we may remove Σ from beneath the integral in both Eqs. 10 and 11. When Eq. 5 us used, the expressions for the flux and the dose simplify to

$$N(s) = N_o(E_o) \int_o^{E_o} \exp\{-[\Sigma\bar{s}(E) + U^2]\} \frac{(dU/dE)}{\sqrt{\pi}}\, dE \qquad (12)$$

and

$$D(s) = N_o(E_o) \int_o^{E_o} \exp\{-[\Sigma\bar{s}(E) + U^2]\} \frac{f(E)}{\sqrt{\pi}} (dU/dE)dE \qquad (13)$$

The integrals in both Eqs. 12 and 13 must be evaluated numerically.

A further simplification is obtained in the limiting case, where the attenuation due to nuclear interactions is negligible, as it would be for ions of sufficiently low energy. In that case, the cross section is assumed to go to zero, and the expressions for the flux and the dose reduce to

$$N(s) = N_o(E_o) \int_o^{E_o} e^{-U^2} \frac{(dU/dE)}{\sqrt{\pi}}\, dE \qquad (14)$$

and

$$D(s) = N_o(E_o) \int_o^{E_o} e^{-U^2} \cdot f(E) \frac{(dU/dE)}{\sqrt{\pi}}\, dE.$$

The latter expression for the flux is equivalent to the classical expression, derived by Evans[3] and others. It can be obtained from basic principles as follows.

We assume that the distribution of ranges for particles with initial energy E_o is Gaussian, with a variance $[\sigma(E_o)]^2$:

$$P(R) = \frac{1}{\sqrt{2\pi}\,\sigma(E_o)} \exp\left\{-\left[\frac{R-R(E_o)}{\sqrt{2}\,\sigma(E_o)}\right]^2\right\},$$

where $R(E_o)$ is the mean range. The flux at a given distance s is contributed to by all particles whose range is greater than s. If the initial flux is $N_o(E_o)$ at s = 0, then the flux at s is given as

$$N(s) = N_o(E_o) \int_s^\infty \frac{1}{\sqrt{2\pi}\,\sigma(E_o)} \exp\left\{-\left[\frac{R-R(E_o)}{\sqrt{2}\,\sigma(E_o)}\right]^2\right\} dR \quad (15)$$

If we change variables from R to W, where W is given as

$$W = \frac{R-R(E_o)}{\sqrt{2}\,\sigma(E_o)},$$

Eq. 15 becomes

$$N(s) = N_o(E_o) \int_{\frac{s-R(E_o)}{\sqrt{2}\,\sigma(E_o)}}^\infty e^{-W^2} \frac{dW}{\sqrt{\pi}},$$

which is equivalent to Eq. 14.

F. Nuclear Interactions

Energy deposition from nuclear interactions arises from two sources -- direct and indirect. The direct contribution comes from the deexcitation of the compound nucleus formed by the interaction of the target atom with the bombarding ion. A certain fraction of this deexcitation energy is released at the point of impact, and it is this fraction which comprises the direct contribution. The indirect portion aroses from secondaries produced at points within the medium other than the position of interest.

1. Direct Contribution

The total number of interactions, per unit length of travel, of ions with energy E, due to those particles whose initial energy is E_o, is given by

$$r^o(E,s) = N(E,s)\ \Sigma(E).$$

The total energy release at s from the direct contribution is then

$$D_{dir}(s) = \int_o^{E_o} N(E,s)\ \Sigma(E)\ G(E)\ dE,$$

where G(E) is the energy deposited at s per nuclear interaction with a particle of energy E.

2. Indirect Contribution

Let $H(E',s' \rightarrow s)$ be the energy released at s due to a nuclear interaction

of an ion of energy E' at s'. Then the total indirect contribution to the linear energy transfer, denoted $D_n(s)$, is given by

$$D_n(s) = \int ds' \int dE' N(E',s') \Sigma(E') \, H(E',s' \rightarrow s). \qquad (16)$$

The simple form of Eq. 16 belies the inherent difficulties involved with its evaluation; although, as will be indicated, N(E,s) can be calculated, the function $\Sigma(E)$ is usually not well known. Furthermore, even less is known about the function $H(E',s' \rightarrow s)$.

For the work in this report, we neglect the contributions to the dose and flux from secondary particles.

G. Variance of the Path-Length Distribution

The path-length distribution is a function of several processes; we assume that each of these processes is independent of others. We further assume that each process contributes in a random manner to the deviations in the path-length distribution. Therefore, the total variance in the distribution can be expressed as a sum of terms, each of which represents the variance due to a given process.

In this section, we discuss the different processes and show how each contributes to the total variance.

1. Energy-Loss Fluctuations

The process of ionization-energy loss occurs in a random fashion, so that one expects that, over a finite energy interval, the path-length distribution of particles with given energy will be Gaussian. The classical derivation of the expression for the associated variance, made by Lewis,[6] is given below.

Suppose that a particle has an energy E_{tot}. From Lewis, the average number of collisions experienced by the particle per unit distance of travel, in which an energy loss T occurs, is given by the expression

$$N_T(T) \, dT = \frac{k \, dT}{2 \, E_{tot} \, T^2}, \qquad (17)$$

where constant k is given as

$$k = 2\pi \, n_e \, Z_p^2 \, M_p \, e^4/m_e,$$

and where n_e is the number of electrons per unit volume of the target and M_p and Z_p are the mass and atomic number of the incident particle. The

function $N_T(T)$ is often referred to as the collision spectrum.

Equation 17 is valid in the nonrelativistic limit. It is also assumed that the velocity of the incident particle is much greater than that of the k electrons of the target atom.

Now, in traversing an increment of distance Δs, the average number of collisions in which an energy loss T occurs is given by

$$N_T(T)\, dT\big|_{\Delta s} = \frac{k\, dT}{2\, E_{tot}\, T^2}\, \Delta s.$$

Since the collisions occur randomly, the standard deviation associated with the average number $N_T(T)dT$ is equal to the square root of that number. The variance $\langle N_c^2 \rangle$ in the number of collisions is therefore equal to

$$\langle N_c^2 \rangle = \frac{k\, dT}{2\, E_{tot}\, T^2}\, \Delta s.$$

Because each collision is associated with an energy loss T, the variance in the total energy loss over the distance Δs is given as

$$\langle \delta\, E_{tot}^2 \rangle = T^2\, \langle N_c^2 \rangle = \frac{k\, dT}{2\, E_{tot}} \cdot \Delta s. \tag{18}$$

For each value of T, there is a corresponding variance given by Eq. 18. Inasmuch as the collisions associated with each value of T are independent, the variances for all values of T are additive. Therefore, the net variance in the total energy loss associated with an incremental distance Δs is given by the sum

$$\langle \Delta\, E_{tot}^2 \rangle = \sum_{\text{All } T} \frac{k\, dT}{2\, E_{tot}}\, \Delta s,$$

and in the limit, by

$$\langle \Delta\, E_{tot}^2 \rangle = k \int_{T_{MIN}}^{T_{MAX}} \frac{dT}{2\, E_{tot}}\, \Delta s. \tag{19}$$

It can be shown that the maximum energy loss in a single collision is given by $\epsilon\, E_{tot}$, where

$$\epsilon = 4\, m_e / [M_p (1 + m_e/M_p)^2]. \tag{20}$$

A discussion of the lower limit is given by Bloch, who shows that it

can usually be neglected.[8] Integrating Eq. 19 using Eq. 20 we have

$$\langle \Delta E_{tot}^2 \rangle = \frac{4\pi n_e Z_p^2 e^4}{(1+m_e/M_p)^2} \Delta s. \tag{21}$$

Equation 21 gives the variance in the energy loss produced by collisions in Δs.

Evans[3] gives an argument to show that the relationship between an energy variance and the corresponding variance in the path-length distribution is given as

$$\langle \Delta R^2 \rangle = \frac{1}{[f(E)]^2} \langle \Delta E_{tot}^2 \rangle, \tag{22}$$

where E_{tot} is the mean energy of the particles in question. This can be argued as follows. At some energy E_{tot}, a change in energy, ΔE_{tot}, produces a corresponding change in path length Δs, given by Eq. 1. The term Δs is then the contribution to the total path length due to the energy change ΔE_{tot}. Therefore, if ΔE_{tot} represents an uncertainty in the energy change, then the corresponding uncertainty in the contribution to the total path length is again Δs, and $\langle \Delta E_{tot}^2 \rangle$ is the square of ΔE_{tot}. Equation 22 then follows.

Substituting the expression given by Eq. 21 into Eq. 22 we obtain

$$\langle \Delta R^2 \rangle = \frac{4\pi n_e Z_p^2 e^4}{(1+m_e/M_p)^2} \cdot \frac{\Delta s}{[f(E)]^2},$$

which is the contribution to the variance in the path length due to collisions in Δs. Since collisions within each increment Δs are independent from those in any other increment, the net variance over a group Δs_i will be the sum of the individual variances. As the Δs_i approaches zero, the sum becomes an integral, and we obtain

$$\langle \Delta R^2 \rangle = \frac{4\pi n_e Z_p^2 e^4}{(1+m_e/M_p)^2} \int_{E_1}^{E_2} \frac{ds}{[f(E)]^2}.$$

Using Eq. 1, we have

$$\langle \Delta R^2 \rangle = \frac{4\pi n_e Z_p^2 e^4}{(1+m_e/M_p)^2} A_p \int_{E_1}^{E_2} \frac{dE}{[f(E)]^3}. \tag{23}$$

This is the expression for the contribution to the variance in the path-length distribution for particles going from an energy E_2 to an energy E_1.

It is valid when the energy range is nonrelativistic, but at very high energies, correction factors must be applied. Furthermore, at very low energies, corrections must be made to take into account the fact that the electrons of the medium are in a bound state.

a. High- and Low-Energy Corrections

At high energies, the collision spectrum deviates from the form given by Eq. 17. Maccabee[9] discusses this effect and gives the modified expression as developed by Vavilov[10] as

$$N_T(T)\,dT = \frac{k\,dT}{2\,E_{tot}\cdot T^2}\left[1 - \beta^2\cdot\frac{T}{T_{max}}\right],$$

with

$$T_{max} = 4\,E_{tot}\,m_e/[M_p(1 + m_e/M_p)^2(1 - \beta^2)].$$

When these relationships are used, the expression for the variance contribution $\langle\Delta R^2\rangle$ becomes, instead of that given by Eq. 23,

$$\langle\Delta R^2\rangle = 4\pi Z_p^2 e^4 n_e A_p \int_E^{E_o} \frac{(1 - \beta^2/2)}{(1 - \beta^2)[1 + (2m_e/M_p)\gamma]}\,\frac{K\,dE'}{[f(E')]^3} \qquad (24)$$

where

$$\gamma = (1 - \beta^2)^{-1/2}.$$

These are the equations given by Sternheimer[11] for calculating the path-length variance due to energy-loss straggling. The quantity β is the ratio of the particle velocity to the speed of light,

$$\beta^2 = 1 - \left[\frac{M_o c^2}{E + M_o c^2}\right]^2,$$

where $M_o c^2$, the rest energy per amu, is equal to approximately 931 MeV. The term K is a factor introduced by Sternheimer to take into account the effects due to the binding of the atomic electrons. If the variance is expressed in g/cm^2, then Eq. 24 becomes

$$\langle\Delta R^2\rangle = \frac{4\pi Z_p^2 e^4 n_e A_p}{\rho}\int_E^{E_o} \frac{(1 - \frac{1}{2}\beta^2)}{(1-\beta^2)[1 + (2m_e/M_p)\gamma]}\,\frac{K\,dE'}{[f(E')]^3}$$

where f(E) is in units of MeV-cm^2/g. The term ρ is the density of the target in g/cm^3. If we substitute numerical values in Eq. 25, and define

the function

$$H(E) = \left[\frac{M_o c^2}{E + M_o c^2}\right]^2 , \qquad (26)$$

Eq. 25 becomes

$$\langle \Delta R^2 \rangle = \frac{1.3027 \times 10^{-25} \cdot Z_p^2 n_e A_p}{\rho} \int_E^{E_o} \frac{1 + H(E')}{H(E')\left[1 + (\frac{2m_e}{M_p})/H(E')^{1/2}\right]} \frac{K\, dE'}{[f(E')]^3} . \qquad (27)$$

For the energies of interest, the quantity H(E) varies between approximately 0.15 and 1.0. Since for even the lightest particles of interest (i.e. protons) the ratio $2m_e/M_p$ is much less than 1.0, the term $1 + (2m_e/M_p)/H(E)^{1/2}$ in Eq. 27 is very nearly unity. Consequently, Eq. 27 simplifies to

$$\langle \Delta R^2 \rangle = \frac{1.3027 \times 10^{-25} \cdot Z_p^2 n_e A_p}{\rho} \int_E^{E_o} \frac{1 + H(E')}{H(E')} \frac{K\, dE'}{[f(E')]^3} . \qquad (28)$$

b. The Binding-Correction Term

Sternheimer points out that the quantity K decreases rapidly to unity with increasing energy. For Be, for example, typical values of K for protons are as follows:

MeV	K
1	1.24
2	1.12
10	1.07
50	1.02

Table I gives values of the various terms in the integrand for the energy spectrum ranging from 1 to 500 MeV per amu for neon, in water. On the basis of the approximate numbers shown in this table, it is concluded that the term K can be set equal to unity with no significant error introduced into the calculated values for the variance. This follows for several reasons. First, at those values of the energy range for which K differs at all from unity, the value of the integrand is nearly zero. Second, even if the integrand values were nontrivial in this range (which might be true for some very heavy ions at energies between zero and 5 MeV), the portion of the energy range over which K differs significantly from unity is a small fraction of the total range, so that the contribution from this portion of the range to the total integral is correspondingly small.

Table I. Terms of the integrand in Eq. 28 for neon ions in water.

E (MeV/amu)	H(E)	$f(E)_2$ (MeV-cm^2/g)	$\frac{1 + H(E)}{H(E)} \times \frac{1}{[f(E)]^3}$
500	0.423	278	1.56×10^{-7}
250	0.621	396	4.20×10^{-8}
100	0.816	740	5.52×10^{-9}
50	0.900	1270	1.05×10^{-9}
25	0.947	2400	1.49×10^{-10}
10	0.980	4700	1.94×10^{-11}

Furthermore, in the very-low-energy region where f(E) decreases (for heavy ions), the quantity Z_p^2 also decreases, again tending to reduce the value of the integrand.

Tables II through IV show typical values of the standard deviation as calculated by Sternheimer,[12] which are denoted "reference."

Table II. Comparison of calculated and reference values[a] for the standard deviation in the path-length distribution of protons in Be.

Incident energy (MeV)	Standard deviation (g/cm^2)		% error
	Calculated	Reference	
4	4.052×10^{-4}	4.588×10^{-4}	11.68
10	1.969×10^{-3}	2.055×10^{-3}	4.18
25	9.571×10^{-3}	9.757×10^{-3}	1.91
50	3.190×10^{-2}	3.220×10^{-2}	0.93
70	5.697×10^{-2}	5.739×10^{-2}	0.73
100	0.1048	0.1052	0.43
140	0.1845	0.1850	0.27
250	0.4745	0.4746	0.02
500	1.364	1.360	0.003

a. Ref. 11 and 12

As usual, the standard deviation is taken to be the square root of the variance $\langle \Delta R^2 \rangle$. Also shown are the values calculated neglecting the correction term K. For beryllium, there is only a 2% error for 25-MeV protons. For aluminum, the corresponding error is 5%; it is 12% for lead. These results show that, for the passage of protons through the lighter

elements, the neglecting of variations of K from unity produces very small errors in the calculated values for the variance.

Table III. Comparison of calculated and reference values[a] for the standard deviation in the path-length distribution. The particles are protons in Al.

Incident energy (MeV)	Standard deviation (g/cm^2)		
	Calculated	Reference	% error
4	5.327×10^{-4}	6.440×10^{-4}	17.28
10	2.455×10^{-3}	2.715×10^{-3}	9.58
25	1.133×10^{-2}	1.200×10^{-2}	5.58
50	3.644×10^{-2}	3.798×10^{-2}	3.53
70	6.471×10^{-2}	6.653×10^{-2}	2.74
100	0.1178	0.1202	2.00
140	0.2056	0.2087	1.49
250	0.5224	0.5269	0.85
500	1.479	1.483	0.27

a. Ref. 11 and 12

Table IV. Comparison of calculated and reference values[a] for the standard deviation in the path-length distribution. The particles are protons in Pb.

Incident energy (MeV)	Standard deviation (g/cm^2)		
	Calculated	Reference	% error
4	1.767×10^{-3}	2.303×10^{-3}	23.27
10	6.599×10^{-3}	7.499×10^{-3}	12.54
25	2.591×10^{-2}	2.931×10^{-2}	11.60
50	7.713×10^{-2}	8.540×10^{-2}	9.68
70	0.1318	0.1436	8.22
100	0.2330	0.2514	7.32
140	0.3969	0.4255	6.72
250	0.9723	1.0262	5.25
500	2.6568	2.7562	3.63

a. Ref. 11 and 12.

Although the results given here are for protons only, the order of magnitude of the errors shown in Tables II through IV is the same for all

incident ions. The final expression for the variance due to fluctuations in the ionization energy-loss process is therefore

$$\langle \Delta R^2 \rangle = \frac{1.3027 \times 10^{-25} n_e Z_p^2 A_p}{\rho} \int_E^{E_o} \frac{1 + H(E')}{H(E')} \frac{dE'}{[f(E')]^3} , \qquad (29)$$

with the function H(E) given by Eq. 26.

2. Initial Energy Spread of the Beam

In general, a beam of particles is not monoenergetic, but has some sort of spread centered around a most probable energy. To include the effect of this spread on the path-length distribution, we assume that the energy distribution of the beam is well represented by a Gaussian, with a variance $\langle E_o^2 \rangle$ and with a most probable energy E_o. Associated with this variance in the energy is a constant variance in the path-length distribution. This is calculated as follows. The relationship between an energy interval ΔE_o and the corresponding distance of travel Δs_o is given by Eq. 1. If we interpret ΔE_o as the uncertainty in the initial energy, then the corresponding uncertainty in the path length is given as

$$\Delta s_o = A_p \frac{\Delta E_o}{f(E_o)}.$$

This is a constant uncertainty over the entire path length of the particles. The associated variance in the path-length distribution is therefore

$$\langle \Delta s_o^2 \rangle = \left[\frac{A_p}{f(E_o)} \right]^2 \langle \Delta E_o^2 \rangle .$$

Strictly speaking, a Gaussian distribution in the initial energy of the beam can lead to a Gaussian distribution in the path lengths only if f(E) is constant over the energy range of the distribution. For most beams of interest, however, the initial energy spread will be sufficiently small so that f(E) is nearly constant over the energy range.

3. Multiple-Scattering Contributions

As a charged particle travels through a medium, it undergoes what is commonly termed small-angle multiple scattering. This arises principally from electromagnetic interactions between the charged particle and the nucleus. When these interactions lead to a large-angle scattering, it is either due to (i) inelastic interactions arising from the short-range nuclear forces, or (ii) the very infrequent scattering also due to the electromagnetic

interactions. If the interaction arises out of the first cause, it is termed a "nuclear interaction," and is neglected for the reasons discussed earlier.

Obviously, there is no fine line between small-angle multiple scattering and large-angle Rutherford scattering. However, because of the strong angular dependence of the Rutherford law, the probability of an angular change produced as the result of an interaction is a rapidly decreasing function of the angle, so that only very small angles contribute appreciably to the angular spreading of a beam of particles.

The result of the scattering process is that the particles spread slowly as they traverse the medium, so that an "average" trajectory would look something like that shown in Fig. 1, rather than a straight line. Therefore, if x denotes the penetration distance of a particle into the medium -- i.e., measured along the initial direction of the beam -- then for a mean distance of travel $\bar{s}$ corresponding to a given energy E, there will be, because of the scattering process, a distribution of penetration depths. In other words, even if all the particles traveled exactly the same distance $\bar{s}$ -- i.e., in the absence of any statistical fluctuations in the energy-loss process -- multiple scattering would still lead to a distribution in the penetration distances traveled by these particles.

Of primary concern are the flux and dose as functions of penetration depth into the medium. We must therefore find some method of relating the mean distance of travel $\bar{s}$ of a group of particles to corresponding mean penetration distance x.

In order to arrive at expressions for the dose and flux in terms of the penetration distance x, we must convert from the distribution $M(s,\bar{s})$ to a distribution $M'(x,\bar{s})$. This is defined as the fraction of particles, all having slowed down to energy E from energy E_o, that are at a penetration distance x. To do this we proceed by calculating the mean square difference between the path length s and the penetration distance x, as a function of s, denoted as $\langle(s-x)^2\rangle$.

Referring to Fig. 1, we can deduce the relationship between a small change Δs in the distance of travel of a given particle, and the corresponding change Δx in the penetration distance,

$$\Delta x = \Delta s \cos \varphi,$$

where φ is the angle that the particle makes with the x direction. The change in the square of the difference $(s-x)^2$ is therefore given approximately

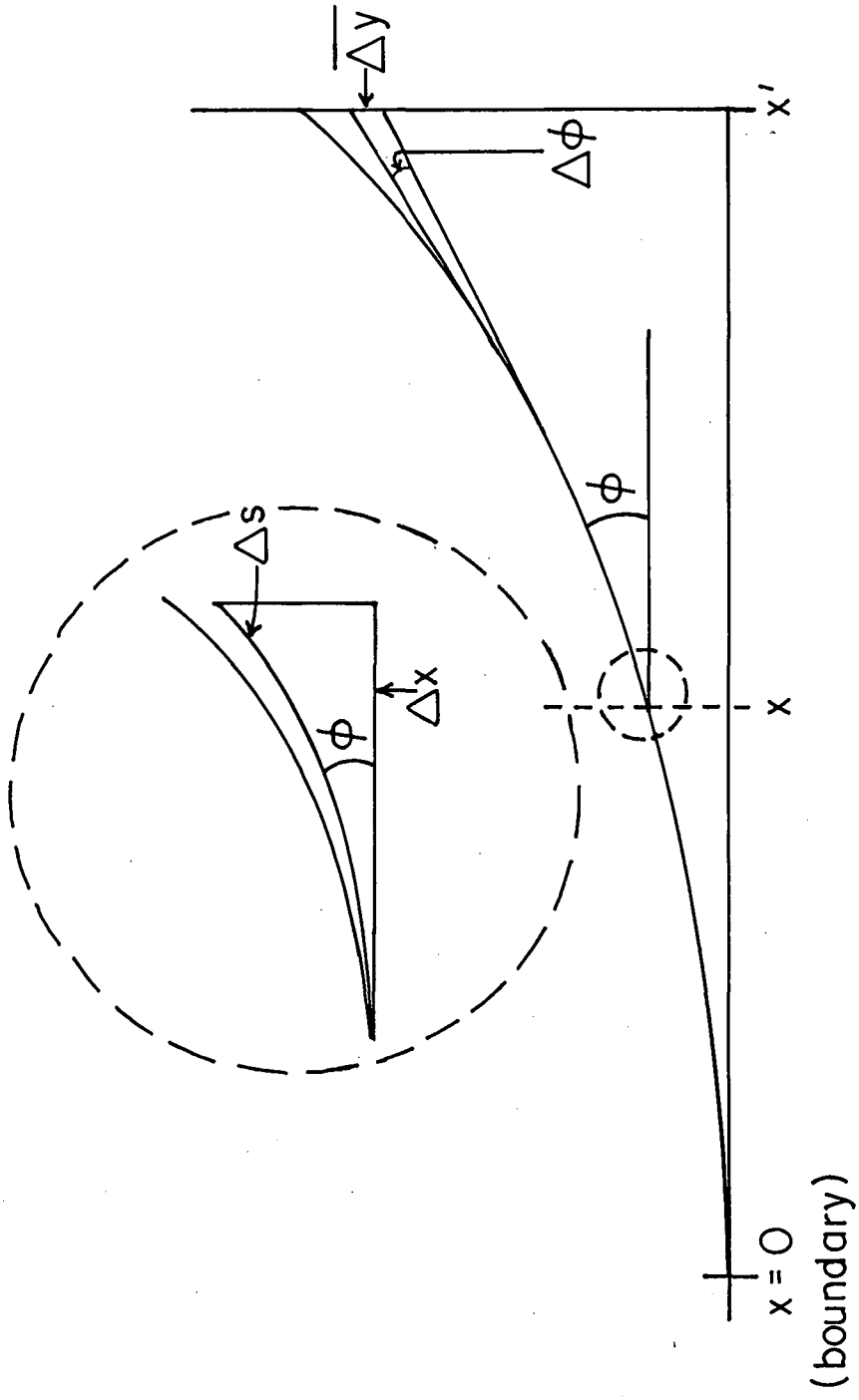

Fig. 1. Geometric model used in analyzing multiple-scattering effects.

as

$$\Delta(s - x)^2 = [\Delta s(1 - \cos \bar{\varphi})]^2,$$

where $\bar{\varphi}$ is the mean angle of the particles within ds. Again, making the assumption of independence of events, the net value of the mean square difference is given as the sum

$$\langle (s - x)^2 \rangle = \sum [(1 - \cos \bar{\varphi})\Delta s]^2. \qquad (30)$$

Expressions for calculating $\bar{\varphi}$ are developed in a subsequent section.

We now proceed to the development of the penetration-distance distribution. For a given distance of travel, the distribution function of the difference $(s - x)$ may be approximated by a Gaussian. The quantity $\langle (s - x)^2 \rangle$ given by Eq. 30 is then an estimate of the variance of this distribution. Since we are considering a particular value of s, then $\langle (s - x)^2 \rangle$ also represents the variance in the distribution of penetration distances corresponding to the distance of travel s.

Thus, if the distribution in $(s - x)$ is given as

$$P(s - x) = \frac{1}{\sqrt{2\pi}} \exp \{-[(s - x) - D_o]^2/2\kappa^2\},$$

where the variance κ^2 is the mean square difference given by Eq. 30, and D_o is the mean about which the distribution is centered, then the distribution in penetration distances is

$$P(x) = \frac{1}{\sqrt{2\pi}} \exp \{-[x - \bar{x}]^2/2\sigma^2\}.$$

The quantity $\bar{x}$ is the mean value of the penetration distance, and is estimated simply as the difference between s and the mean difference between s and x. Thus,

$$\bar{x} \approx s - \{\langle (s - x)^2 \rangle\}^{1/2}. \qquad (31)$$

We may summarize as follows. For a given value of the energy E, the mean penetration distance is given by Eq. 31; the contribution to the variance in the penetration distance distribution from multiple scattering is given by Eq. 30.

4. Initial Angular Spread of the Beam

Typically, a beam of particles is not unidirectional, but instead has some angular distribution centered about a most probable value. The effect of this distribution is most easily taken into account as follows. In the

previous section, the multiple-scattering effects were discussed and characterized in terms of a mean angle $\bar{\varphi}$, which is a function of the mean distance of travel in the medium. The calculation of $\bar{\varphi}$ is discussed in a later section, but it is clear that the initial value chosen for the mean angle will have a direct influence on all values of $\bar{\varphi}$. Thus, the effect of an initial angular spread in the beam is taken into account by imposing a suitable initial condition on $\bar{\varphi}$ in the multiple-scattering calculation. The exact method of introducing this condition is demonstrated in the later section dealing with the calculation of the mean angle due to multiple scattering.

Alternatively, one could equally well calculate a constant variance due to the angular spread, to be added to the variance of the penetration-distance distribution. The former approach is more efficient from a computational point of view, and for this reason it is chosen.

III. PHYSICAL PROCESSES

The previous section was devoted to the derivation of expressions that describe Bragg and flux curves, and energy spectra. These expressions contained functions that represented certain physical processes -- namely ionization loss, nuclear interactions, and multiple scattering. For example, it was assumed that the nuclear-interaction cross section could be represented by an energy-dependent function $\Sigma(E)$.

The purpose of this section is to discuss these phenomena in detail and to derive expressions that can be used to calculate values for the functions.

A. Energy Loss

The process of energy loss is extremely complex. Steward has calculated the stopping power for ions of arbitrary energy and mass in an arbitrary medium.[13] In Steward's method the problem is treated in two main parts, one for ion atomic numbers less than 10 and the other for ion atomic numbers greater than 10. This division is based on the fact that experimental stopping-power data are available for ions with $Z < 10$ for all energies for which the atom is not completely stripped, whereas such data are not at all complete for ions with $Z > 10$.

For the lower-atomic-number region, Steward calculates the stopping power, using experimental data and a modified version of the method developed by Northcliffe for low energies.[1] For the region of $Z > 10$, Steward uses the nuclear and electronic stopping-power theory of Lindhard et al.,[14,15] with adjustments made in order to obtain agreement with fission-product range data at low energies. At intermediate energies, charge-state data developed from experimental Ar range-energy data in Al are extended to other ions and stopping media. At high energies, a modified form of Bethe's theory, as developed by Barkas and Berger, is used for all ions.[16]

The values of $f(E)$ used throughout this work are obtained by using the methods of Steward. The values of the mean excitation energy used in connection with the Bethe equation are those given by Turner.[17]

It should be mentioned that high-energy δ rays are occasionally produced, and that these energetic electrons influence the energy-deposition process. The phenomenon is discussed in detail by Segrè.[18] He shows that in part because the probability for the production of an electron of energy T is approximately proportional to $1/T^2$, so few δ rays of significant energy

are produced that their effect can be neglected.

B. Nuclear Reactions

In order to calculate the energy deposition even from the primary particles alone, it is necessary to know the value of the total reaction cross section as a function of energy. One must in principle specify exactly what is meant by this cross section. Too often, the literature is confusing by giving vague references to such terms as "reaction cross section," "inelastic cross section," etc. We shall remove any possible ambiguity by defining the total reaction cross section to be that which describes any nuclear interaction that removes a particle from the beam, excluding Rutherford scattering, which is treated elsewhere, in the section on multiple-scattering corrections.

For most of the cases of interest -- namely very heavy ions with energies on the order of a few hundred MeV per amu -- experimental data are essentially nonexistent; consequently, we must rely on theoretical considerations.

Following the treatment by Blatt and Weisskopf,[19] we develop below a simple formulation for the calculation of the reaction cross sections. If we consider the range of energies sufficiently high so that the wavelength of the beam particle is much less than the characteristic dimension of the medium nuclei, then one would expect that the reaction cross section would be on the order of the total geometric cross section -- assuming, of course, that any interaction leads to a compound nucleus. If we let R represent the radius of this geometric cross section, then at sufficiently high energies the microscopic cross section is given by

$$\eta = \pi R^2 .$$

The radius of a nucleus may be expressed in the form

$$r = r_o \cdot A^{1/3} - SKT,$$

where A is the atomic weight of the nucleus, r_o is the nuclear unit radius, and SKT may be interpreted as an overlap parameter. Since the radius of the geometric cross section is simply the sum of the radii of the incoming particle and the target nucleus, we have

$$R = r_p + r_t, \qquad (32)$$

where the subscripts "p" and "t" refer to the particle and target, respectively.

At low energies, the Coulomb barrier obviously plays a role in the interaction process. It can be shown[19] that if R, given in Eq. 32 in this

case, is the classical distance of closest approach, and V(R) represents the potential at this distance, then the cross section is given by

$$\eta = \pi R^2 \left[1 - \frac{V(R)}{E_{c.m.}}\right] \quad \text{for } E_{c.m.} > V(R), \text{ and}$$
$$\eta = 0 \qquad\qquad \text{for } E_{c.m.} < V(R), \tag{33}$$

where $E_{c.m.}$ is the total energy of the particle in the center-of-mass system. The potential is given by

$$V(R) = \frac{Z_p Z_t e^2}{R}, \tag{34}$$

where Z_t is the nuclear charge. Equation 33 reflects the fact that classically the potential barrier cannot be crossed with less than a given amount of energy.

The exact form of the Coulomb correction is of secondary importance, since for almost all cases of interest in this study, $E_{c.m.}$ is much greater than V(R). Hence, the presence of the Coulomb barrier has almost no effect on the cross section for the energies of interest.

We must now consider the fact that the incoming particle exhibits wave properties, especially in the energy region where the equivalent wavelength is not trivially small. If the wavelength is denoted by $\lambda\!\!\!^{-}$, then the uncertainty in the position of the particle is also given by $\lambda\!\!\!^{-}$. Hence, one would expect that the "effective radius" of the particle-plus-target cross section would be enhanced by this amount. Thus, a better estimate of the cross section is

$$\eta = \pi(R + \lambda\!\!\!^{-})^2 \left[1 - \frac{V(R + \lambda\!\!\!^{-})}{E_{c.m.}}\right] .$$

At very high energies, $\lambda\!\!\!^{-}$ approaches zero and the cross section is given simply by πR^2. As the energy decreases, the cross section increases as the wave length becomes important. Finally, there is a sharp drop in the cross section near energies comparable to the potential threshold. Using Eqs. 33 and 33 we obtain the complete expression for the reaction cross section:

$$\eta = \pi[r_o(A_p^{1/3} + A_t^{1/3}) + \lambda\!\!\!^{-} - 2SKT]^2 \left[1 - \frac{Z_t Z_p e^2}{E_{c.m.}[r_o(A_p^{1/3} + A_t^{1/3}) + \lambda\!\!\!^{-}]}\right] \tag{35}$$

Blatt and Weisskopf have calculated the cross sections for protons and alpha particles using the results of a wave-mechanics treatment. The results given by Eq. 35 are found to be in excellent agreement, for energies

significantly greater than $V(R + \lambda\!\!\!^{-})$. Igo has calculated the variation of the cross section with energy in the low-energy region for α particles.[20] The behavior given by Eq. 34 agrees well with his results.

It is convenient to express both the particle wavelength and center-of-mass total energy in terms of the laboratory energy E, in units of MeV per amu. These are given by the relationships

$$\lambda\!\!\!^{-} = \frac{\hbar c}{A_p(2E \cdot M_o c^2 + E^2)^{1/2}} \quad \text{and}$$

$$E_{c.m.} = \frac{A_p A_t}{A_p + A_t} E,$$

where $(M_o c^2)$ is the rest mass of an amu expressed in energy units (approx 931 MeV). Substituting numerical values, we obtain

$$\lambda\!\!\!^{-} = \frac{1.977 \times 10^{-11}}{A_p(1862\ E + E^2)^{1/2}} . \qquad (36)$$

The Values of r_o and SKT

Most important in the use of Eq. 35 is the value of the nuclear unit radius r_o. In general, r_o varies somewhat from one nucleus to another; however, inasmuch as the concept of a nuclear radius is somewhat vague, it is permissible to use a single value of r_o for all nuclei.

Most earlier analyses of nuclear interactions have been made using a simpler model in which the parameter SKT was not considered. With this model, many attempts have been made to assign a value to r_o. Evans[3] has summarized the various methods utilized prior to 1955. These include:

a. Analysis of the β decay of certain isotopes to infer the value of the classical Coulomb-energy radius;

b. Quantum-mechanical corrections to the classical Coulomb-energy radius, leading to an equivalent electromagnetic radius;[21]

c. Analysis of isotopic shift in line spectra;[22]

d. Measurement of the characteristic electromagnetic radiations from μ-mesonic atoms;[21,23,24]

e. Analysis of fine-structure splitting of electronic x-ray levels in heavy atoms;[25]

f. Measurement of the lifetime of α ray emitters;[26]

g. Analysis of anomalous scattering of α particles;[27]

h. Measurement of the cross sections for nuclear reactions;[28]

i. Measurement of the elastic scattering of fast neutrons by nuclei.

Later attempts to measure r_o include the following. Willoughby measured the mean free path of α particles in emulsions and calculated a value for r_o of 1.23 fermis.[29] Williams[30] measured the reaction cross section for 1.4-GeV neutrons, and calculated a value of 1.28 for r_o. Note that at very high energies Eqs. 35 and 36 apply equally well for neutrons. Thomas has calculated the cross sections for compound-nucleus formation using two different models.[31] The first model, based on a square-well nuclear potential, gives results that agree reasonably well with experimental data when a value for r_o of approximately 1.5 is used. The second model, based on a diffuse nuclear potential, fits experimental data well with a value for r_o of 1.17. Longo and Moyer measured the reaction cross sections for 1.4- to 4.0-GeV protons.[32] The corresponding value of r_o lies between 1.25 and 1.35 fermis. The result of Zerby,[33] as reported by Wallace,[34] for the proton cross section in oxygen yields a value for r_o of 1.17.

By use of these and other early works as guidelines, and by making use of the analysis of nuclear charge distribution by Hofstadter,[35] a set of values for r_o and SKT was found that fitted reasonably well the literature data. These values, 1.4 F for r_o and 0.4 F for SKT, were used in obtaining all the calculated results presented in this work.

C. Multiple Scattering

The scattering process is important for several reasons. First, as was discussed earlier, the beam spreading associated with the scattering introduces a variance in the path-length distribution. An analysis of the process is required, therefore, in order to calculate the mean angle of deflection, $\bar{\varphi}$, from which this variance contribution is obtained.

Similarly, a knowledge of the mean angle allows one to calculate the amount of travel by the ions in a direction perpendicular to the original direction of motion of the ions. This in turn can be used to estimate (i) the minimum beam diameter necessary so that the multiple scattering does not significantly dilute the beam, and (ii) the degree of beam attenuation resulting from geometrical spreading.

Various attempts have been made to treat the multiple-scattering problem in detail, some meeting with more success than others. Bichsel gives an

extensive review of the work in the field.[36] Unfortunately, none of these treatments is directly applicable to the problem of very heavy, high-energy ions in matter. Some of the past work done is discussed briefly below, primarily to furnish background for the rest of this section.

The basic limitation of most of the treatments of the multiple-scattering process is that the assumption is made that the ratio of the atomic number of the incoming ion to that the stationary medium is quite small. This allows the use of c.m. results, which are quite simple in form, in the laboratory (lab) system.

Molière[37] and Goudsmit and Saunderson[38,39] obtained solutions to the problem of a parallel beam of ions impingent on an infinite slab. Bethe demonstrated the conditions under which the two solutions were equivalent.[40] Because of the simplicity of the scattering law in the case of light projectiles and heavy targets, Molière succeeded in performing certain transformations on the general solution which yielded a result in a much more tractable form.

Because for a great many of the cases of interest the atomic number ratio of the projectile to target is unity or larger, the transformations by Molière do not appear to be possible. Consequently, methods that make use of the results of Molière, such as that of Bichsel and Uehling,[4] and Overas[41] are not directly applicable in this case.

Various authors have attempted to estimate the multiple-scattering effects by making direct use of the scattering law to calculate such quantities as the mean square angle as a function of position. Segrè[18] and Rossi[42] both discuss some of the more common methods. Although this avenue of attack seems the most immediately promising for this work, none of the published methods and results is directly applicable. This is again primarily because most authors have used the scattering law in the form restricted to the c.m. system.

Furthermore, in many of the methods, such as those given by Williams,[43] Mather and Segrè,[44] and Snyder and Scott,[45] the approximations used do not adequately handle the wide energy range of interest here. Since in this work the variation in energy is often very large, it is felt that it would be best to start from the fundamental scattering law, following in part the methods outlined by others, but modifying to (a) transfer to the lab system of coordinates, and (b) treat in a more rigorous manner the problem of energy

dependence.

In the following analysis, we first develop the equations that describe the basic scattering law. These are then used to obtain expressions for the mean square angle of deflection of the beam particles, which is in turn used to estimate the mean angle of deflection, $\bar{\varphi}$. Finally, these results are used to calculate the mean square beam spread and contribution to the path-length variance as functions of penetration distance.

1. Scattering Law

The quantity $P(\theta)d\theta$ is defined as the number of collisions per unit distance of travel of a particle, which deflect the trajectory of the particle by an angle which is within $d\theta$ of θ. The classical Rutherford scattering formula for this probability is given by Rossi as[42]

$$P(\theta)d\theta = \frac{1}{4} N_a Z_p^2 Z_t^2 r_e \cdot \frac{1}{A_t}\left(\frac{m_e c}{\beta p_{c.m.}}\right)^2 \cdot \frac{2\pi \sin\theta\, d\theta}{\sin^4(\theta/2)} , \qquad (37)$$

where N_a is Avogadro's number, r_e is the classical electron radius, m_e is the electron mass, and $p_{c.m.}$ is the momentum of the particle. This equation applies to the c.m. system of coordinates; it may be valid in the lab system if the mass of the incident particle is much less than that of the atoms of the medium. Since for many cases of interest to this study this is not so, Eq. 37 must instead be considered in the c.m. system only.

For the purposes of this treatment, it will be convenient to leave the angle θ in the c.m. system, but to transform the momentum term into the lab system.

From the expressions derived by Halliday,[46] the relation between the momentum in the lab and c.m. systems is

$$p_{c.m.} = \left(\frac{1}{1+\gamma}\right) p_L , \qquad (38)$$

where $$\gamma = A_p/A_t .$$

Using Eq. 38 in Eq. 37 and dropping the subscript on the lab momentum term, we have

$$P(\theta)d\theta = \frac{\pi}{2} \frac{N_a Z_p^2 Z_t^2}{A_t} r_e \left(\frac{m_e c}{\beta p}\right)^2 \frac{\sin\theta\, d\theta}{\sin^4(\theta/2)} (1+\gamma)^2 . \qquad (39)$$

The limitations on the validity of Eq. 39 must be discussed. At extremely small angles, this equation fails because the electrons of the

scattering atom screen the particle from the field of the nucleus. Rossi[42] states that Eq. 39 is valid for angles significantly larger than $\lambda\!\!\!^{-}/r_a$, where $\lambda\!\!\!^{-}$ is the de Broglie wavelength of the incident particle divided by 2π and r_a is the radius of the atom; whereas, for angles less than $\lambda\!\!\!^{-}/r_a$, Eq. 39 grossly overestimates the scattering probability. In fact, one can see that the equation is singular for $\theta = 0$.

Various attempts have been made to modify Eq. 39 in order to take into account the screening effect. Using an atomic potential of the form $V = (Z_t Z_p e^2/r) \exp(-r/r_a)$, Goudsmit and Saunderson[38,39] show that the scattering-probability law takes the form

$$P(\theta)d\theta = \frac{8\pi N_a Z_p^2 Z_t^2}{A_t} r_e \left(\frac{m_e c}{\beta p}\right)^2 \frac{\sin\theta\, d\theta}{[\theta^2+\theta_1^2]^2} (1+\gamma)^2 , \qquad (40)$$

where

$$\theta_1 = \lambda\!\!\!^{-}/r_a . \qquad (41)$$

By use of the expression in Eq. 38 and the classical expression for r_a,

$$r_a = \frac{1}{\alpha^2} r_e Z_t^{1/3} ,$$

with

$$\alpha = e^2/\hbar c ,$$

Eq. 41 is transformed to

$$\theta_1 = \frac{Z_t^{1/3}}{137} \frac{m_e c}{p} (1+\gamma) . \qquad (42)$$

Note that θ_1 is in c.m., whereas p is the lab momentum.

Williams has derived corrections to the scattering law given in Eq. 40 for high energies, using a simple model for the charge distribution within the nucleus.[43] He shows that the fact that the charge is not concentrated in a single dimensionless point does not materially affect the scattering law for angles less than $\theta_2 \approx \lambda\!\!\!^{-}/r_n$, where r_n is an assumed radius for the nucleus. On the other hand, for $\theta > \lambda\!\!\!^{-}/r_n$, the scattering probability goes to zero much more rapidly than predicted by Eq. 39. Using for r_n the expression

$$r_n = 0.49\, r_e A_t^{1/3} ,$$

we can estimate an upper limit, θ_2, for nonzero values of the scattering probability:

$$\theta_2 \approx \frac{\lambda\!\!\!^{-}}{0.49\, r_e A_t^{1/3}} \cong 280\, A_t^{-1/3} \cdot \frac{m_e c}{p}\,(1+\gamma). \tag{43}$$

It is convenient to express the various quantities appearing in Eqs. 40, 42, and 43 in energy rather than momentum units. To do this, we use the relativistic relation between momentum and energy,

$$p^2 = 2A_p^2 M_o E + A_p^2 E^2/c^2, \tag{44}$$

where E is in units of energy per amu, and M_o is the rest mass per amu.

The quantity β in terms of E is

$$\beta = \left[1 - \left(\frac{M_o c^2}{E + M_o c^2}\right)^2\right]^{1/2}. \tag{45}$$

Using Eqs. 44 and 45 in 40, 42, and 43, and rearranging terms, we obtain

$$P(\theta)d\theta = (8\pi N_a r_e^2)(m_e c^2)^2 \cdot \frac{1}{HH(E)} \frac{\sin\theta d\theta}{[\theta^2 + \theta_1^2]^2} \left(\frac{Z_p^2 Z_t^2}{A_p^2 \cdot A_t}\right)(1+\gamma)^2 \tag{46}$$

with

$$HH(E) = \left[\frac{E(E + 2\,M_o c^2)}{E + M_o c^2}\right]^2 \tag{47}$$

$$\theta_1 = \frac{Z_t^{1/3}\,(1+\gamma)}{137\, A_p} \quad \frac{m_e c^2}{[E(E + 2M_o c^2]^{1/2}},$$

and

$$\theta_2 = \frac{280(1+\gamma)}{A_t^{1/3} \cdot A_p} \quad \frac{m_e c^2}{[E(E + 2M_o c^2)]^{1/2}}.$$

If we substitute numerical values, these equations reduce to

$$P(\theta)d\theta = 0.3139 \left(\frac{Z_p^2 Z_t^2}{A_p^2 \cdot A_t}\right)(1+\gamma)^2 \cdot \frac{1}{HH(E)} \frac{\sin\theta\, d\theta}{[\theta^2 + \theta_1^2]^2}, \tag{48}$$

with

$$HH(E) = \left[\frac{E(E + 1862)}{E + 931}\right]^2,$$

$$\theta_1 = 3.73 \times 10^{-3} \quad \frac{Z_t^{-1/3}(1+\gamma)}{A_p} \quad \frac{1}{[E(E + 1862)]^{1/2}}, \tag{49}$$

and $$\theta_2 = \frac{143.1\ (1 + \gamma)}{A_t^{1/3} \cdot A_p} \cdot \frac{1}{[E(E + 1862)]^{1/2}} \cdot \qquad (50)$$

2. Mean Square Angle of Deflection

We are now ready to calculate the mean square angle of deflection, denoted $\langle\varphi^2\rangle$, as a function of distance of travel. Since each scattering is independent and represents a very small fraction of the total scattering angle, the change in $\langle\varphi^2\rangle$ in a distance element Δs is

$$\Delta\langle\varphi^2\rangle \cong \Delta s \int \varphi_L^2 P_L(\varphi_L) d\varphi_L \ , \qquad (51)$$

where φ_L is the scattering angle of a single collision (lab), and $P_L(\varphi_L)$ is the corresponding probability of occurrence per unit length. In the limit as $\Delta s \to 0$ we have

$$\frac{d}{ds}\langle\varphi^2\rangle = \int \varphi_L P_L(\varphi_L) D\varphi_L \equiv \varphi_s^2 \ , \qquad (52)$$

where φ_s^2 is the mean square angle change per unit distance of travel.

Now, since all expressions describing the scattering process are in the c.m. system, we must transform Eq. 52 as follows. Since there is a unique relation between an angle φ_L lab and the corresponding angle θ in the c.m. system, we may write

$$P_L(\varphi_L) d\varphi_L = P(\theta) d\theta .$$

Substituting into Eq. 52, then, we obtain

$$\varphi_s^2 = \int_{\theta_1}^{\theta_2} \varphi_L^2(\theta) P(\theta) d\theta , \qquad (53)$$

where the functional dependence of φ_L on θ is indicated.

We now seek a simple means of relating φ_L to the c.m. angle. Halliday[46] has shown that this relationship is given by the expression

$$\tan \varphi_L = \frac{\sin \theta}{\cos \theta + \gamma} \ . \qquad (54)$$

From an examination of the expression for θ_2 given by Eq. 50, we can conclude that for nearly all cases of interest, θ_2 is less than unity. Further, one can show that for those small energies for which θ_2 exceeds unity, the corresponding residual range of the ions is so small that the

multiple-scattering effects within that range are negligible. Therefore, we may replace Eq. 54 by the simpler expression

$$\varphi_L = \frac{\theta}{1 + \gamma} .$$

Substituting this expression for θ_L into Eq. 53 we obtain

$$\varphi_s^2 = \frac{1}{(1 + \gamma)^2} \int_{\theta_1}^{\theta_2} \theta^2 P(\theta) d\theta. \tag{55}$$

The integral in Eq. 55 is easily evaluated by using the expression for $P(\theta)$ given by Eq. 48. The result is

$$\varphi_s^2 = 0.15696 \frac{Z_p^2 Z_t^2}{A_p^2 \cdot A_t} \cdot \frac{1}{HH(E)} \left\{ \ln \left[\left(\frac{\theta_2}{\theta_1} \right)^2 + 1 \right] - \right\} 1 \quad , \tag{56}$$

and θ_2/θ_1 is, from Eqs. 49 and 50,

$$(\theta_2/\theta_1) = \frac{3.836 \times 10^4}{(A_t Z_t)^{1/3}} , \tag{57}$$

and HH(E) is given by Eq. 47. Note that if θ_2 as calculated from Eq. 50 is greater than π, then the value of θ_2 is to be taken as π instead. In that case, the term θ_2/θ_1 is

$$\theta_2/\theta_1 = \frac{842.2 \cdot A_p [E(E + 1862)]^{1/2}}{Z_t^{1/3}(1 + \gamma)} . \tag{58}$$

Using these expressions for φ_s^2, we can proceed with the calculation of the mean square angle of deflection.

From Eq. 52, we have

$$\frac{d}{ds} \langle \varphi^2 \rangle = \varphi_s^2(E), \tag{59}$$

where we have indicated the dependence of φ_s^2 on the particle energy. This unique dependence on the energy is established by Eq. 56.

As an initial condition, we specify that

$$\langle \varphi^2 \rangle \Big|_{s=0} = \varphi_o^2.$$

Integrating Eq. 59, then, from s = 0 to some value s, we have

$$\langle\varphi^2\rangle = \varphi_o^2 + \int_o^s \varphi_s^2(E')ds'$$

and

$$\langle\varphi^2\rangle = \varphi_o^2 + A_p \int_E^{E_o} \frac{dE'}{f(E')}\, \varphi_s^2(E').$$

For a perfectly collimated beam, φ_o is zero. However, if the initial beam has an angular distribution that can be represented by a Gaussian with some standard deviation, then φ_o is equal to this standard deviation.

The mean angle of deflection $\bar{\varphi}$ is estimated to be the square root of the mean square angle. Thus we write

$$\bar{\varphi} = [\langle\varphi^2\rangle]^{1/2}.$$

3. Scattering for Multiple Materials

The difficulty involved in treating a target composed of more than one type of atom is that there is no unique relationship between the c.m. and lab systems. That is, for each type of target atom, there is a different c.m. system. Consequently, it is necessary to resort to further approximations in order to arrive at results that are applicable in the lab system. The method used is as follows.

The scattering probability function given by Eq. 46 is rewritten

$$P(\theta)d\theta = \left(\frac{N_a\rho}{A_t}\right)\left\{8\pi r_e^2\cdot(m_e c^2)\cdot\frac{1}{HH(E)}\cdot\frac{\sin\theta\, d\theta}{[\theta^2+\theta_1^2]^2}\left(\frac{Z_p Z_t}{A_p}\right)^2(1+\gamma)^2\right\}\frac{1}{\rho},$$

where $(N_a\rho/A)$ is the number of atoms of the scatterer per cubic centimeter, and ρ is the total density of the scattering medium. The term in the braces is then interpreted as the probability of scattering into $d\theta(\theta)$ per atom of scattering material.

The scattering probability for scattering atom type "i" is hence

$$P_i(\theta)d\theta = \frac{8\pi N_i}{\rho}\,(r_e\cdot m_e c^2)^2\cdot\left[\frac{Z_p Z_i(1+\gamma_i)}{A_p}\right]^2\cdot\frac{1}{HH(E)}\,\frac{\sin\theta\, d\theta}{[\theta^2+\theta_1^2]^2},$$

where N_i is the number of type "i" atoms per cubic centimeter, and ρ is the total density of the medium.

The mean square angle change per unit distance, due to type "i" atoms,

is then

$$(\varphi_s^2)_i = 2.606 \times 10^{-25} \left(\frac{N_i}{\rho}\right)\left[\frac{Z_p Z_i}{A_p}\right]^2 \cdot \frac{1}{HH(E)} \left\{\ln\left[\left(\frac{\theta_2}{\theta_1}\right)^2 + 1\right] - 1\right\},$$

where the results embodied in Eq. 56 have been used. Also, by use of Eqs. 57 and 58, we have

$$\left(\frac{\theta_2}{\theta_1}\right)_i = \frac{3.836 \times 10^4}{(A_i Z_i)^{1/3}} \qquad \text{for } \theta_2 < \pi$$

and

$$\left(\frac{\theta_2}{\theta_1}\right)_i = 842.2 \frac{A_p[E(E + 1862)]^{1/2}}{Z_i^{1/3}(1 + \gamma_i)} \quad \text{for } \theta_2 \geq \pi.$$

We now consider the problem of obtaining an estimate of the net mean square scattering angle. Equation 52 may be written as

$$\frac{d}{ds} \langle \varphi^2 \rangle = \sum_i \int \varphi_L^2 P_i(\varphi_L) d\varphi_L = \Sigma(\varphi_s^2)_i \,, \tag{60}$$

where the $P_i(\varphi_L)$ are the probabilities due to the various scattering species.

The mean square angle at s is then obtained, as before, by integration of Eq. 60 from s = 0 to s.

4. Multiple-Scattering Effects

Earlier, it was shown that the scattering process leads to a contribution to the variance in the path-length distribution. Other effects that can be calculated from the equations describing the scattering are discussed below.

a. Radial Spreading

Of particular interest is the function $\langle y^2 \rangle$, which is defined as the mean square distance of travel in a direction perpendicular to the initial direction of travel, and is a function of the mean distance of travel s. For simplicity, it is denoted as the mean square radial spread. This function characterizes the general shape of the beam within the medium, and can be used to estimate the minimum beam size necessary to ensure against excessive effects due to spreading.

Suppose the mean-square beam spread at some positions in the medium is given as $\langle y^2 \rangle$. Clearly, then, if the initial dimensions of the beam are much greater than $[\langle y^2 \rangle]^{1/2}$, the effect of radial spreading will be small.

That is, the fractional change in the beam dimensions will be much less than unity.

On the other hand, if the beam radius, say, is much smaller than the value of $\langle y^2 \rangle$ at some distance s, then the beam at that point will have smeared out to the extent that the shapes of the flux and dose curves are grossly altered from what they would be for a large-diameter beam.

We proceed to the calculation of the function $\langle y^2 \rangle$. Referring to Fig. 1, we can express the change in the mean-square radial spread at x' due to a change in the mean angle of deflection φ at some $x < x'$. Thus, we have

$$\Delta y \equiv [\Delta\langle y^2 \rangle]^{1/2} = (x' - x)\Delta\varphi \ ,$$

so that

$$\Delta\langle y^2 \rangle = (x' - x)^2 \, \Delta\langle \varphi^2 \rangle \ . \tag{61}$$

The change in the mean square angle is given by Eq. 51 and substituting into Eq. 61 we have

$$\Delta y^2 = (x' - x)^2 \cdot \varphi_s^2 \, \Delta s \ . \tag{62}$$

Recognizing that the contributions to the mean square radial spread are additive, we obtain

$$\langle y^2 \rangle = A_p \int_E^{E_o} (x - x')^2 \varphi_s^2 \frac{dE'}{f(E')} + (\Delta y_o)^2 \ , \tag{63}$$

where we have interchanged the variables x and x' for convenience. The quantity $(\Delta y_o)^2$ is the contribution to the radial spread variance at x due to an initial angular spread of the beam particles. Thus, if φ_o is the initial mean angle of the beam particles, then reference to Fig. 1 and Eq. 62 shows that $(\Delta y_o)^2$ is

$$(\Delta y_o)^2 = x^2 \varphi_o^2 \ ,$$

where $(\Delta y_o)^2$ is evaluated at a penetration distance x.

It is shown later that, in many cases, the term $(\Delta y_o)^2$ dominates the right-hand side of Eq. 63, even for quite small values for φ_o. In other words, the mean beam deflection can be a strong function of the initial angular spread. Numerical examples are presented in the section dealing with results.

The variable x' is related to the energy E' through the expressions in Eqs. 31 and 5.

Equation 63 thus gives an expression for the variance in the radial spread distribution for particles having reached an energy E. We may define a mean beam deflection as the square root of $\langle y^2 \rangle$. This is another measure of the amount of radial spreading of the beam.

b. Beam-Spreading Attenuation

As the beam spreads, there may be an effective geometric attenuation of the flux and dose; i.e., the particles are spread out over a larger area. A very rough estimate of this effect is given as follows.

Let y_o be the radius of the initial beam. At some penetration distance x, suppose that the mean-square radial spread is $\langle y^2 \rangle$. Then at that point, one can say that the beam "effective radius" is estimated to be $y_o + y$, where y is the mean beam deflection. Therefore, the attenuation factor will be simply

$$f = \left(\frac{y_o}{y_o + y} \right)^2 = \left(\frac{1}{1 + y/y_o} \right)^2 . \qquad (64)$$

As the ratio y/y_o increases, one would expect this function to more nearly represent the attenuation of the center-line flux and dose.

For the experimental situation in which the sensitive-area dimensions of a detector are much larger than the maximum value of y, there is no attenuation of the form given by Eq. 64. Similarly, if the beam were very broad and the diameter of the sensitive area of the detector were small, no attenuation would result. On the other hand, the function f would be expected to give the proper attenuation for the situation in which (i) the ratio y/y_o is large, and (ii) the counter diameter is small compared with y_o.

c. Range Shortening

Because the particles follow curved paths, the effective range in the medium is somewhat less than if the particles all traveled in straight lines. If R is the effective range of the particles and S_R is the corresponding mean distance of travel, then Eq. 31 gives their relationship as

$$R = S_R - \langle s - x \rangle \Big|_R , \qquad (65)$$

where $\langle s - x \rangle \big|_R$ is the mean difference at the range.

The choice of definition of the range is somewhat arbitrary, and several are in common usage. For the purposes of evaluating the expression in Eq. 65, the value chosen for the range is immaterial, since $\langle s - x \rangle$ is

virtually constant in the vicinity of the end of the range. That this is so follows from the fact that when the mean angle of deflection becomes significant, the mean energy is so low that the residual range is a minute fraction of the total range. That is, although the particles are traveling at large oblique angles, their remaining distance of travel is so small that the contributions to $\langle s - x \rangle|_R$ are negligible.

The degree of range shortening is often expressed in terms of a quantity called the percentage detour factor, which is defined by Berger and Seltzer[7] as

$$D = \frac{100 \langle s - x \rangle|_R}{S_R} .$$

IV. RESULTS

Presented in this section are the results of calculations based on the analyses presented in the preceding sections. For the most part, these calculations were performed by using the program BRAGG,[47] which was written to solve the various equations developed in this work. The first part of this section deals with those results related in particular to the multiple-scattering process. Also presented here are comparisons with the results of other workers. The second part of this section is devoted to the presentation of Bragg and flux curves for various ions in different targets. Also presented are results pertinent to the energy spectra at the Bragg peak. The effects of using different ions in the same medium, and of using the same ions in different media, are discussed. The next section deals with the importance of initial energy and angular spreads of the beam. Finally, experimental results of the Bragg, flux, and spectral curves are compared with the corresponding theoretical calculations.

A. Multiple-Scattering Calculations

The multiple-scattering process may be considered separately from the other processes occurring in the medium as the mean angle of deflection and the mean beam deflection are essentially functions of the particle energy only, and do not appreciably depend on the actual number of particles reaching this energy.

1. Comparison with the Literature

Other workers have studied the scattering of protons in media for which the lab and c.m. systems are equivalent.

Berger and Seltzer have calculated the percentage detour factor for protons of various energies incident on various absorbers.[7] These results are reproduced in Fig. 2. Table V gives various values taken from this figure.

Table V. Comparison of multiple-scattering results for an incident beam of 100-MeV protons.

Absorber	Percentage detour factors	
	Berger and Seltzer	Calculations, this work
Lead	2.28	1.49
Copper	0.756	0.57
Aluminum	0.306	0.24
Beryllium	0.087	0.069

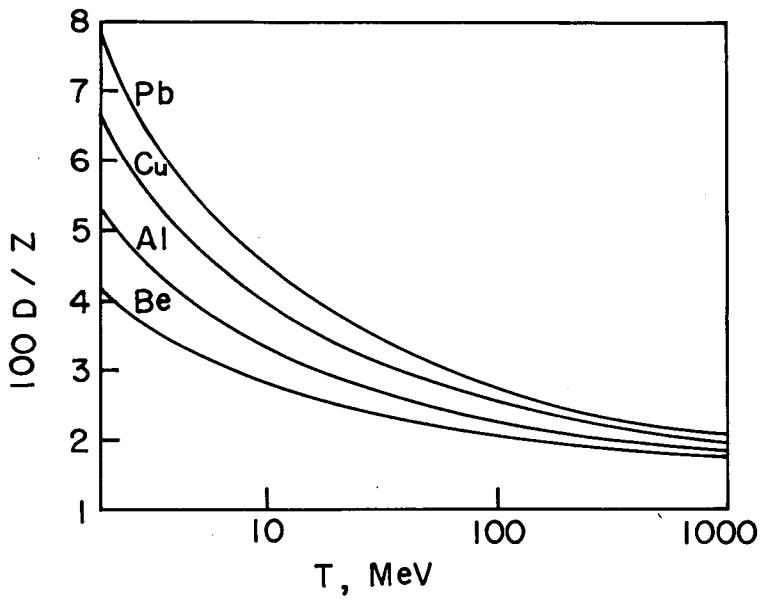

XBL 677-4367

Fig. 2. Ratio of percentage detour factor to the atomic number of the medium for protons.

Also given in the table are the corresponding results obtained by using the analysis of this work.

Berger and Seltzer also give the results of Monte Carlo calculations performed by Berger[48] for the angular distribution of 338.5-MeV protons slowed down to 2 MeV in copper and lead. These results are shown in Fig. 3, which can be used to estimate the mean angle of deflection. These estimates, along with the calculated values, are shown in Table VI.

Table VI. Comparison of multiple-scattering results for an incident beam of 338.5-MeV protons.

	Mean angle of deflection (deg)	
Absorber	Estimates from Berger and Seltzer	Calculations, this work
Lead	30 to 40	44
Copper	15 to 25	21

Looking at Fig. 3, we see that in both cases the curves are skewed towards the high end. Consequently, the mean angle of deflection is somewhat greater than the most probable angle. For lead, the mean angle would appear to lie in the vicinity of 30 to 40 deg. This agrees reasonably well with the calculated value of 44 deg for the mean angle, as shown in Table VI. For copper, Fig. 3 indicates that the mean angle lies in the range from 15 to 25 deg. This is compared to a calculated angle of 21 deg.

In comparing the two sets of results, it should be pointed out that the Monte Carlo data are based on the case histories of only 5000 particles. Consequently, a good deal of uncertainty is attendant, especially in the upper and lower angular regions, where the figures are based on very few events.

Preston and Koehler[49] have measured the radial intensity of a beam of protons passed through various thicknesses of different absorbers. From these measurements, they calculate the standard deviation in the radial spread. Their results are presented in Table VII, along with the results obtained by using the methods in this work (note that the SD in the radial spread is equivalent to the square root of the mean square radial spread). In the table, E_o is the initial beam energy, T is the thickness of the absorber traversed by the beam, σ_{exp} is the experimentally determined value of the radial SD, and σ_c is the corresponding calculated value. The

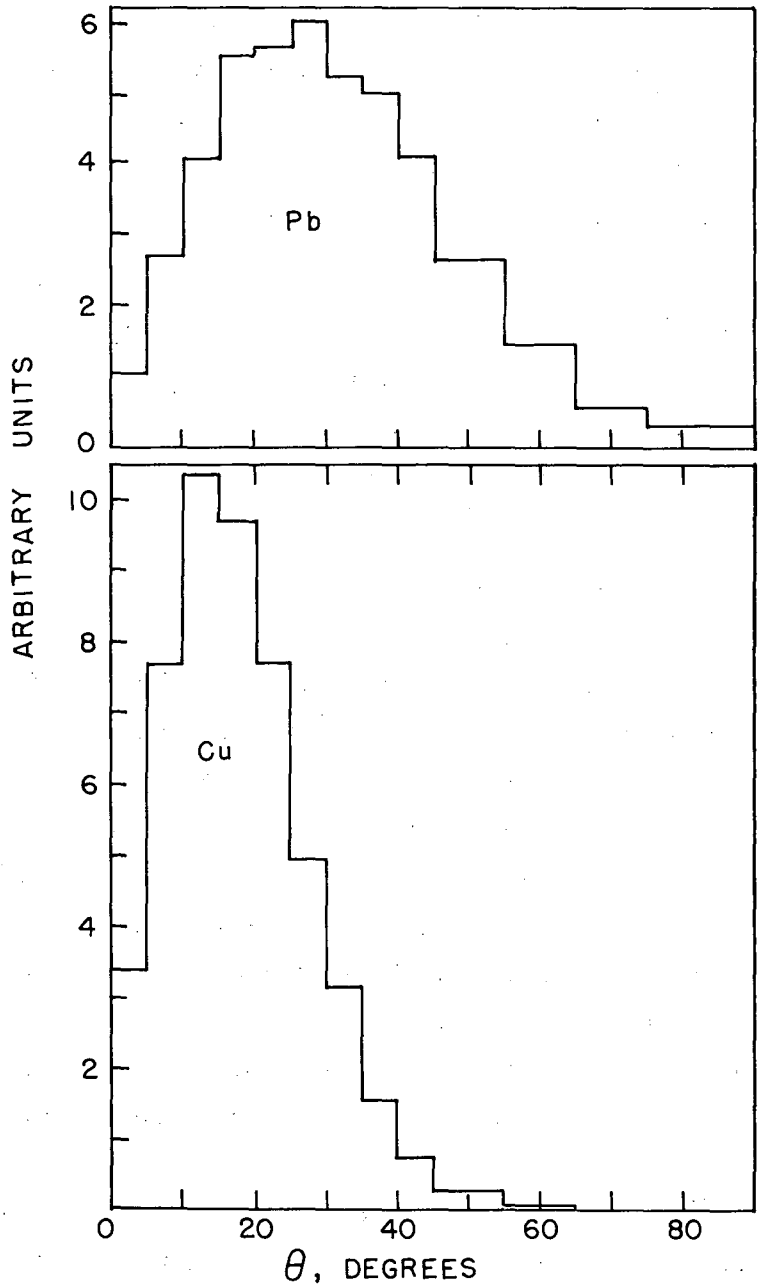

XBL 677-4371

Fig. 3. Angular distribution of protons slowed down from 338.5 MeV to .2 MeV in lead and copper, based on 5000 Monte Carlo histories.

results are generally in excellent agreement.

Table VII. Comparison of multiple-scattering results.

Absorber	E_o (MeV)	T (cm)	σ_{exp} (mm)	σ_c (mm)
Aluminum	158	2.54	0.35	0.55
		5.08	1.62	1.64
		6.38	2.35	2.40
		7.62	3.24	3.29
		8.25	3.43	3.78
	112	2.54	0.97	0.79
		3.81	1.66	1.57
		4.44	2.06	2.08
Water	127	5.7	1.15	1.11
		8.7	2.18	2.22
		11.4	3.46	3.66

2. Scattering Effects for Various Ions and Materials

In this section, we present the results of calculations of the multiple-scattering effects for various ions in different materials. From the equations describing small-angle scattering, it can be seen that the scattering effects decrease as the ratio of the atomic numbers of the beam and target increases. One can see this most easily by recognizing that as this ratio increases, the maximum angle of scattering decreases. Hence, for a given absorber, and a given range, one would expect the mean beam deflection and the percentage detour factor to decrease as the atomic number of the beam particles increases.

To illustrate these effects, calculated values of the percentage detour factor, the standard deviation in the radial spread, and the mean angle of deflection -- all at the Bragg peak -- are tabulated for various ions in water, copper, and uranium. Tables VIII and IX give the results for ions in water, with the Bragg peak at 5.0 and 10.0 g/cm^2. Tables X and XI show similar results for copper and uranium, with the peaks at 5.0 g/cm^2.

In all cases, it is clearly demonstrated that the scattering effects decrease markedly as the atomic number of the beam particles increases. For example, for the Bragg peak at 5.0 g/cm^2 of water, the degree of beam spreading goes down by a factor of approximately 5 in going from a beam of

protons to one of neon ions. A similar decrease is calculated for the

Table VIII. Multiple-scattering results for water with the Bragg peak at 5.0 g/cm^2.

Beam particle	Percentage detour factor	Mean beam deflection (g/cm^2)
P	0.114	0.168
He	0.0285	0.083
C	0.0088	0.046
Ne	0.0051	0.035
A	0.0025	0.024
Kr	0.0012	0.017
Xe	0.0007	0.013

Table IX. Multiple-scattering results for water with the Bragg peak at 10.0 g/cm^2.

Beam particle	Percentage detour factor	Mean beam deflection (g/cm^2)
P	0.108	0.328
He	0.027	0.162
C	0.0083	0.090
Ne	0.0048	0.068
A	0.0024	0.047
Kr	0.0011	0.032
Xe	0.0007	0.026

Table X. Multiple-scattering results for copper with the Bragg peak at 5.0 g/cm^2.

Beam particle	Percentage detour factor	Mean beam deflection (g/cm^2)
H	0.628	0.388
He	0.159	0.193
C	0.0475	0.105
Ne	0.0269	0.0791
A	0.0141	0.0554
Kr	0.0066	0.0383
Xe	0.0042	0.0300

Table XI. Multiple-scattering results for uranium with the Bragg peak at 5.0 g/cm^2.

Beam particle	Percentage detour factor	Mean beam deflection (g/cm^2)
H	2.54	0.772
He	0.669	0.390
C	0.193	0.207
Ne	0.108	0.155
A	0.0548	0.108
Kr	0.0261	0.0740
Xe	0.0168	0.0577

other cases. It should also be pointed out that in all cases, the rate of change of beam spreading with respect to increasing beam-ion mass decreases at the higher masses. Thus, there is a greater effect in going from protons to neon than there is in going from neon to xenon.

An extremely important result is the magnitude of the lower limit on the beam dimensions predicted by the calculations. For a proton beam with the Bragg peak at 10 cm H_2O, this limit is on the order of 0.75 to 1.5 cm, whereas for neon the lower limit is approximately 0.1 to 0.2 cm.

It is also interesting to examine the variation of the multiple-scattering effect with absorber, for a given beam particle. Tables XII and XIII show the results for protons and neon ions in miscellaneous absorbers. For comparison purposes, the initial energies are chosen such that the Bragg peak occurs at 5.0 cm.

Table XII. Multiple-scattering results for protons in various absorbers with the peak at 5 g/cm^2.

Absorber	Percentage detour factor	Mean beam deflection (g/cm^2)
Al	0.256	0.250
Cu	0.628	0.390
Ag	1.11	0.515
Pb	2.22	0.722
U	3.88	0.962

Table XIII. Multiple-scattering results for neon ions in various absorbers, with the peak at 5 g/cm^2.

Absorber	Percentage detour factor	Mean beam deflection (g/cm^2)
Al	0.011	0.051
Cu	0.027	0.075
Ag	0.047	0.103
Pb	0.092	0.145
U	0.172	0.197

As expected, the scattering effects increase with increasing absorber atomic weight for both cases. Again, it is seen that neon ions produce scattering effects that are less than those produced with protons by a factor of 5.

B. Bragg, Flux, and Spectral Curves for Monoenergetic Beams

In this section, results are presented for the case in which the initial beam of particles is assumed to be perfectly collimated (zero angular spread) and to be monoenergetic. In later sections, the effects due to finite energy and angular spreads are discussed.

Presented here are Bragg curves, flux curves, and energy spectra at the Bragg peak, not only for ions ranging from protons to xenon and having a variety of energies, but also for a number of different targets ranging from water to uranium.

In a discussion of Bragg curves, there are two quantities of particular interest. One is the ratio of the dose at the peak to that at the incident surface, denoted as the peak-to-plateau ratio. The other is the width of the Bragg peak, measured at those two points at which the dose is equal to one-half the dose at the peak. This is called the full width at half maximum, which we shall abbreviate to the "peak width" for convenience.

Also of considerable importance is the shape of the spectrum at the Bragg peak. Of particular interest are the average energy at the peak and the full width at half maximum.

With regard to the calculations, it should be pointed out that for the very heavy, high-energy ions, there will be some secondary-particle generation, primarily in the initial portions of the path length. Conse-

quently, the calculations are expected to be somewhat in error in this region. In fact, since most secondaries are generated near the incident surface, with relatively few being produced in the vicinity of the Bragg peak, one would expect the calculated peak-to-plateau dose ratio to be somewhat high.

Since there are relatively few secondaries generated near the Bragg peak, the shape of the peak is determined principally by the primary particles. In particular, the full width at half maximum of the peak is a relatively slowly varying function of the parameter r_o, which is known reasonably well. Consequently, it is to be expected that the calculated half widths are fairly accurate.

1. Effect of Different Ions

We consider first the following question: given a particular target, and given that the Bragg peak is to be at a particular depth, then how will the shapes of the various curves be affected by using different ions? Qualitatively, one would expect these effects not to be trivial. In particular, the various contributions to the variance in the path-length distribution are all strong functions of the charge and atomic weight of the beam ions, as well as of the charge and atomic weight of the target.

For a monoenergetic beam, the principal contributors to the variance are the processes of energy straggling and multiple scattering. For each of these, it is easily seen that the variance contribution decreases as the charge of the beam particles increases. Therefore, those aspects of the penetration process that are dependent on the path-length variance should be noticeably affected by changing the character of the bombarding ion.

We consider first the case in which the target material is water. Figure 4 shows the Bragg curves for various ions in water, with the Bragg peak at 5.0 g/cm^2. Figure 5 shows the flux curves for the same ions and Fig. 6 shows the spectra at the peak. The basic features of these results are depicted in Table XIV, which gives the peak-to-plateau dose ratio, the Bragg-peak full width at half maximum, and the average energy at the Bragg peak for each case. Also, the peak-to-plateau ratio and the Bragg-peak width are plotted as functions of the atomic number of the beam in Figs. 7 and 8.

As shown by these tables and figures, the peak-to-plateau dose ratio

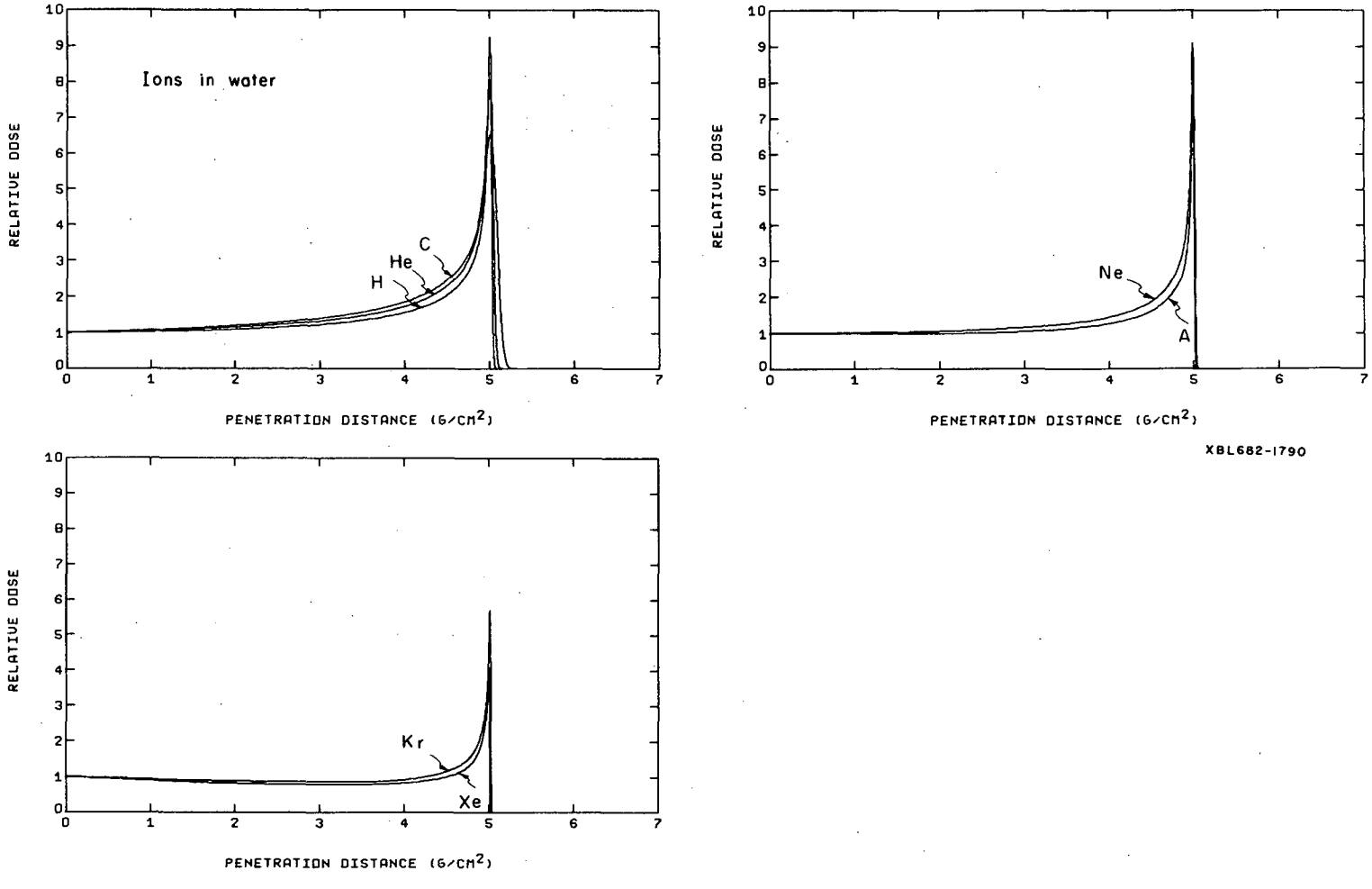

Fig. 4. Bragg curves for ions in water, with the peak at 5 g/cm^2: (a) H, He, and C; (b) Ne and A; (c) Kr and Xe.

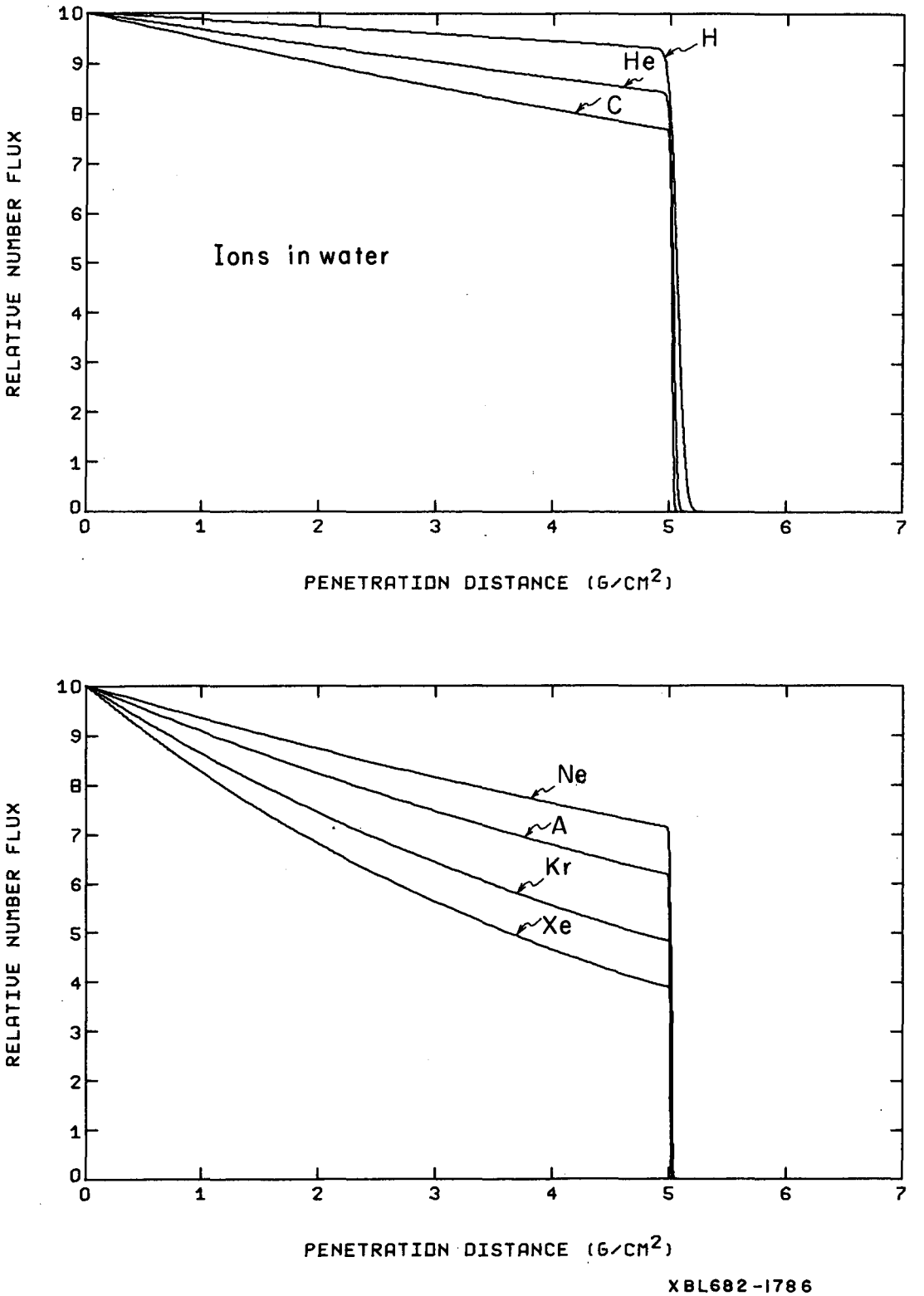

Fig. 5. Flux curves for ions in water with the peak at 5 g/cm^2: (a) H, He, and C; (b) Ne, A, Kr, and Xe.

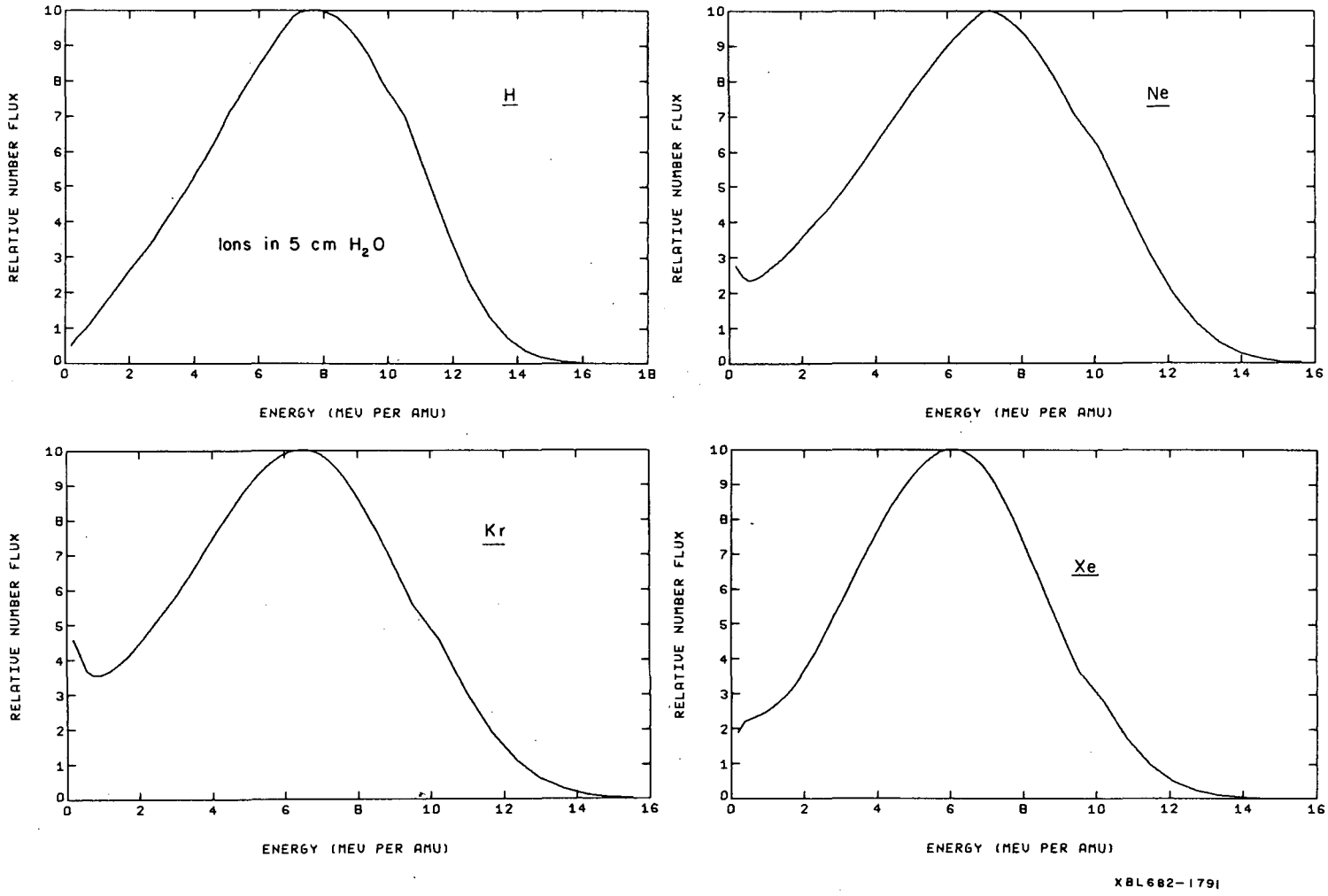

Fig. 6. Spectra at the Bragg peak for ions in water, with the peak at 5 g/cm^2: (a) protons; (b) neon; (c) krypton; (d) xenon.

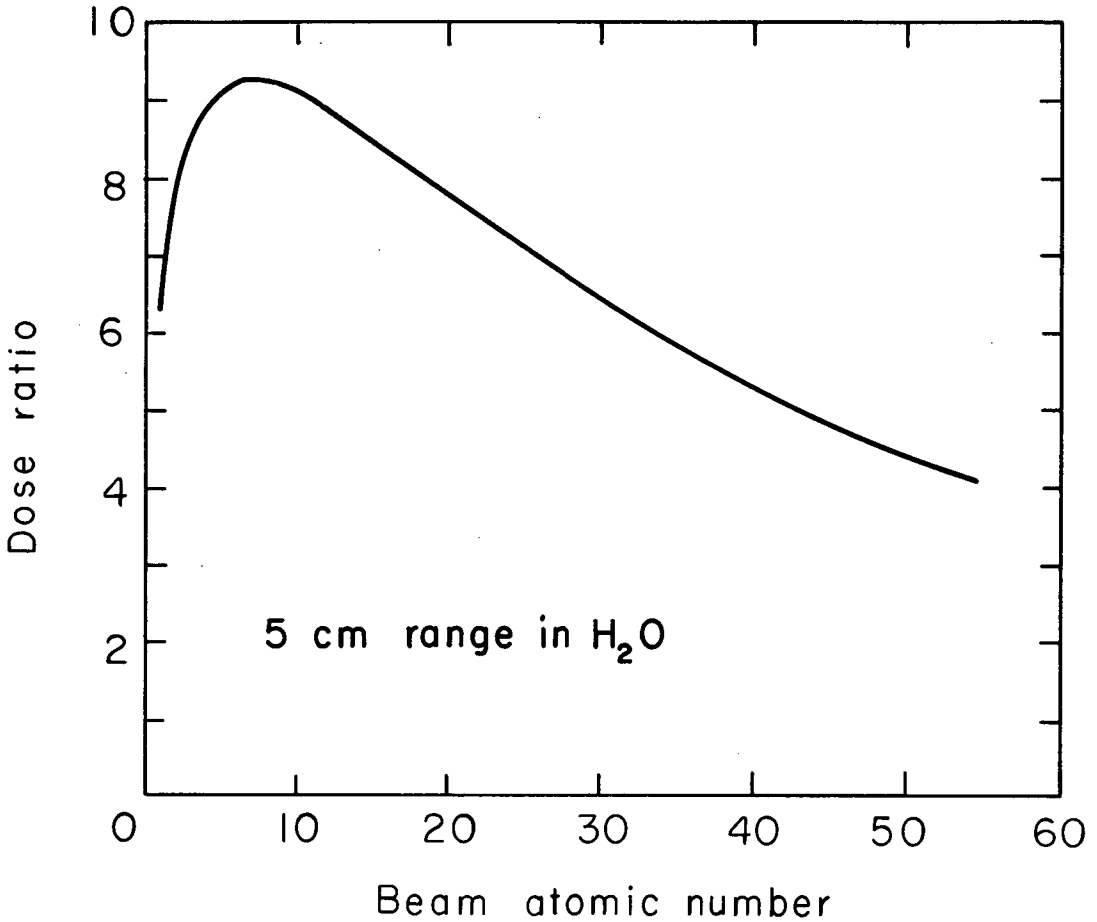

XBL682-1775

Fig. 7. Peak-to-plateau dose ratio for ions in water, with the peak at 5 g/cm^2.

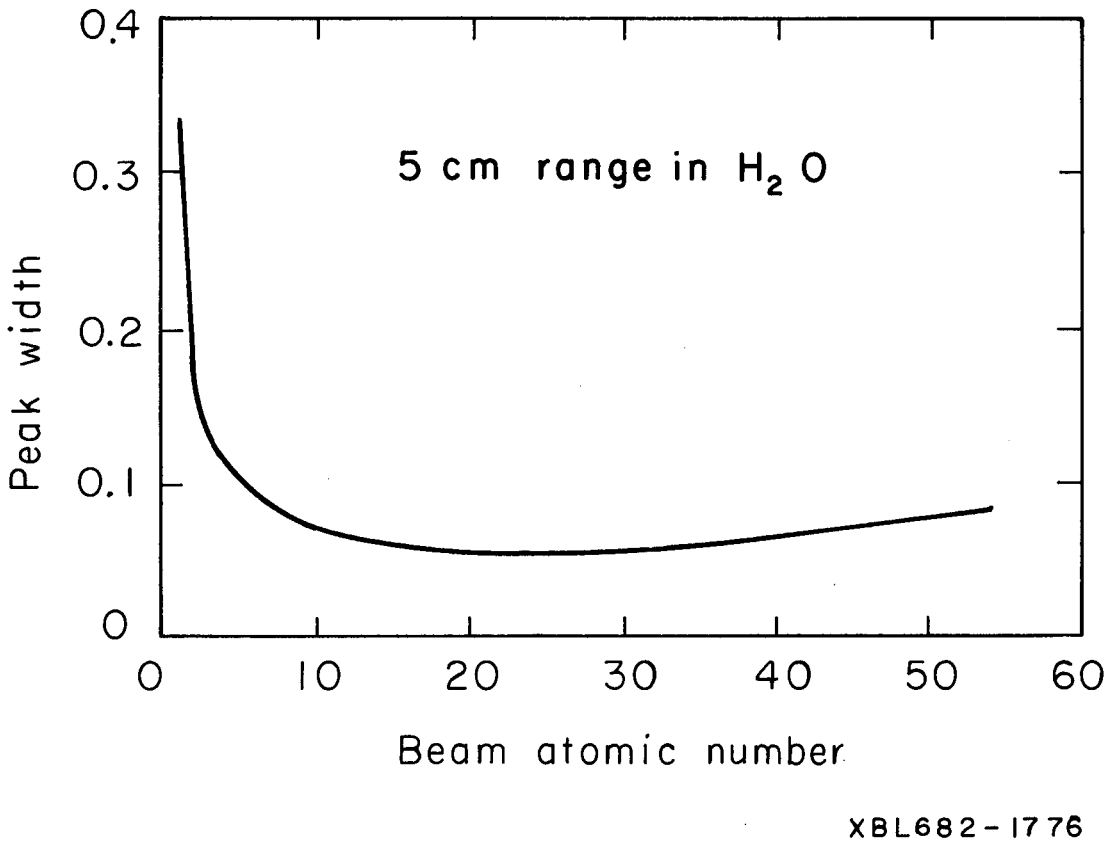

Fig. 8. Bragg peak width for ions in water, with the peak at 5 g/cm^2.

Table XIV. Results for ions in water, with the Bragg peak at 5 g/cm^2.

Beam ion	Initial energy (MeV/amu)	p-p dose ratio	Peak width (g/cm^2)	Peak ave. energy (MeV/amu)
H	79.75	6.53	0.336	7.33
He	79.40	8.04	0.170	4.93
C	147.5	9.24	0.092	6.25
Ne	197.2	9.09	0.075	6.70
A	263.0	8.12	0.057	6.39
Kr	381.1	5.69	0.063	6.14
Xe	471.0	4.08	0.085	5.84

reaches a maximum value for a value of the beam atomic number between 6 and 8. Beyond a value of 10, the dose ratio falls off monotonically.

On the other hand, the peak width falls off extremely rapidly with increasing atomic number, up to a value of approximately 20. For greater values of atomic number the width increases quite slowly. This behavior can in part be explained by considering the effective charge of the ions as they traverse the medium.

Referring to Eq. 29 we see that the straggling variance is directly proportional to Z_p^2 and inversely proportional to the cube of the stopping power, which is in turn proportional to the square of the charge. Hence, the variance is approximately inversely proportional to the fourth power of the charge of the beam particle. We must also recognize that the peak width is directly related to the variance.

Now, consider first the lighter particles. They retain their total charge for essentially the whole range, so that the effective charge goes up as the atomic number. Hence the variance decreases rapidly with increasing atomic number for small atomic numbers. For the heavier elements, however, charge exchange becomes an important process, so that the ion charge no longer is proportional to the atomic number. Hence, the rate of decrease of the half width would be expected to decrease with increasing atomic number. This is obviously not the complete picture, since the peak shape is also determined by the shape of the stopping-power function. However, the same type of argument regarding effective charge applies.

The behavior of the peak-to-plateau dose ratio can be explained, at least partially, in a similar manner. A decrease in the path-length

variance implies that the ions of a given energy are closer together in the target. Consequently, the low-energy (high dE/dx) ions will deposit more energy in less space, and the dose in the vicinity of the peak will rise.

The drop-off of the ratio at high values of Z_p is again due, in part, to the ion-exchange process. Also, the nuclear reaction cross section becomes increasingly important for ions of increasing atomic number, so that more and more particles are removed from the beam.

It is interesting to note that the peak width is nearly constant for values of Z_p ranging from approximately 20 to 40. Also, it should be noted that the average energy at the Bragg peak is relatively independent of the beam ion.

2. Effect of Different Energies

Suppose one wishes to produce Bragg peaks at various penetration depths within a given medium, using a given ion. It would be useful to be able to predict the changes in the various features of the physical process as functions of the depth at which the peak is produced, or alternatively, as functions of the initial beam energy. This section presents results that depict these functional dependences.

We consider two separate systems: protons incident on a water target, and neon ions incident on a water target. These cases serve to demonstrate the relationship between the initial beam energy and such quantities as the peak-to-plateau dose ratio and the Bragg peak width.

The results for the two systems are embodied in Figs. 9 through 12 and Tables XV and XVI. In general, the peak-to-plateau dose ratio goes

Table XV. Variations with initial energy for protons incident on water.

Initial energy (MeV/amu)	Mean range (g/cm^2)	p-p dose ratio	Peak width (g/cm^2)	Peak ave. energy (MeV/amu)	Mean beam deflection (g/cm^2)
50	2.20	6.70	0.153	4.70	0.074
100	7.64	6.26	0.489	9.05	0.247
150	15.58	5.51	0.988	13.25	0.492
200	25.58	4.76	1.61	17.36	0.792
300	50.50	3.36	3.23	24.08	1.523
400	80.61	2.26	5.91	31.64	2.385
500	114.8	1.47	8.26	38.36	3.342

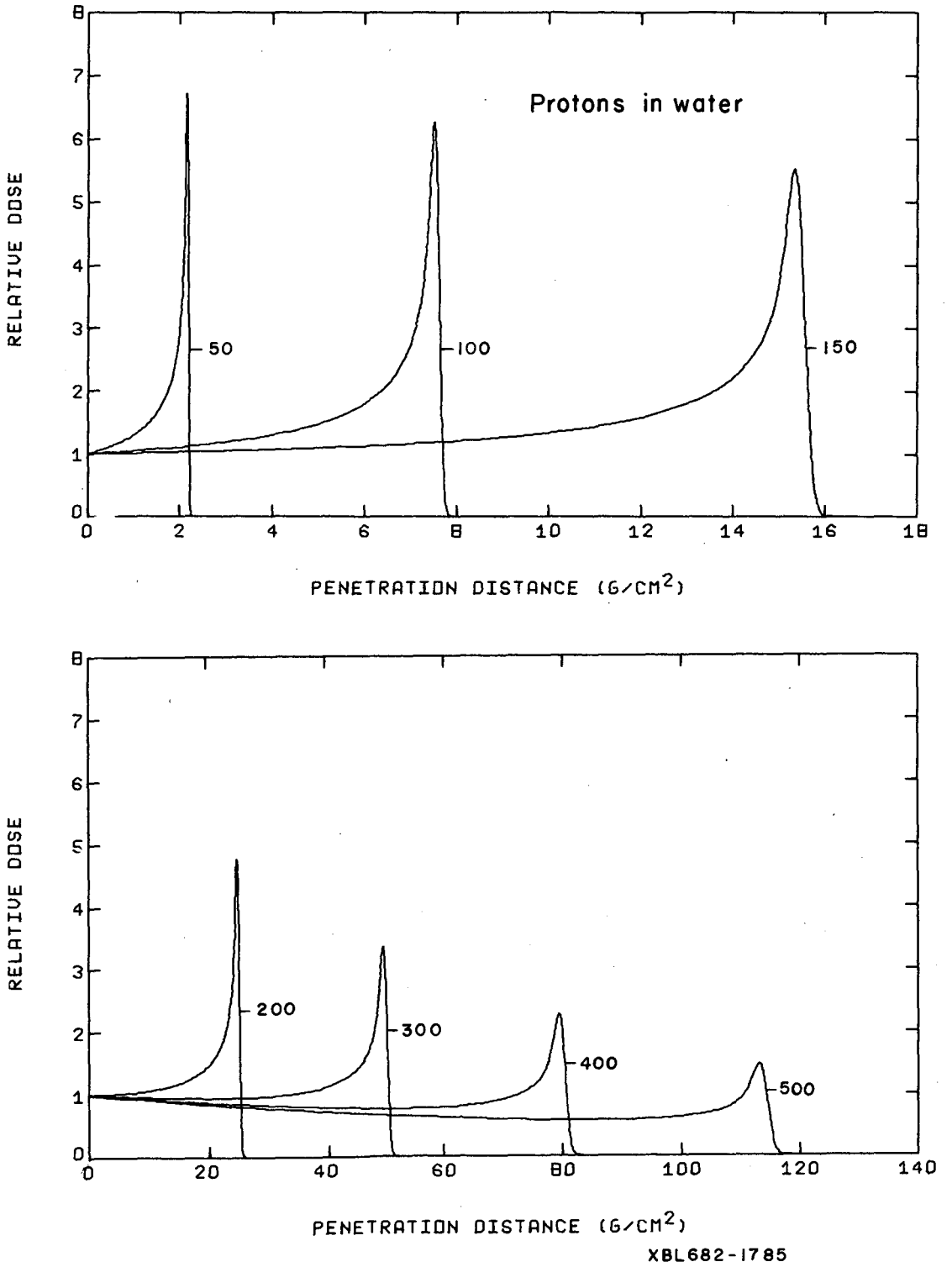

Fig. 9. Bragg curves in water for protons with initial energies ranging from 50 to 500 MeV.

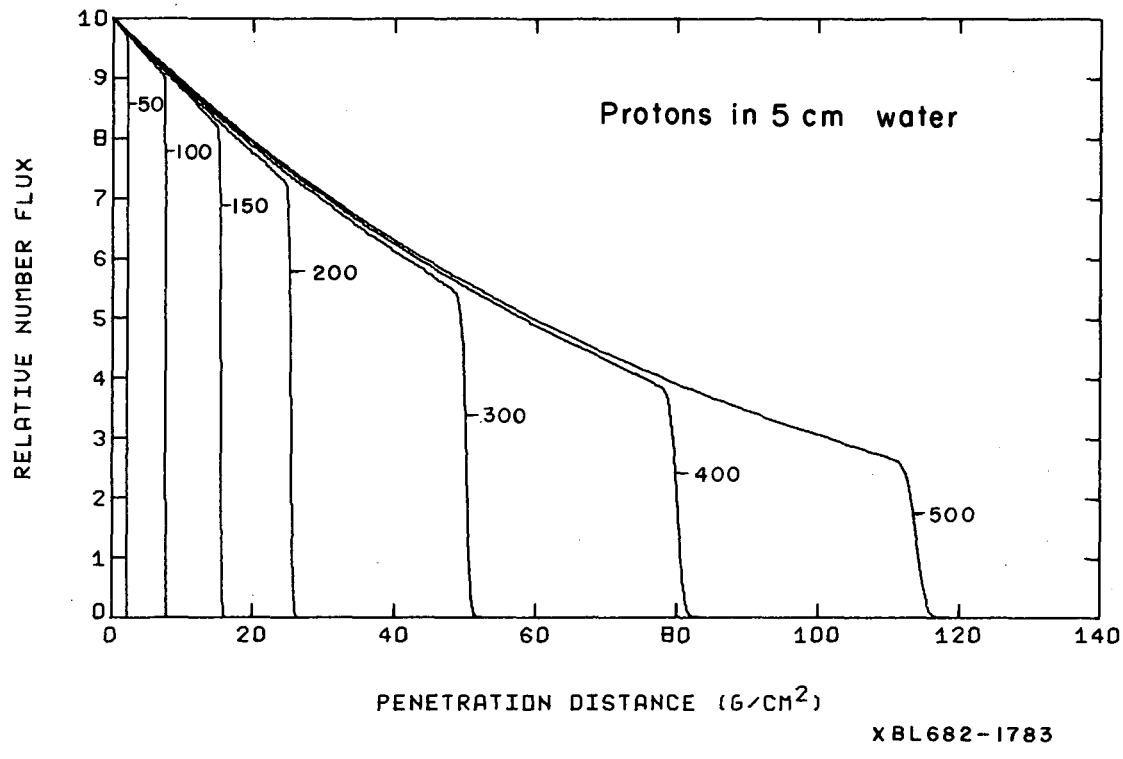

Fig. 10. Flux curves in water for protons with initial energies ranging from 50 to 500 MeV.

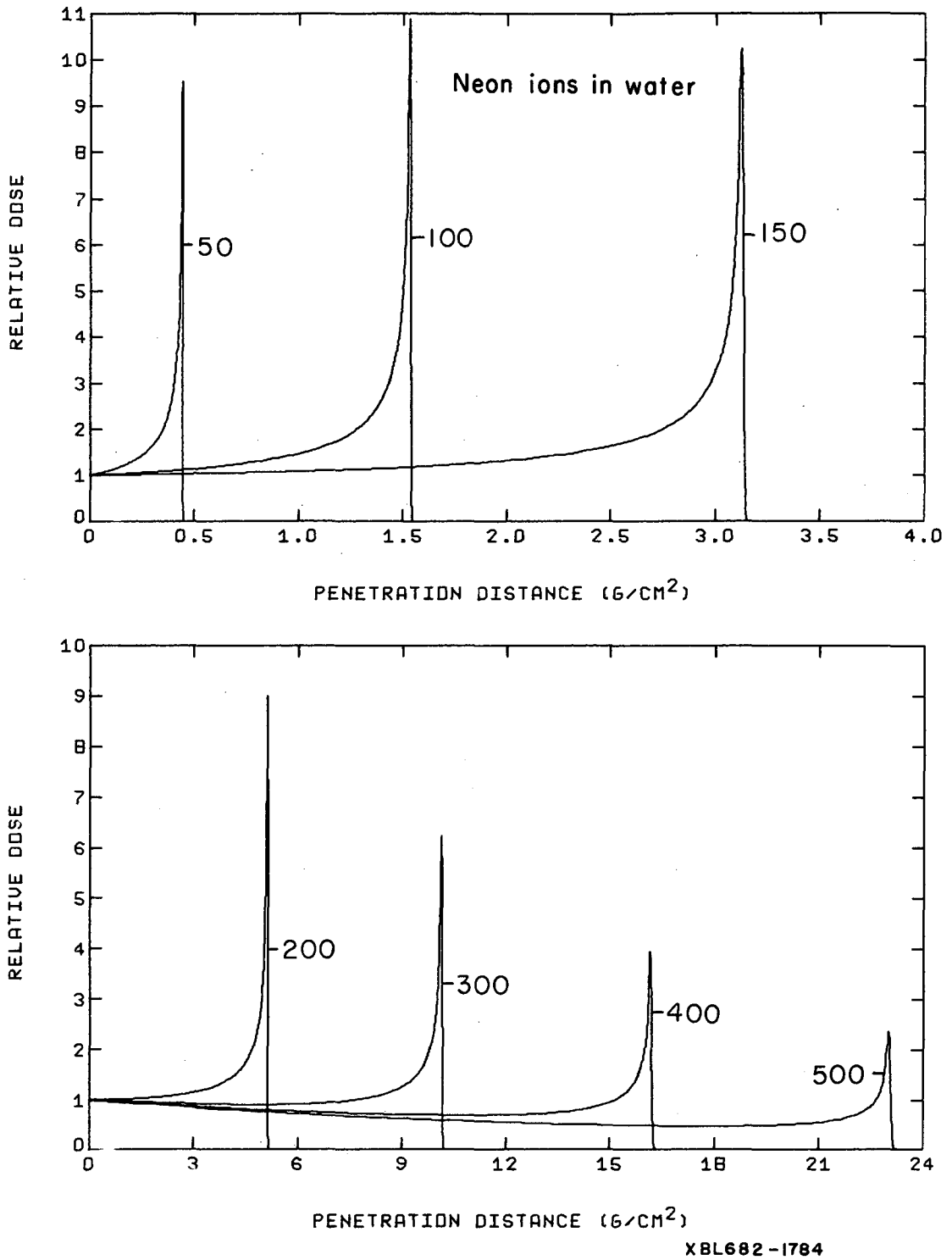

Fig. 11. Bragg curves in water for neon ions with initial energies ranging from 50 to 500 MeV/amu.

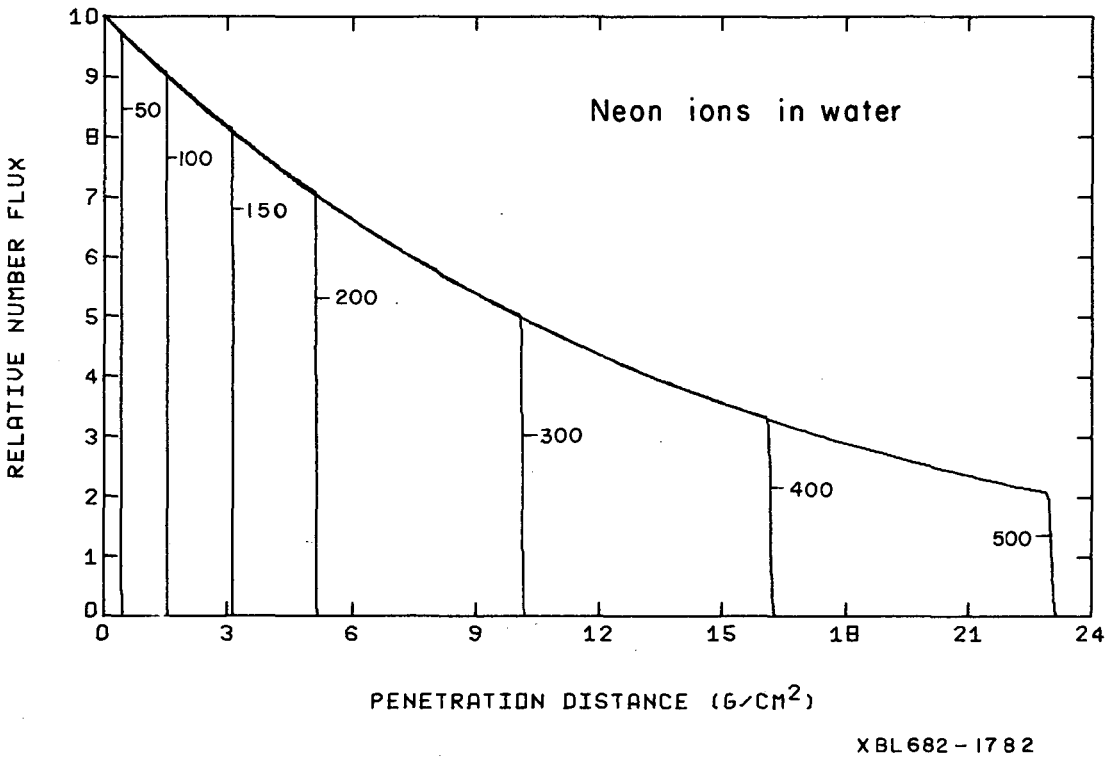

Fig. 12. Flux curves in water for neon ions with initial energies ranging from 50 to 500 MeV/amu.

Table XVI. Variations with initial energy for neon ions incident on water.

Initial energy (MeV/amu)	Mean range (g/cm^2)	p-p dose ratio	Peak width (g/cm^2)	Peak ave. energy (MeV/amu)	Mean beam deflection (g/cm^2)
50	0.445	9.52	0.012	1.54	0.003
100	1.538	10.86	0.032	3.30	0.011
150	3.134	10.23	0.052	5.10	0.022
200	5.143	8.99	0.076	6.76	0.036
300	10.15	6.22	0.135	10.05	0.069
400	16.21	2.35	0.209	13.27	0.107
500	23.08	9.52	0.291	15.89	0.150

through a maximum and then decreases monotonically with increasing energy. The peak width and peak average energy are increasing functions of the initial energy.

C. Consequences of Initial Energy and Angular Spreads

Actually, no beam can be perfectly collimated or monoenergetic. Generally, the energy distribution is approximately Gaussian and has a very narrow width. Also, as a result of many factors, there is a small angular distribution in the particles as they impinge upon the target. It will be shown that even very small widths in the initial energy and angular distributions can have strong influences on the shape of the Bragg and flux curves, and on the energy spectra.

We consider the case of protons and neon ions incident on water targets, with the Bragg peaks at 5 g/cm^2, and study the effects due to changes in the initial energy distribution. Figures 13, 14, and 15 show the Bragg, flux, and spectral curves for protons incident on water, for various values of the standard deviation in the initial energy distribution. Table XVII gives the peak-to-plateau dose ratio, the peak width, and the average energy

Table XVII. Variation with initial energy spread for protons in water with the Bragg peak at 5.0 g/cm^2 (initial energy = 79.75 MeV/amu).

Initial energy standard deviation (MeV/amu)	p-p dose ratio	Peak width (g/cm^2)	Peak average energy (MeV/amu)
0	6.54	0.338	7.23
0.25	6.23	0.377	7.70
0.50	5.62	0.475	8.76

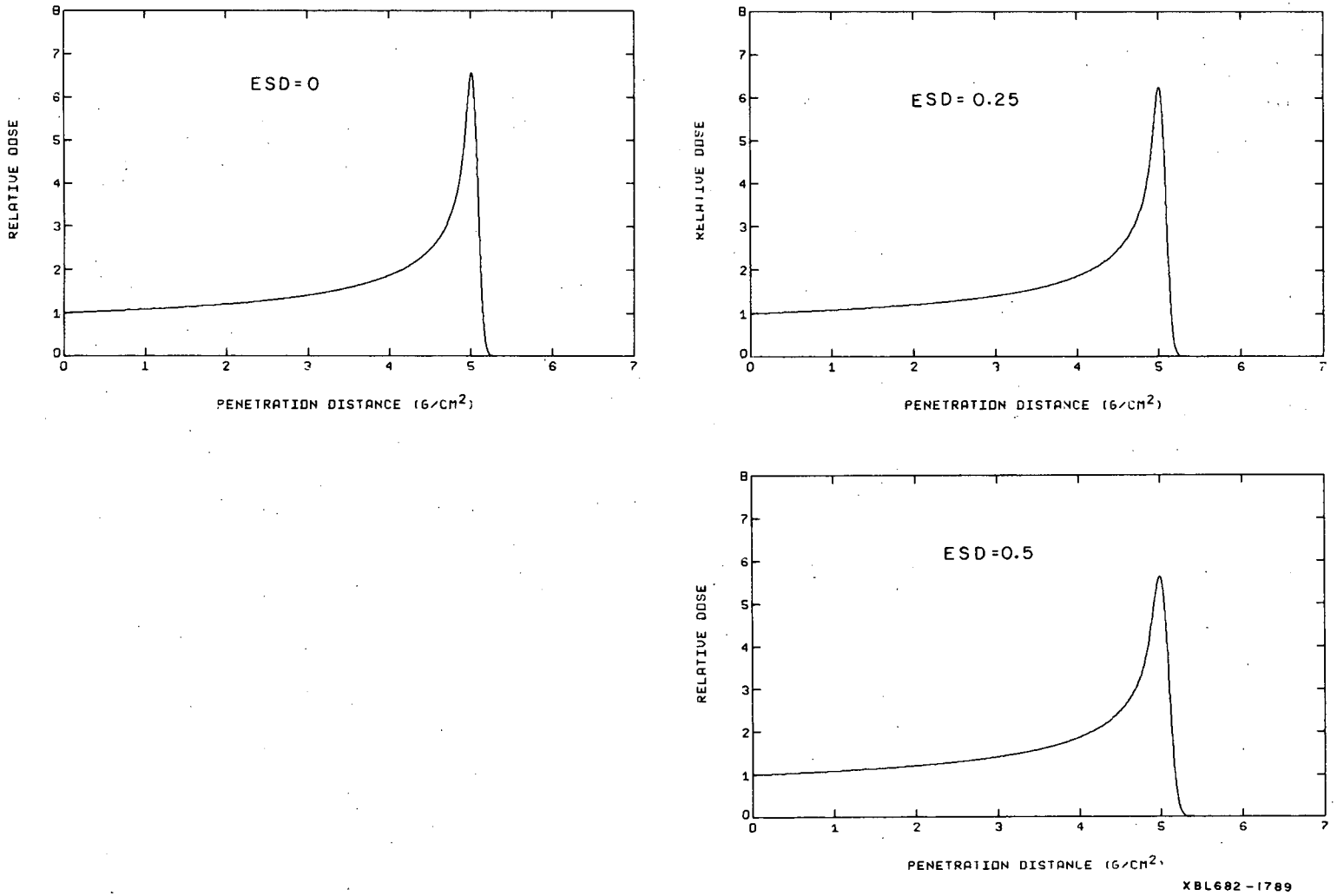

Fig. 13. Bragg curves for protons with a 5 g/cm^2 range in water, for various values of the standard deviation in the initial energy spread.

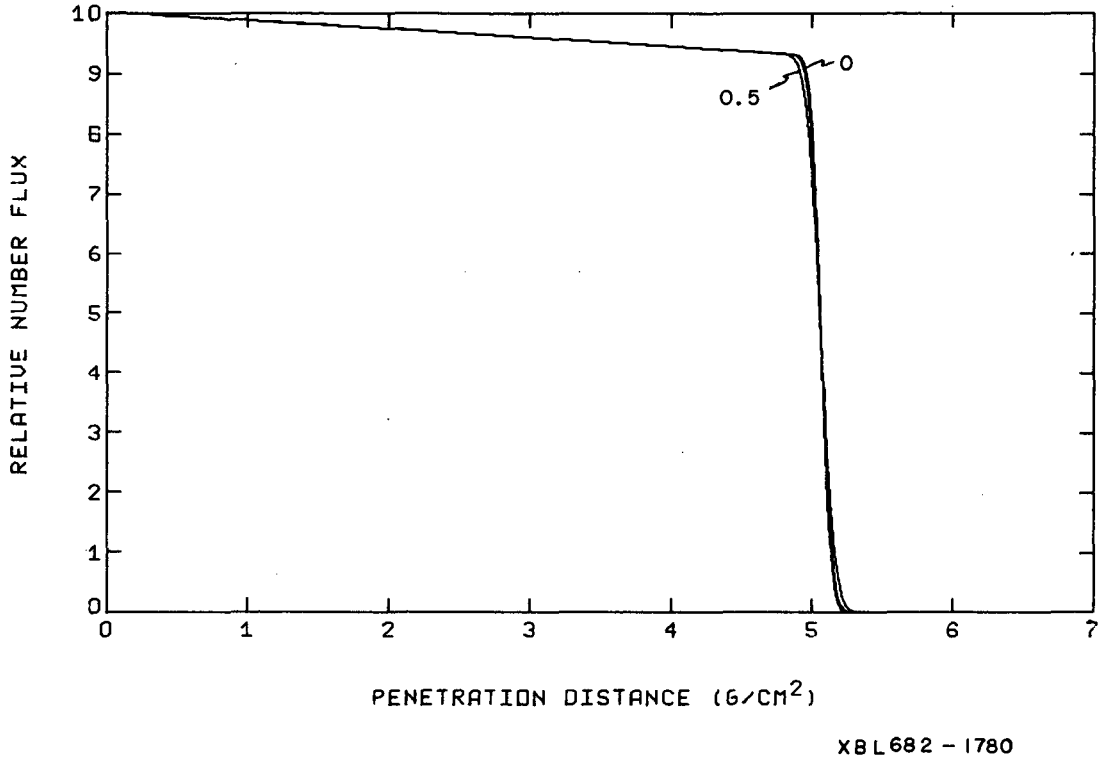

Fig. 14. Flux curves for protons with a 5 g/cm^2 range in water, for various values of the standard deviation in the initial energy spread.

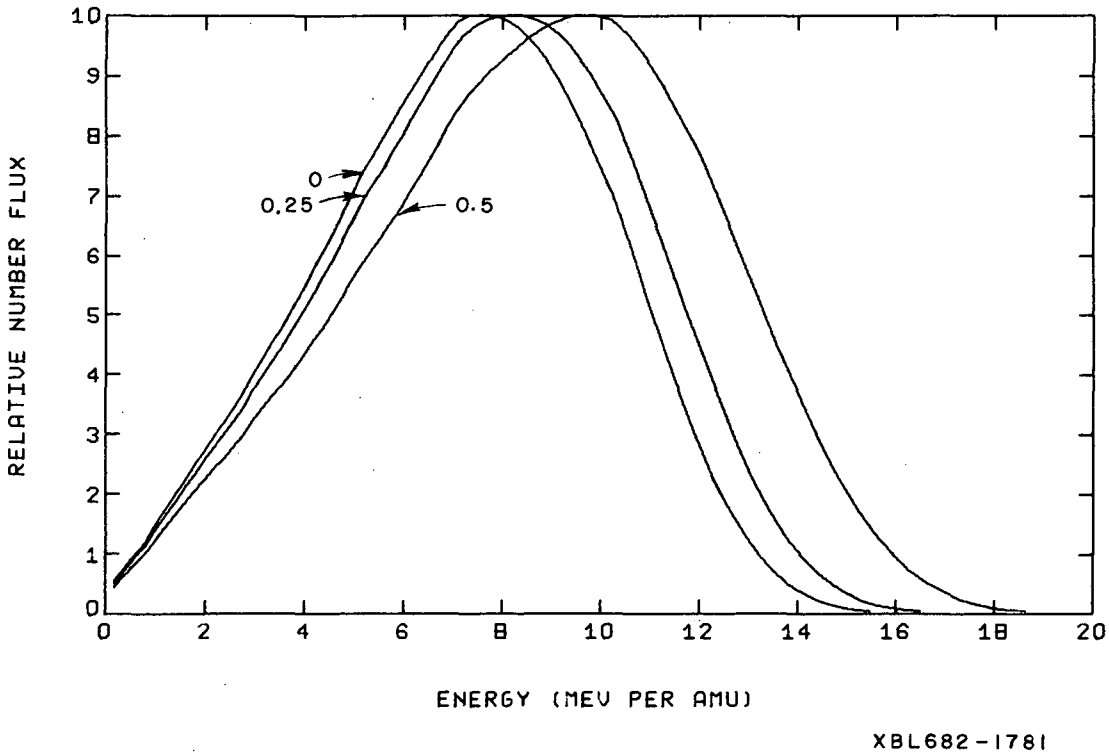

Fig. 15. Spectra at the Bragg peak for protons with a 5 g/cm^2 range in water, for various values of the standard deviation in the initial energy spread.

at the peak for different values of the standard deviation. Figures 16 and 17 and Table XVIII show similar results for neon ions incident on water.

Table XVIII. Variations with initial energy spread for neon ions in water with the Bragg peak at 5.0 g/cm^2 (initial energy = 197.2 MeV/amu).

Initial energy standard deviation (MeV/amu)	p-p dose ratio	Peak width (g/cm^2)	Peak average energy (MeV/amu)
0	9.09	0.075	6.70
0.25	8.00	0.099	5.00
0.50	6.66	0.149	10.55

In general, these results show that a value for the standard deviation of less than 1 percent of the mean initial energy can alter the Bragg and spectral curves significantly. Consider the neon case as an example. An initial standard deviation of 0.5 MeV per amu, or approximately 0.25 percent of the initial energy, produces a change in the peak-to-plateau ratio of approximately 25 percent, a change in the average energy at the peak of approximately 35 percent, and a change in the peak width of nearly 100 percent. Interestingly enough, there is very little effect on the shape of the flux curve for the given changes in the standard deviation.

The degree to which an initial angular spread of the beam particles influences the physical process is dependent in part on the initial size of the beam. This comes about in the following manner. It was shown in Section III-C-4-a that the degree of radial spreading is dependent on the initial mean angle of the beam particles (see Eq. 63). In Section III-C-4-b an estimate was made of the effects due to the beam spreading. Thus, the initial angular distribution leads to an increase in the effective beam attenuation due to the divergence of the beam.

Whether or not this effect is significant depends on the initial beam size relative to the degree of beam spreading. Thus, if the amount of beam spread is much less than the initial beam radius, then the effective attenuation is unimportant. On the other hand, even if the degree of spreading is comparable to, or greater than, the initial beam diameter, the effect on the experimental measurements is small if the detector has a sensitive area radius much larger than that of the beam at the end of the beam range -- that is, if the detector is large enough to detect even

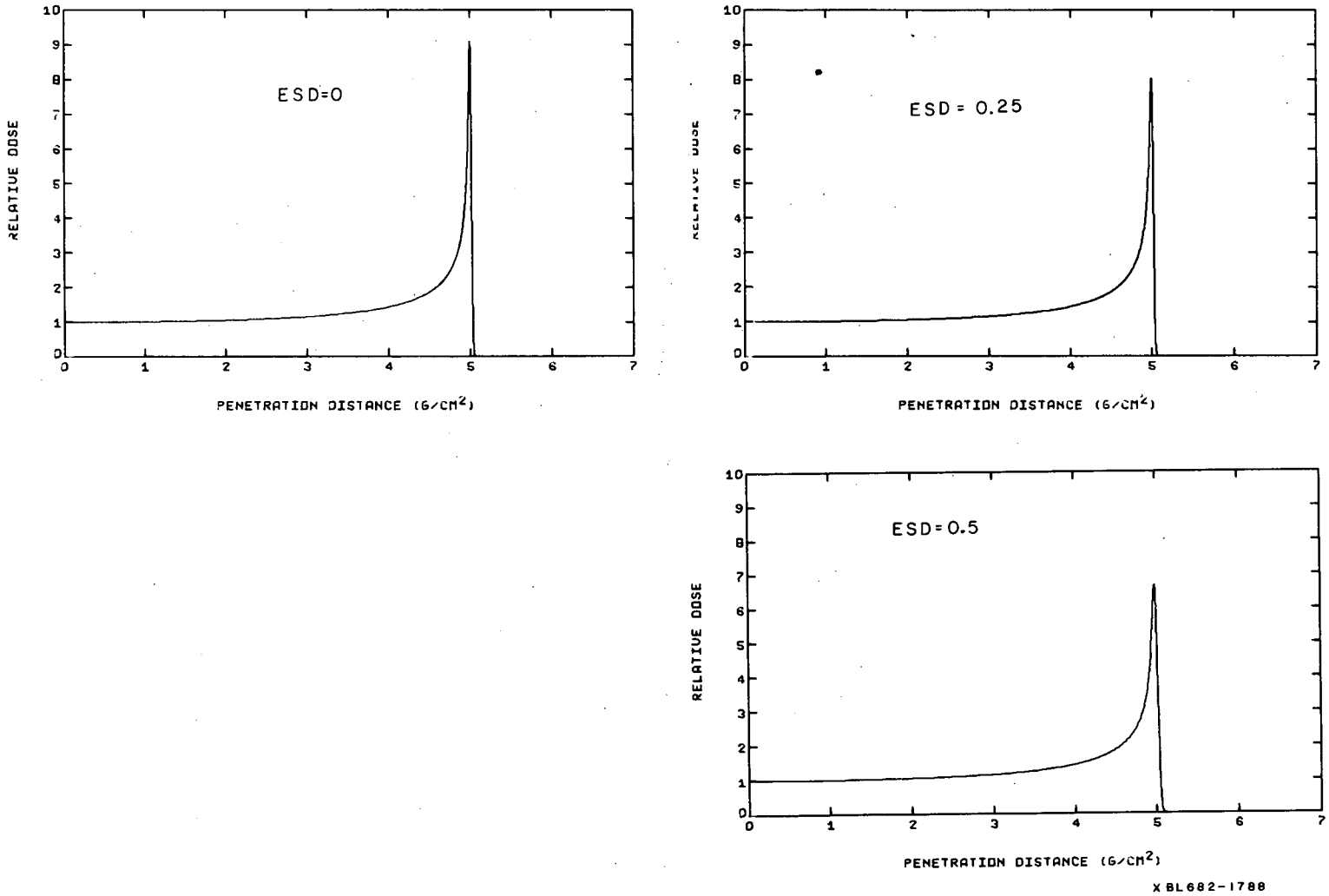

Fig. 16. Bragg curves for neon ions with a 5 g/cm^2 range in water, for various values of the standard deviation in the initial energy spread

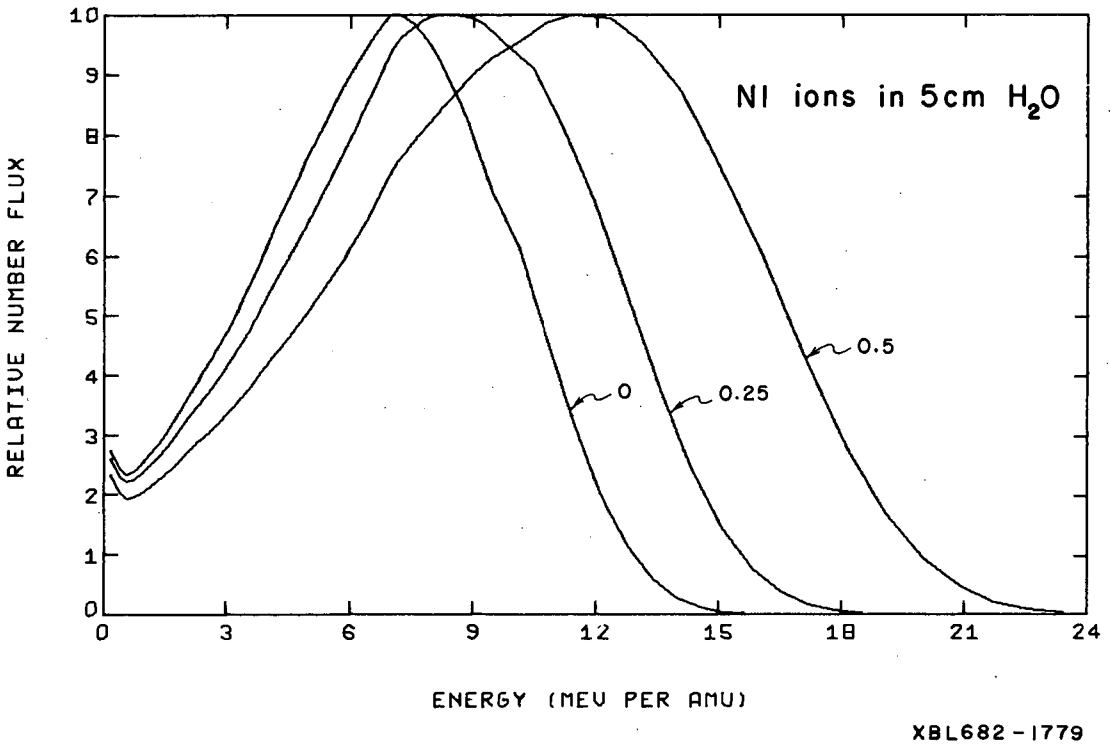

Fig. 17. Spectra at the Bragg peak for neon ions with a 5 g/cm^2 range in water, for various values of the standard deviation in the initial energy spread.

those particles that have traveled large radial distances.

To illustrate these aspects, the case of neon ions incident on water targets is used. As before, the Bragg peak is taken to be at 5 g/cm^2. Table XIX shows the variation of the peak-to-plateau dose ratio and the peak width with the standard deviation of the initial angular spread for various beam diameters. Figure 18 shows the calculated Bragg curves as functions of the standard deviation and beam diameter. Note that these results refer

Table XIX. Effects due to the initial beam size and the initial angular spread for neon ions in water with the Bragg peak at 5 g/cm^2.

Initial beam diameter (cm)	Initial angular standard deviation (deg)	Mean beam deflection (g/cm^2)	p-p dose ratio	Bragg peak width (g/cm^2)
∞	0.0	0.035	9.09	0.075
∞	0.5	0.056	9.09	0.075
∞	1.0	0.094	9.08	0.075
∞	2.0	0.178	8.95	0.078
1.0	0.0	0.035	7.95	0.076
1.0	0.5	0.056	7.36	0.076
1.0	1.0	0.094	6.43	0.076
1.0	2.0	0.178	4.87	0.079
0.5	0.0	0.035	7.01	0.076
0.5	0.5	0.056	6.08	0.076
0.5	1.0	0.094	4.80	0.077
0.5	2.0	0.178	3.06	0.079

to center-to-line measurements only. As expected, the smaller the beam diameter, the greater effect a given initial standard deviation has on the dose ratio. The effects can be extremely large, as illustrated by the results for a beam of 0.5 cm diameter. For an angular spread with a standard deviation of 1 deg, the peak-to-plateau ratio is 32 percent less than with no angular spread!

D. Comparison with Experimental Results

Several sets of experimental results are available, from which it is possible to make comparisons with the theoretical shapes of the Bragg, flux, and spectral curves. In making these comparisons, several points should be borne in mind. First, for sufficiently high-energy particles, nuclear interactions become important and a variety of secondary particles may be

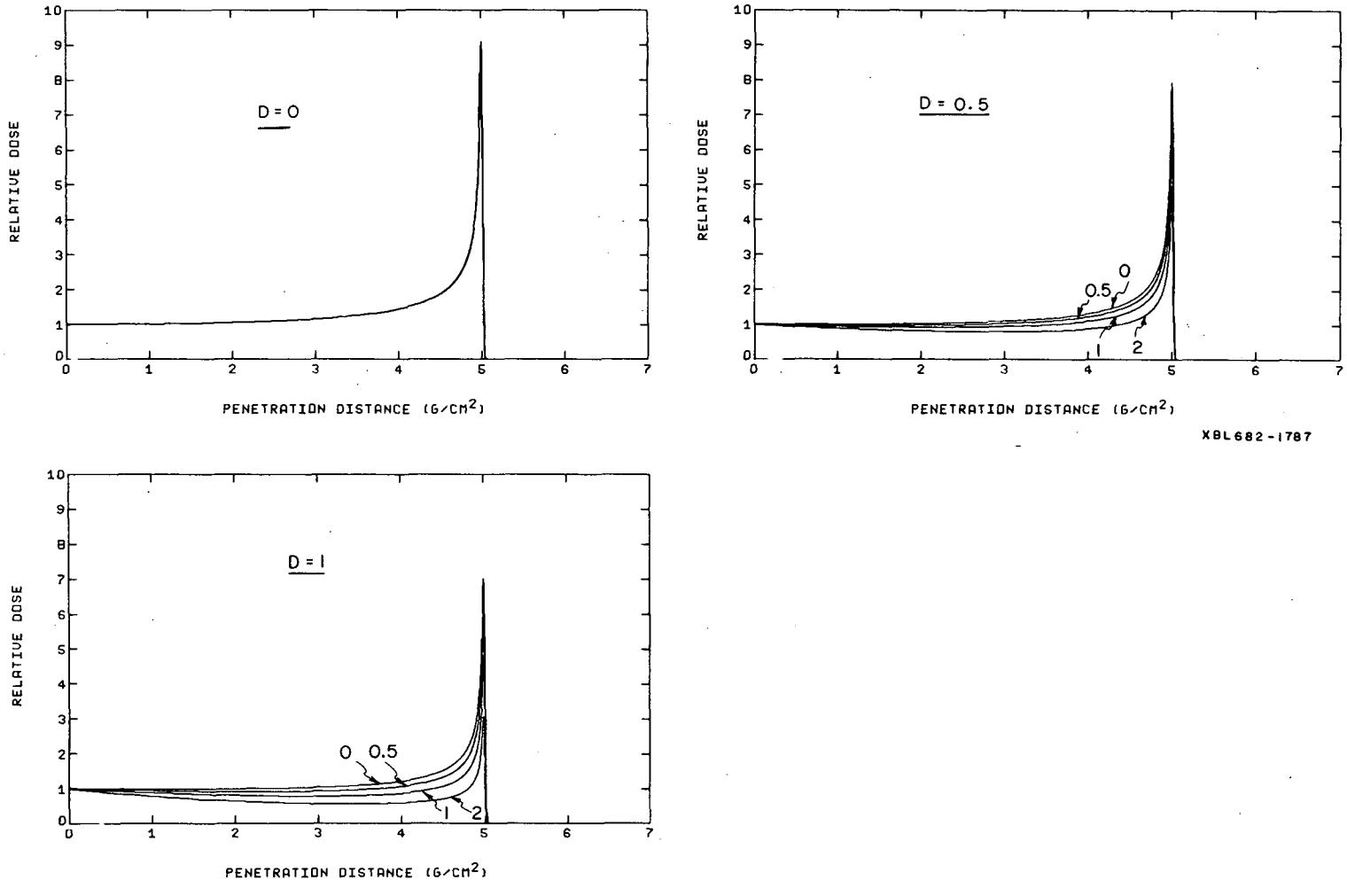

Fig. 18. Bragg curves for neon ions with a 5 g/cm^2 range in water, for various values of the initial beam diameter (D), and for

produced. In these cases, one would expect to note differences between the theoretical and experimental results. Since the great majority of secondaries would be expected to be generated towards the incident surface, with relatively few being produced near the vicinity of the Bragg peak, the theoretical curve shapes in this region should be reasonably accurate.

One uncertainty in making comparisons between experiment and theory arises because in most experimental arrangements, it is very difficult to estimate the degree of angular and energy spread of the ion beam incident on a target; it was shown earlier that these initial distributions can strongly affect the measured curves.

The effects due to the initial angular spread can usually be nearly eliminated by using a large enough beam or by utilizing a detector with sufficiently large diameter, or by a combination of both. These also eliminate the effective attenuation due to the inherent beam spreading from multiple scattering.

On the other hand, the effects resulting from a finite width in the initial energy distribution cannot be eliminated, and they are present in the measured data. Usually, however, a reasonable estimate can be made of the upper limit on the degree of energy spreading. Consequently, the theoretical results that would be obtained if the exact initial energy spread were known can be bracketed.

In addition to the uncertainty in the initial energy spread, the mean energy of the beam is known only to within a certain accuracy. Furthermore, the beam generally passes through one or more thin slabs of various materials prior to entering the main target. These slabs are associated with miscellaneous pieces of experimental apparatus such as counters, collimator edges, etc., and they degrade the beam energy somewhat. In general, the degree of energy degradation is small, but it does enhance somewhat the uncertainty in the initial energy of the ions incident on the target.

It is sometimes necessary, then, to vary the assumed initial energy and energy spread until the best comparison is found. The optimum values have all been found to be well within the experimental uncertainties.

It should also be mentioned that none of the experimental results cited was obtained with the intention of making comparisons with theoretical calculations. Consequently, various details, such as beam diameter, are in

some cases known only approximately, hence leading to uncertainties that can be difficult to estimate.

1. 47-MeV Protons in Water

Raju and Welch[50] have measured the Bragg curve in water from protons generated by the 88-inch cyclotron at the Lawrence Radiation Laboratory. The nominal energy of these protons was 47 MeV, and this value is believed to be accurate to within 1 percent. However before entering the water absorber, the beam passed through various materials, such as detector faces, etc., which degraded the proton energy somewhat; consequently, the energy of the particles at the water face is not precisely known.

The beam diameter was estimated to be 0.5 in., or approximately 1.25 cm, and the detector used to measure the dose distribution was a semiconductor diode with a sensitive volume diameter of less than a millimeter. An upper limit on the standard deviation in the initial energy spread was estimated to be on the order of 0.5 MeV.

By using an assumed initial energy of 43 MeV and an assumed standard deviation in the initial spread of 0.2 MeV, or approximately one-half the estimated upper limit, the Bragg curve is calculated. Included in these calculations is the effective attenuation due to beam spreading. Effects due to initial angular spreading of the beam are neglected, since, for this particular case, a small amount of initial divergence would not significantly influence the results. This is illustrated in Table XX, which shows

Table XX. Effect of initial beam angular divergence for 47-MeV protons in water.

Initial angular standard deviation (deg)	Effective attenuation factor due to beam spreading
0	0.81
0.5	0.81
1.0	0.80
2.0	0.79

that even for an initial standard deviation of 1 deg, there is very little decrease in the effective attenuation factor from beam spreading. The resultant curve is given in Fig. 19, along with the experimental points. The results are in excellent agreement.

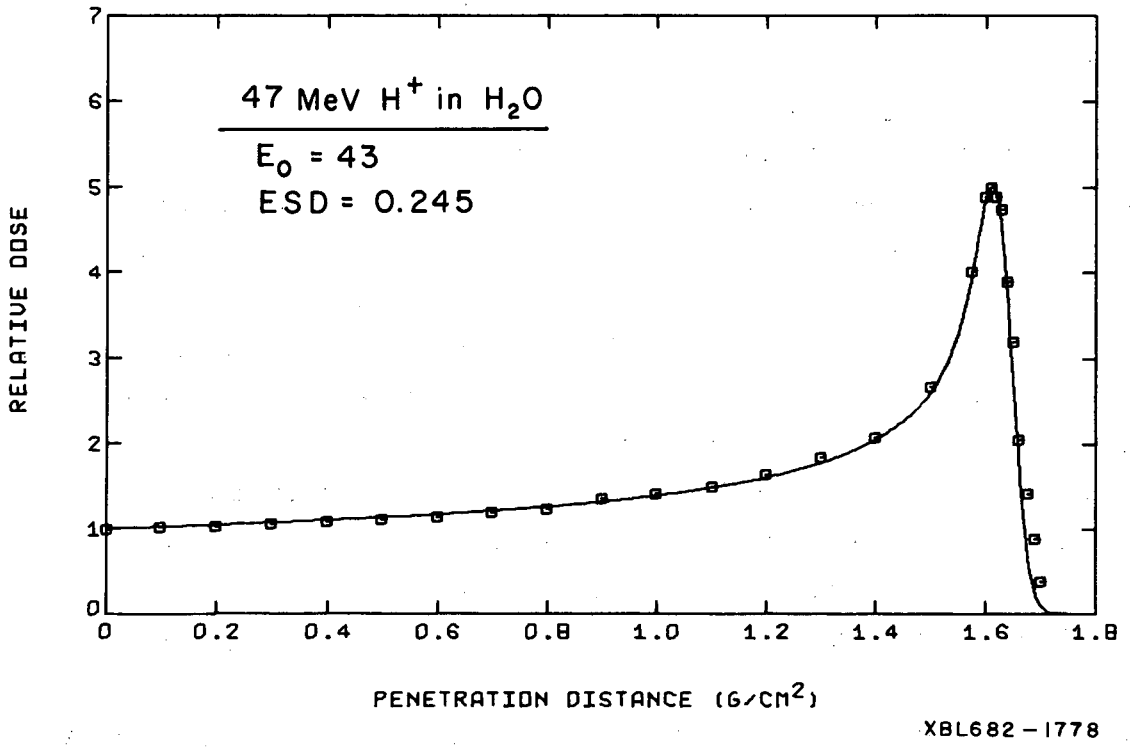

Fig. 19. Experimental and theoretical Bragg curves 47-MeV protons incident on a water absorber.

2. 49-MeV Protons in Aluminum

Raju has also measured the energy spectrum, at the Bragg peak, of protons in aluminum.[51] These particles were produced by the 88-inch cyclotron at the Lawrence Radiation Laboratory, and had an energy of 49 MeV. As indicated earlier, the standard deviation of the initial energy spread is presumably less than 0.5 MeV.

The peak spectrum was calculated for values of the initial energy spread SD of 0 and 0.25 MeV. The peak energies coincide for an assumed initial energy of 48 MeV. The results are shown in Fig. 20 along with the experimental points. The two calculated curves bracket that measured, so that in this case the theory agrees extremely well with the experimental results. As before, the exact energy of the incident protons is not known.

3. Heavy-Ion Beams

Measurement of the heavy-ion beams reported here were done at the Hilac, utilizing the experimental equipment used for investigating the biological effects of heavy charged particles.[52] After the beam has been accelerated to its final energy it passes through an analyzer magnet and is bent 18 degrees relative to its original direction to ensure homogeneity of particle momenta. Next the beam passes through a 1.7-mg/cm^2-thick aluminum foil, which is used as a beam monitor. The beam is then collimated, and passes into a bombardment chamber which contains a set of remotely operated aluminum degrading foils. The back wall of the bombardment chamber can be removed so that different radiation detectors may be placed behind the aluminum degrading foils. The monitor foil is electrically insulated so that with an electrometer the net loss of charge due to secondary electron emission can be measured. With a transmission ionization chamber mounted behind the aluminum foils, it is possible to measure the relative ionization of the ionization-chamber gas as a function of the thickness of the degrading foils in the beam path. When the ionization chamber is replaced by a Faraday cup, it is possible to measure the relative beam current as a function of the absorber thickness. The beam current is proportional to the particle flux times the average charge per particle. If a semiconductor detector is placed behind the absorbers, it is possible to measure the energy spectrum after any thickness of absorber. The energy of the emergent beam particles is approximately 10.4 MeV/amu.

Figures 21 through 35 show both the experimental and the corresponding

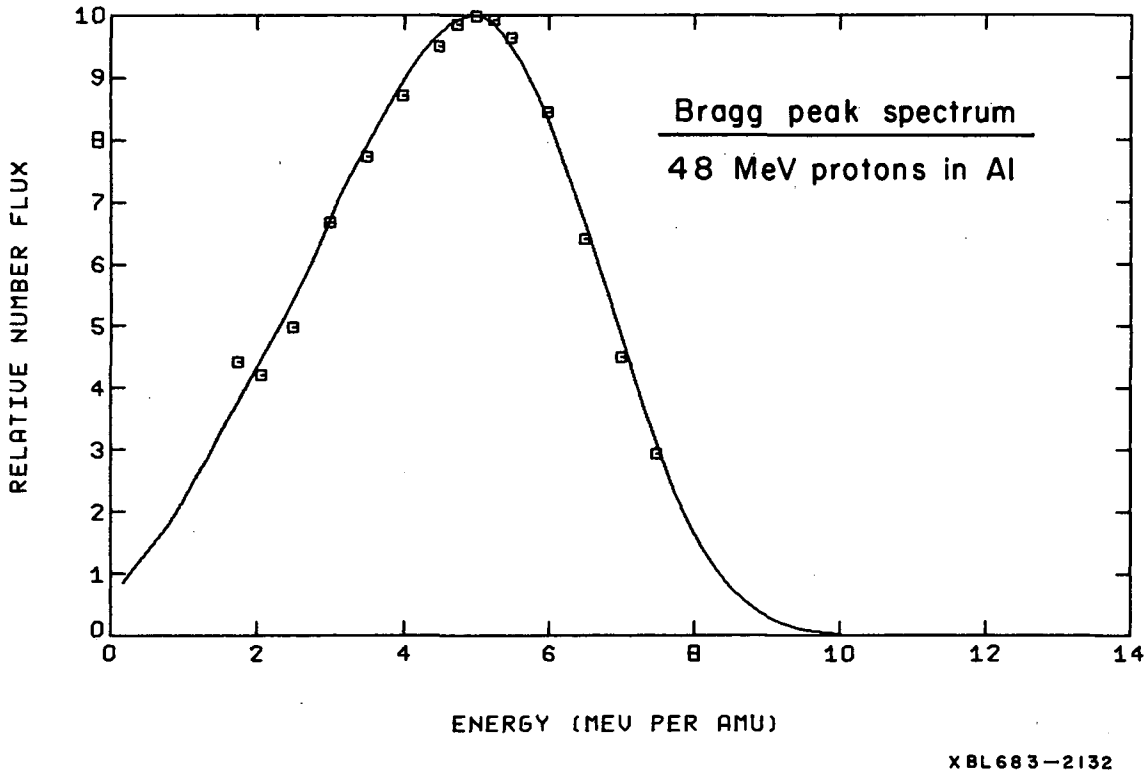

Fig. 20. Experimental and theoretical Bragg peak spectra for 49-MeV protons incident on an aluminum absorber.

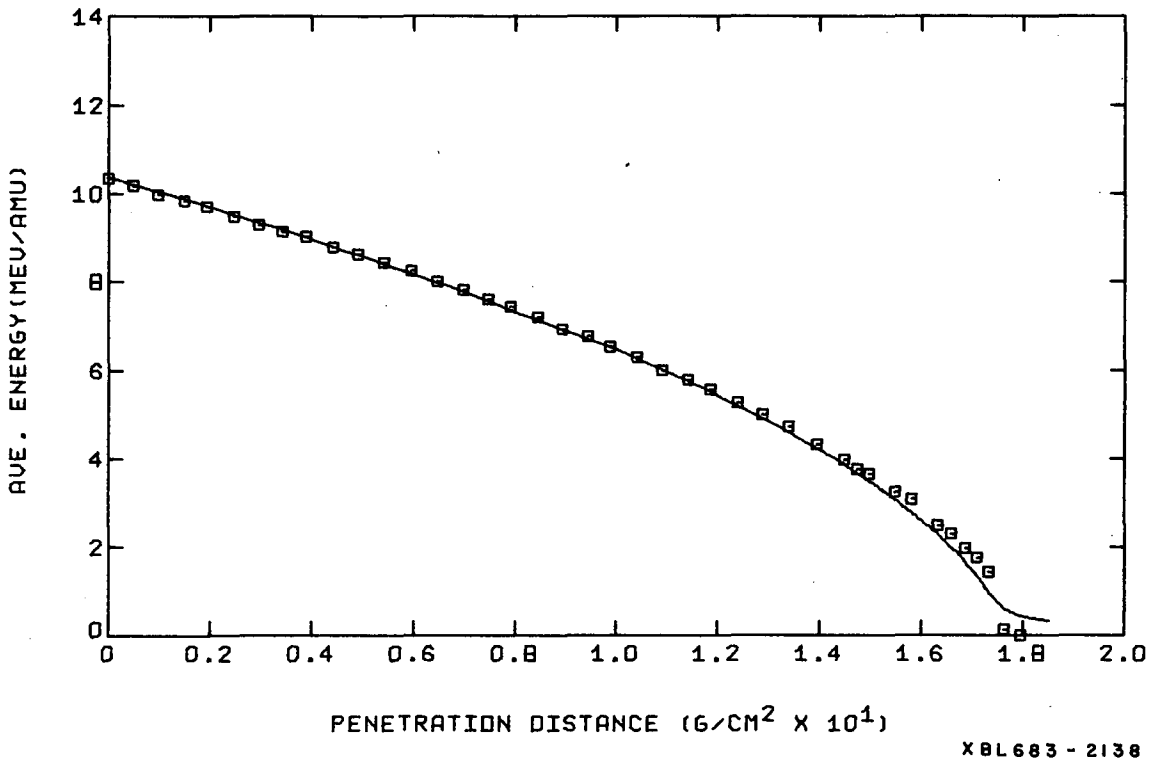

Fig. 21. Average energy versus penetration distance for 10.4-MeV/amu He ions incident on an Al absorber

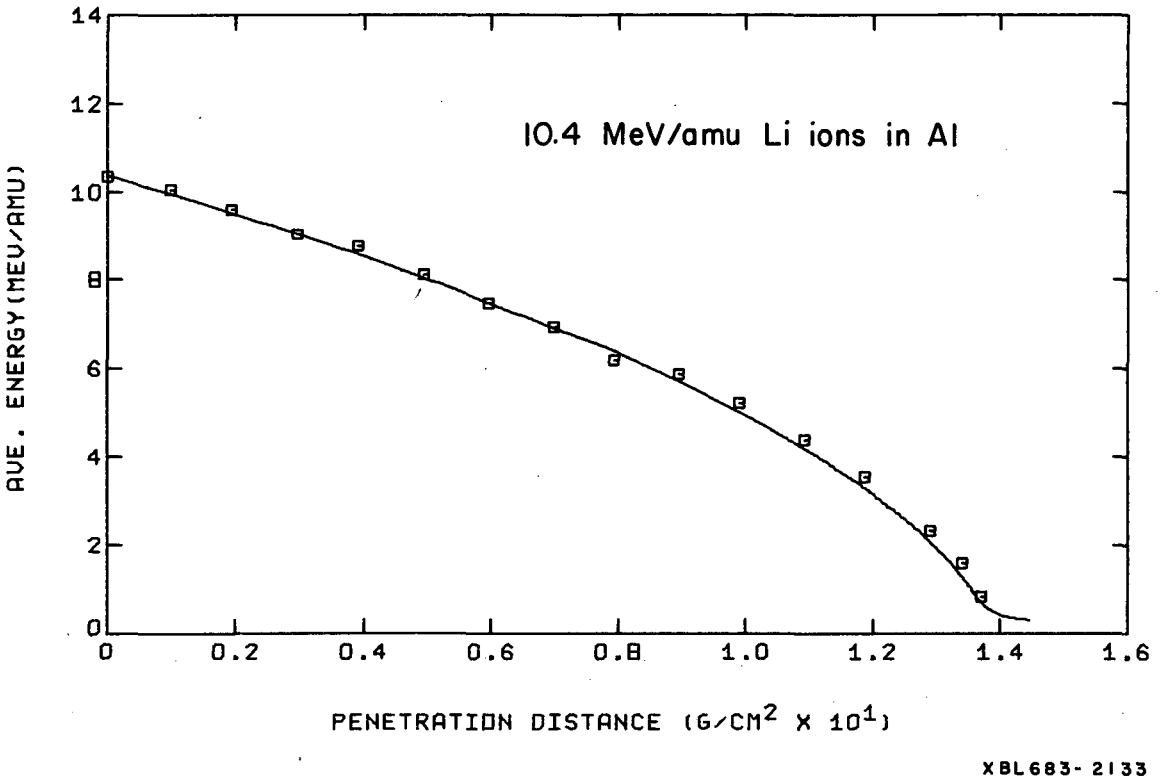

Fig. 22. Average energy versys penetration distance for 10.4-MeV/amu Li ions incident on an Al absorber.

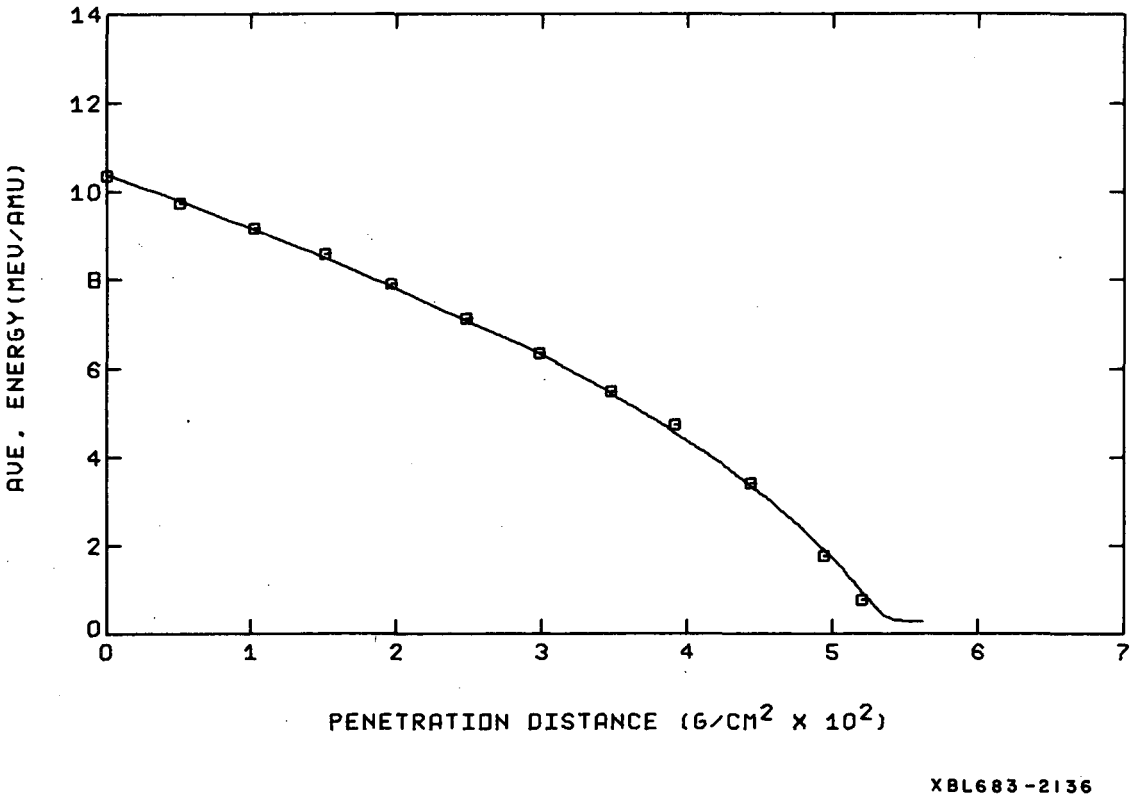

Fig. 23. Average energy versus penetration distance for 10.4-MeV/amu B ions incident on an Al absorber.

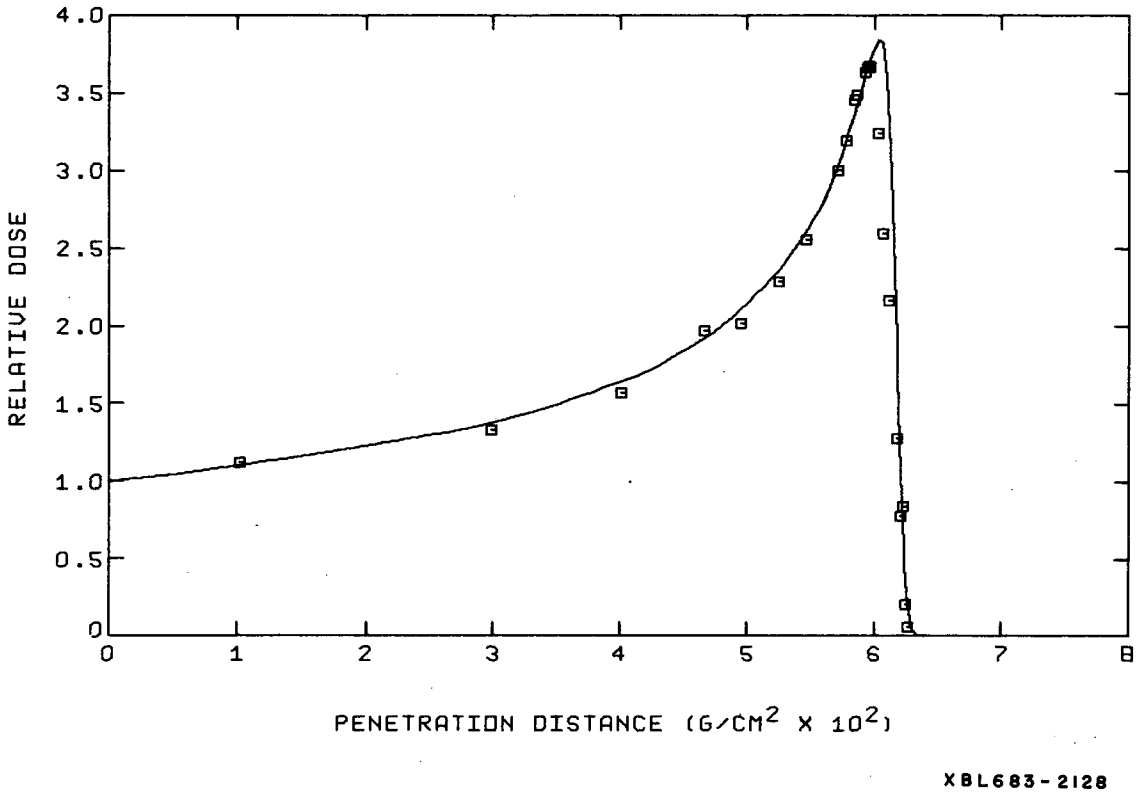

Fig. 24. Bragg curve for 10.4-MeV/amu C ions incident on an Al absorber.

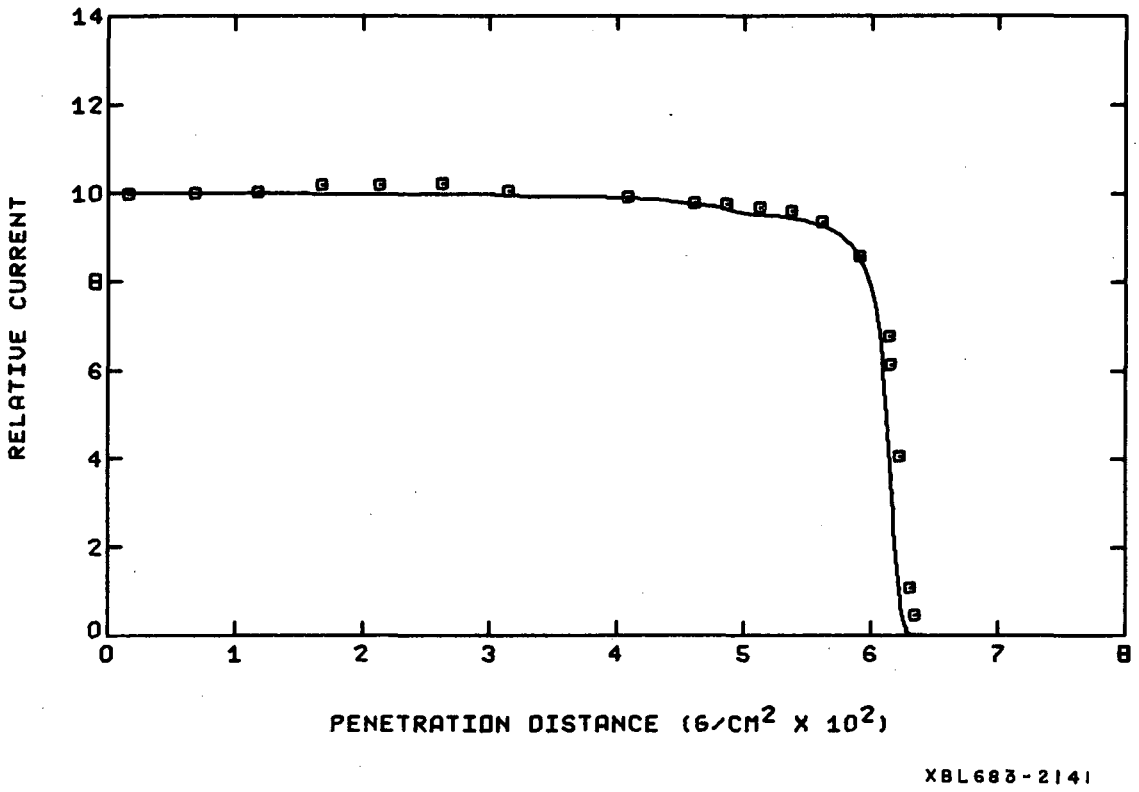

Fig. 25. Relative current versus penetration distance for 10.4-MeV/amu C ions incident on an Al absorber.

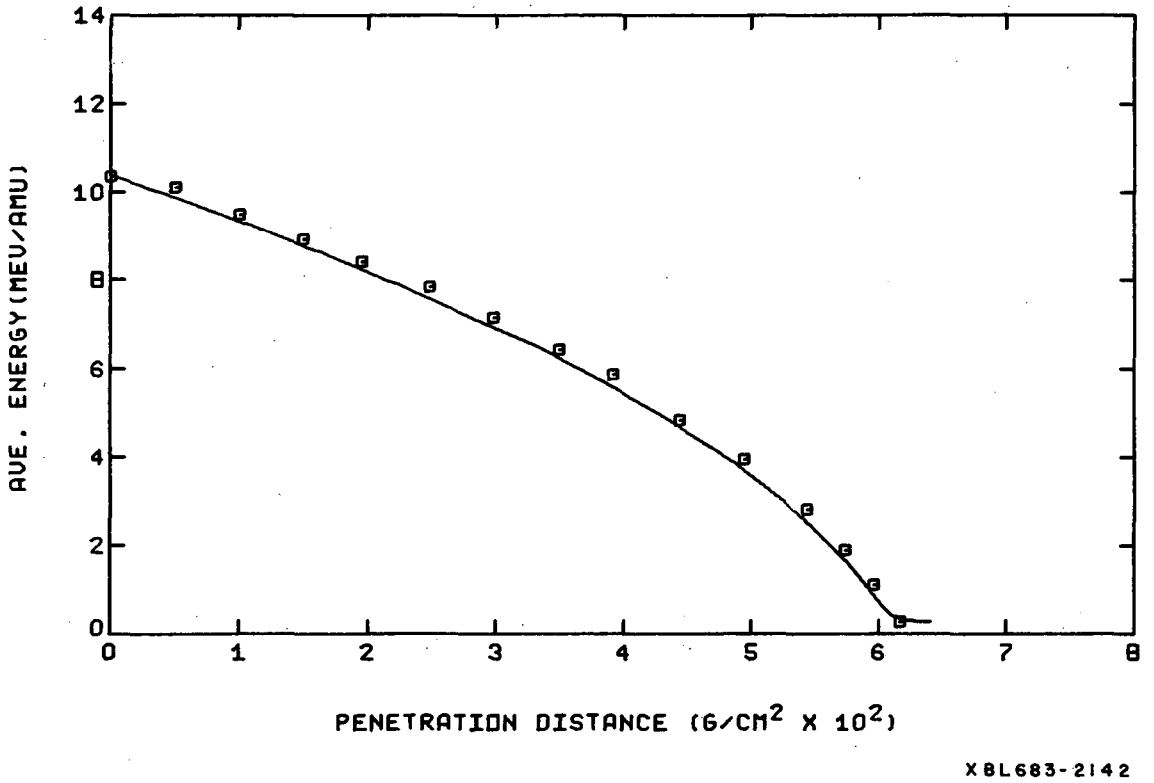

Fig. 26. Average energy versus penetration distance for 10.4-MeV/amu C ions incident on an Al absorber.

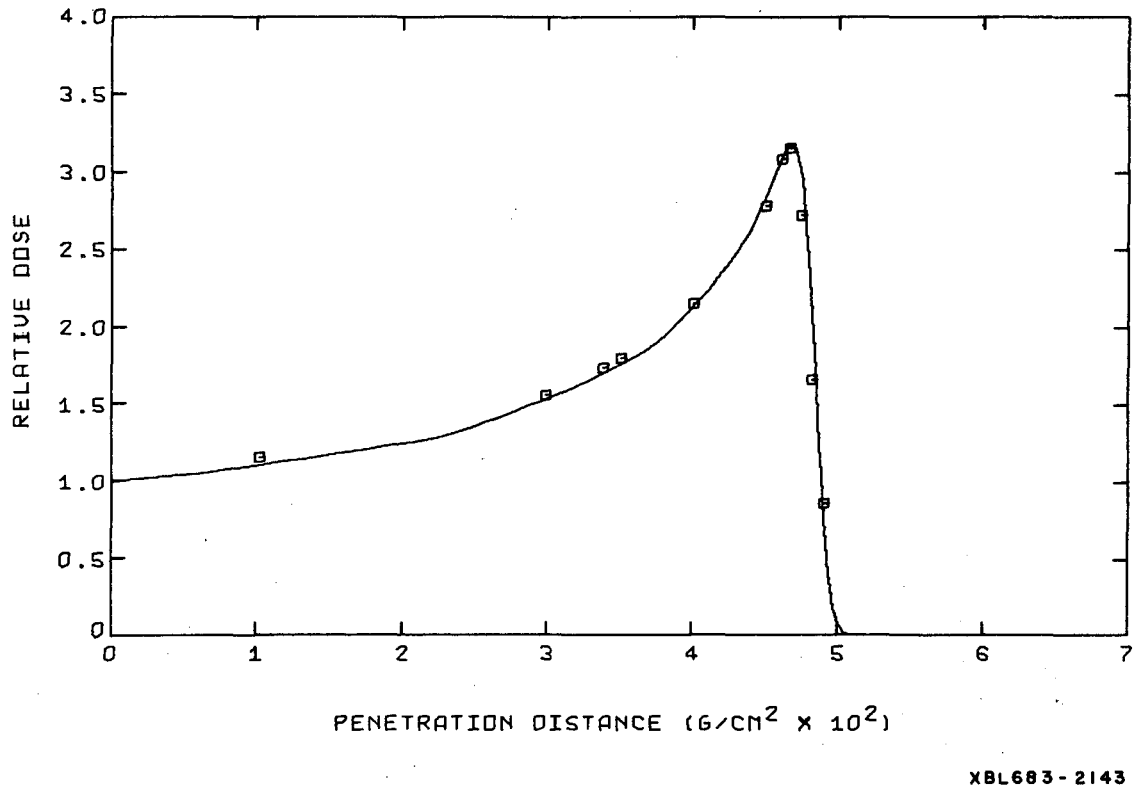

Fig. 27. Bragg curve for 10.4-MeV/amu O ions incident on an Al absorber.

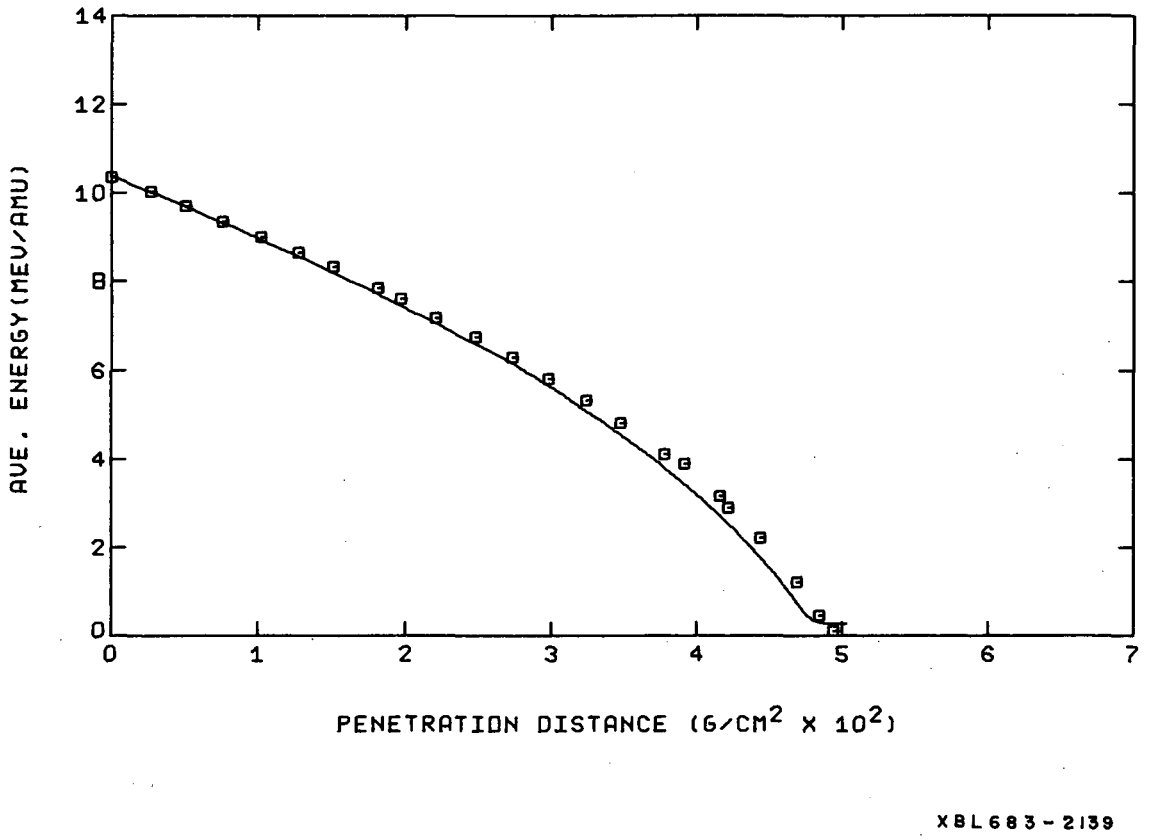

Fig. 28. Average energy versus penetration distance for 10.4-MeV/amu O ions incident on an Al absorber.

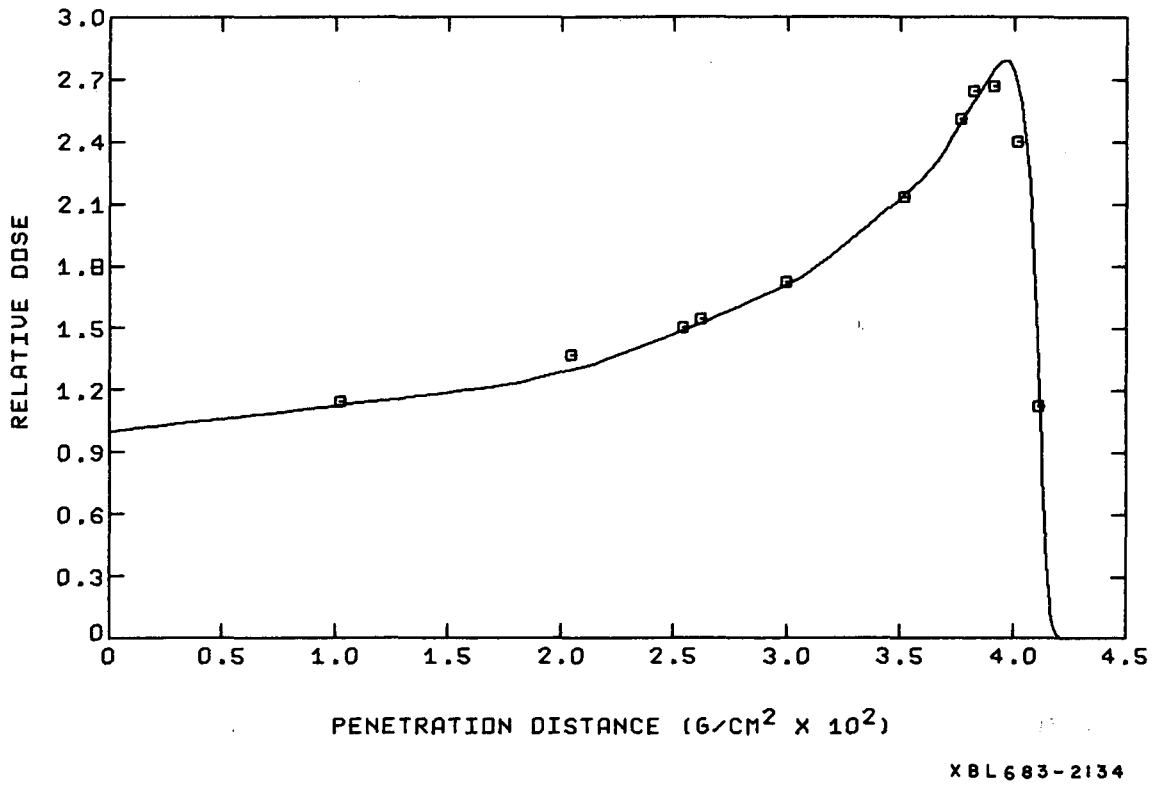

Fig. 29. Bragg curve for 10.4-MeV/amu Ne ions incident on an Al absorber.

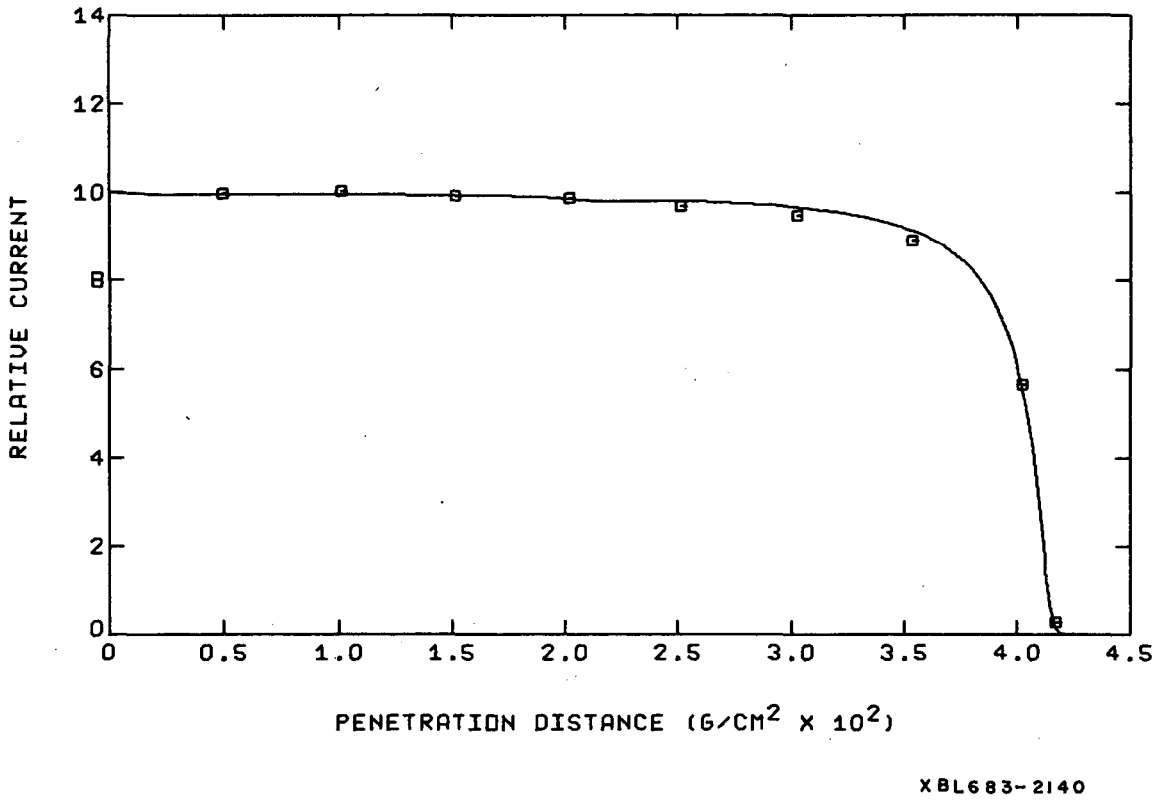

Fig. 30. Relative current versus penetration distance for 10.4-MeV/amu Ne ions incident on an Al absorber.

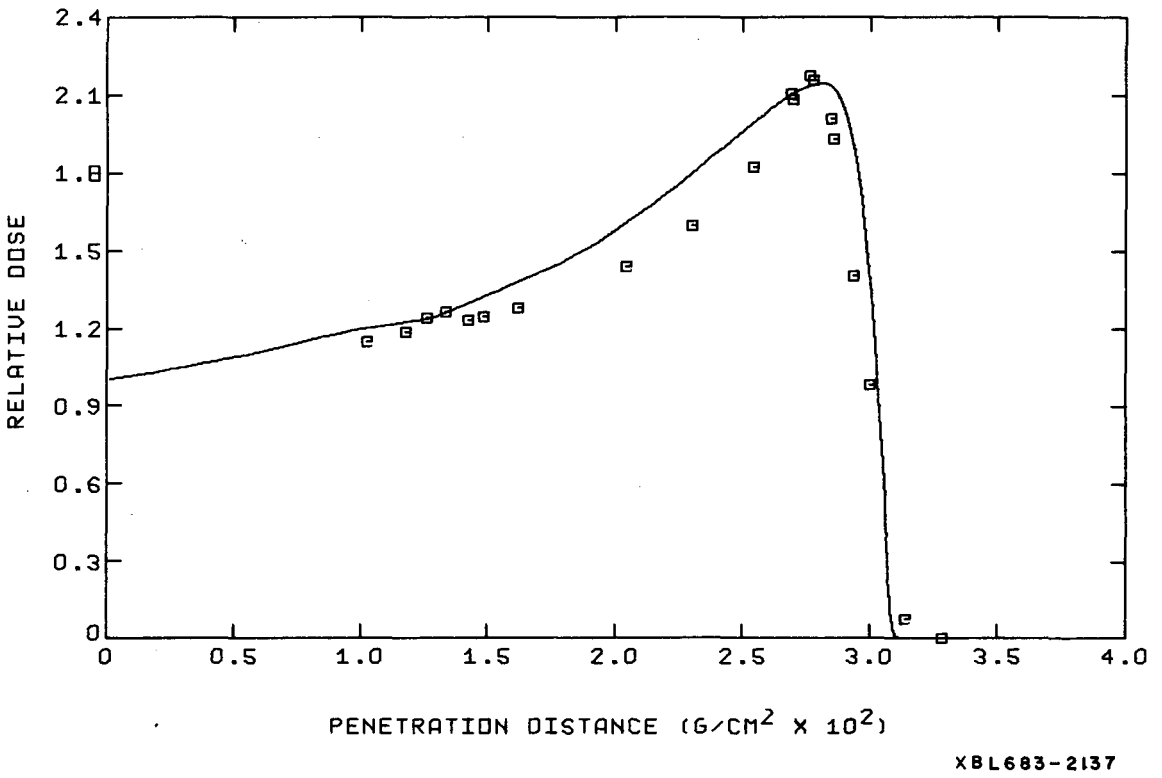

Fig. 31. Bragg curve for 10.4-MeV/amu S ions incident on an Al absorber.

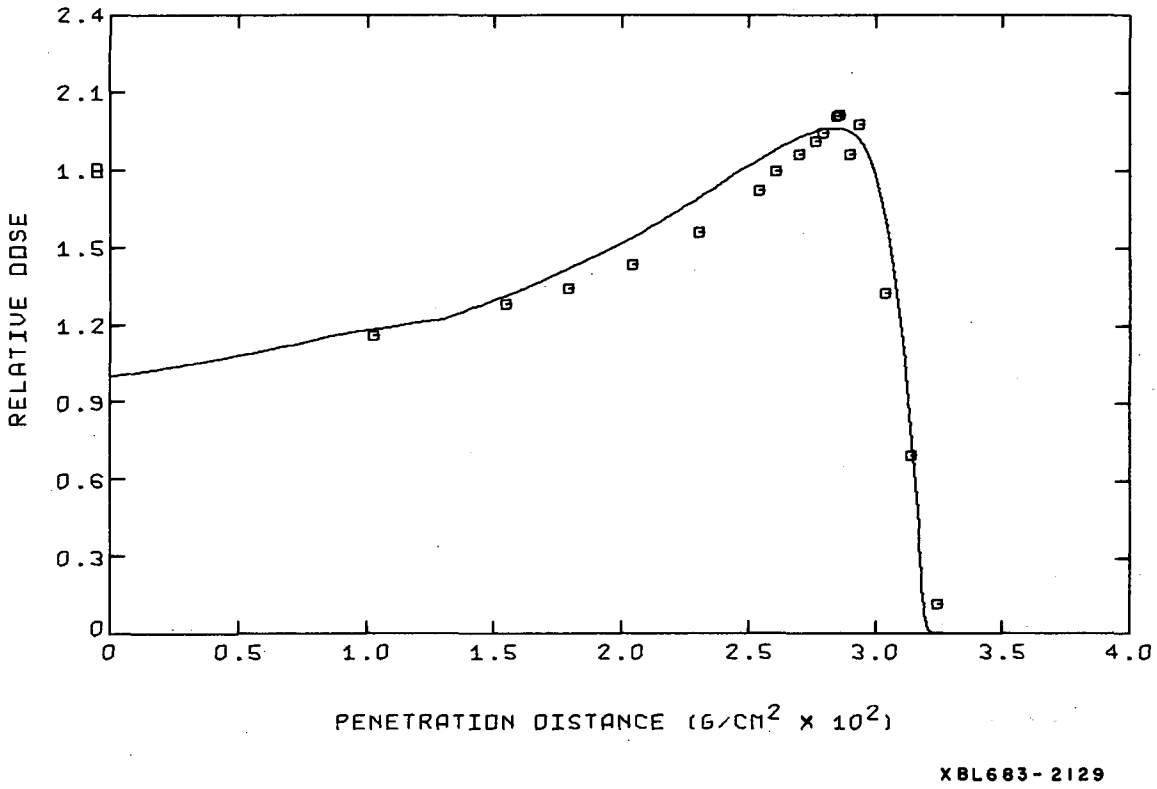

Fig. 32. Bragg curve for 10.4-MeV/amu Al ions incident on an Al absorber.

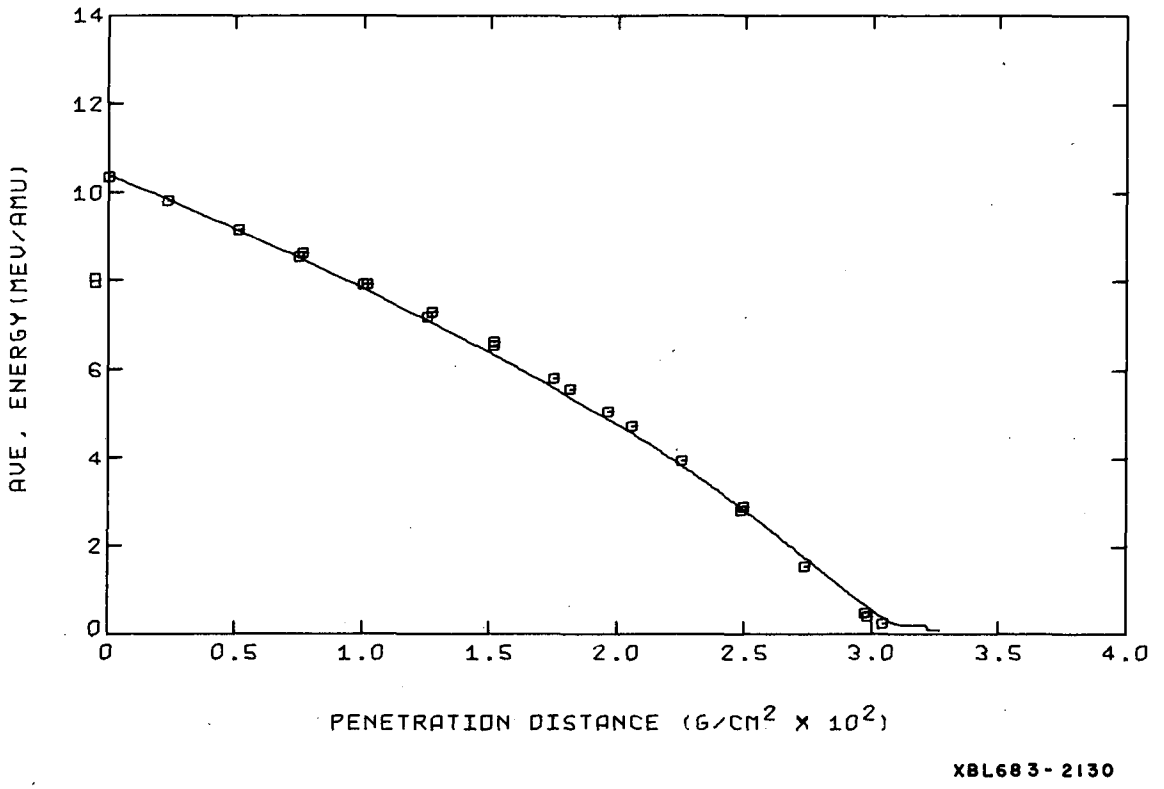

Fig. 33. Average energy versus penetration distance for 10.4-MeV/amu A ions incident on an Al absorber.

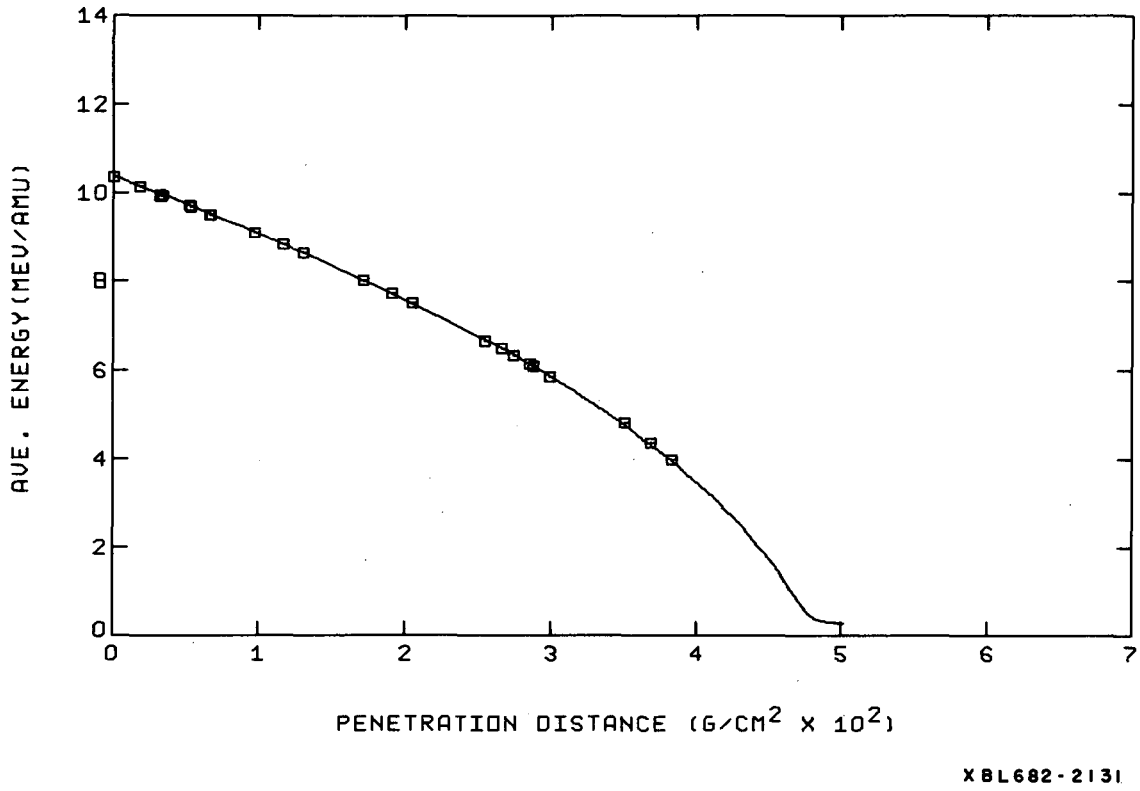

Fig. 34. Average energy versus penetration distance for 10.4-MeV/amu C ions incident on a Mylar absorber.

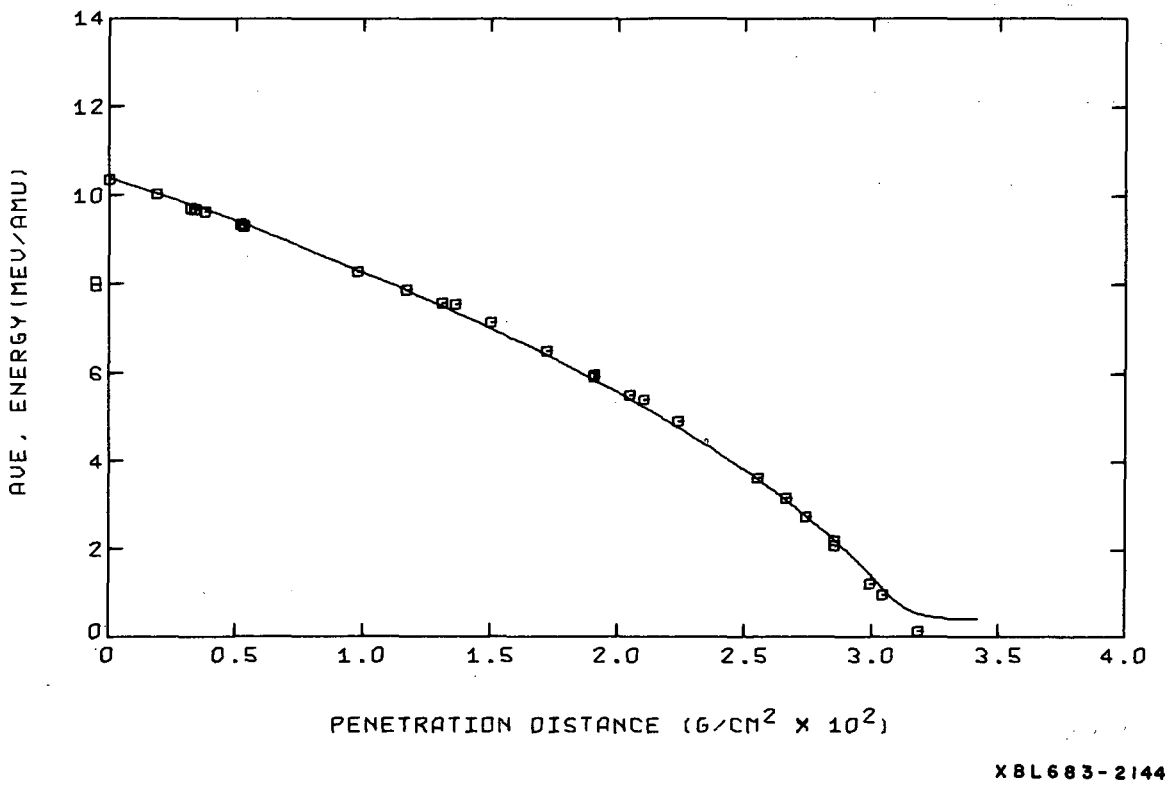

Fig. 35. Average energy versus penetration distance for 10.4-MeV/amu Ne ions incident on a Mylar absorber.

theoretical results for various ions in different absorbers. In general, the agreements are very good, although in certain cases some discrepancies do exist. This is assumed to be the result of the uncertainty in the calculated stopping power in this low-energy region.

V. CONCLUSIONS AND RECOMMENDATIONS

The methods developed here for computing Bragg, flux, and spectral curves are extremely flexible, in that the calculations are done directly in terms of energy-dependent functions for the ionization energy loss and total nuclear-reaction cross section. Thus, the method is directly applicable to any situation in which the important energy-loss processes are ionization and nuclear interactions.

The methods are also more general than previous ones, in that they are able to make corrections for multiple scattering for systems in which the lab and c.m. coordinate systems are not equivalent. Also, effects due to initial angular and energy spreads of the beam have been included in a natural manner.

Calculations have demonstrated that the nature of the initial beam can strongly influence the shapes of the Bragg and flux curves for a given range in a specified material, but the average energy at the Bragg peak is found to be relatively insensitive to the type of ion used.

Within experimental uncertainties, excellent agreement is obtained between experimental Bragg, flux, and peak spectral curves and the corresponding theoretically calculated curves.

The resolving of the uncertainty in some of the experimental data presented here as to the presence or absence of singificant events due to secondary particles would be an important contribution.

In all calculations in this work, it was assumed that the various processes, such as ionization energy loss and multiple scattering, led to distributions that could be represented by Gaussians. In general, this assumption is well founded. However, in certain limiting cases, deviations from Gaussian distributions are significant. For example, at very low energies, plural scattering could cause skewing of the angular distribution of the beam particles. It would therefore be useful to examine the limits within which the assumptions of Gaussian distributions are valid, although for this work there is little doubt as to the validity of these assumptions.

One limitation of this work is in the assumption of a single, homogeneous target medium. An extremely useful extension would be to multiple-slab geometry, allowing more realistic representations of physical systems.

Another basic limitation of these results is that they do not include effects due to secondary particles. Research is being carried on in this

direction, and results including these effects are expected in the near future.

APPENDICES

A. Nomenclature

A_i	Atomic weight of the ith species in the target
A_p	Atomic weight of beam particles
A_t	Atomic weight of target
c	Velocity of light
D	Percentage detour factor
D(s)	Dose at distance s, in MeV/sec-gm
E	Beam particle energy, in MeV/amu
E_o	Initial energy of beam particles, in MeV/amu
$E_{c.m.}$	Total energy in the coordinate system, in MeV
E_{tot}	Total energy of a particle, in MeV
e	Electron charge
$\langle \Delta E_o^2 \rangle$	Variance of initial beam-energy distribution
f	Attenuation factor due to beam spreading
f(E)	Stopping power, in MeV per g/cm^2
K	Binding-effect correction factor
m_e	Electron mass
M_p	Mass of beam particle
$M_o c^2$	Rest energy per amu, $\approx$ 931 MeV
$M(s,\bar{s})$	Path-length distribution function
n_e	Number of electrons per cm^3 in an absorber
N_a	Avogadro's number
N_i	Atomic density of the ith species in the target, in $atoms/cm^3$
$N_e(E)$	Number of particles of energy E
$N_o(E_o)$	Initial particle flux, in $particles/cm^2$-sec
N(s)	Total flux at s, in $particles/cm^2$-sec
N(E,s)	Energy flux at s, in particles per unit energy at E, per cm^2-sec
p	Beam particle momentum
$P(\theta)$	Scattering probability
r_a	Atomic radius
r_e	Classical electron radius
r_n	Radius of nucleus
r_o	Nuclear unit radius, in fermis
R	Mean range of particles in g/cm^2
$\langle \Delta R^2 \rangle$	Contribution to variance in path-length distribution due to energy-loss fluctuations

SKT	Effective overlap parameter
s	Distance of travel in an absorber, in g/cm^2
$\bar{s}(E)$	Mean distance traveled by particles of energy E, in g/cm^2
$\langle \Delta s_o^2 \rangle$	Contribution to variance in path-length distribution due to initial energy spread
x	Penetration distance into the target, in g/cm^2
y	Mean beam deflection, in g/cm^2
y_{o_2}	Initial beam radius
$\langle y^2 \rangle$	Mean square radial spread, in g/cm^2
$\langle \Delta y_o \rangle^2$	Contribution to the variance in the radial-spread distribution due to initial angular spread
Z_i	Atomic number of the ith species in the target
Z_p	Atomic number of beam particles
Z_t	Atomic number of target
β	Velocity ratio
γ	Beam-particle--target-atom mass ratio
θ	Scattering angle in the c.m. system
θ_1	Lower limit on scattering probability
θ_2	Upper limit on scattering probability
$\lambda\!\!\!^{-}$	Wavelength of beam particles, in cm
ρ	Density of target, in g/cm^3
η	Total microscopic nuclear-reaction cross section
$\sigma(E_o)$	Standard deviation in the range distribution for particles of initial energy E_o
$\sigma(E,E_o)$	Standard deviation in the path-length distribution for particles of energy E
$\Sigma(E)$	Total macroscopic reaction cross section, in cm^{-1}
$\bar{\varphi}$	Mean laboratory-system angle of deflection of beam particles
φ_L	Scattering angle in the laboratory system
φ_{o_2}	Standard deviation of initial angular spread
$\varphi_{s_2}^2$	Mean square change in angle of deflection per unit distance
$\langle \varphi^2 \rangle$	Mean square angle of deflection

B. Delta-Function Approximation

We consider the evaluation of the expression given by Eq. 11. For sufficiently small values of $\sigma(E,E_o)$ the term

$$(1/\sqrt{\pi})\cdot\exp\{-U^2\}[dU/dE]$$

behaves like a δ function. Equation 11 then reduces to

$$D(\bar{s}) = N_o(E_o)\exp\{-A_p\int_E^{E_o}[\Sigma(E')/f(E')]\,dE'\}\,f(E), \qquad (A\text{-}1)$$

where the relationship between $\bar{s}$ and E is given by Eq. 5. We wish to learn when this approximation is valid. This may be deduced by the following argument. Consider the exponential term

$$T = \exp\{-U^2\}\,, \qquad (A\text{-}2)$$

where U is given by Eq. 7. For a given value of s, T is the controlling factor in determining how rapidly the total integrand in Eq. 11 goes to zero. Thus, for $U \geq 3$, the contribution to the total integrand is negligible.

Therefore, if each factor in the integrand remains relatively constant over the energy interval within which the integrand differs significantly from zero, then the approximation of Eq. 11 by Eq. A-1 is valid.

We state this mathematically as follows. Let D be the range covered by the variable $\bar{s}(E)$ over which the term T is significantly greater than zero. We may write

$$D = M \cdot \sigma(E,E_o)\,,$$

where M is some constant in the neighborhood of 2 to 4. We wish to calculate the change in energy, ΔE, corresponding to the distance D. From Eq. 1, we find that for a change in $\bar{s}(E)$ equal to D, the corresponding change in energy is approximately

$$\Delta E \approx \frac{D}{A_p}\cdot f(E) = M\cdot\sigma(E,E_o)\cdot f(E)\cdot\frac{1}{A_p}\,. \qquad (A\text{-}3)$$

We now require that the percentage change in each other factor in the integrand be less than some fraction h over the energy interval ΔE given by Eq. A-3. The two functions to consider are

$$G_1(E) = \exp\{-A_p\int_E^{E_o}[\Sigma(E')/f(E')]dE'\} \qquad (A\text{-}4)$$

and $$G_2(E) = f(E) \ . \qquad \text{(A-5)}$$

For a given function $G_i(E)$, the fractional change over an increment ΔE is given approximately as

$$\frac{\Delta G_i}{G_i} \approx \frac{\partial G_i}{\partial E} \frac{\Delta E}{G_i} \ . \qquad \text{(A-6)}$$

Taking the derivatives of both functions in Eqs. A-4 and A-5, using the approximation in Eq. A-6 and the expression for ΔE in Eq. A-3, and requiring that the percentage change of each function over ΔE be less than h, we obtain the criteria

$$\Sigma(E)\ \sigma(E,E_o) < \text{CRIT1} \ , \qquad \text{(A-7)}$$

$$\frac{\partial f(E)}{\partial E}\ \sigma(E,E_o) < A_p\ \text{CRIT1} \ , \qquad \text{(A-8)}$$

where $$\text{CRIT1} = h/M.$$

If both of these requirements are satisfied for a reasonable value of h/M, then Eq. 11 may be replaced by the much simpler form given by Eq. A-1. Similarly, if the inequalities given by Eqs. A-7 and A-8 hold, then the expression for the flux given by Eq. 10 may be replaced by

$$N(\bar{s}) = N_o(E_o) \exp\left\{-A_p \int_E^{E_o} [\Sigma(E')/f(E')]dE'\right\} \ .$$

The value of the constant h/M is obtained experimentally by recognizing that the dose curve and its derivative must be continuous at the point at which the calculation changes from Eq. A-1 to Eq. 11. A priori, one would expect that suitable values would be on the order of 0.05 to 0.10 for h and 1.5 to 2.5 for M. Hence one would expect the largest usable value of h/M to be somewhere in the range 0.02 to 0.07. It is found that for values of CRIT1 greater than approximately 0.04, there clearly are discontinuities in the dose curves. For values less than 0.04, the calculated dose curve remains the same. That is, no change results from decreasing the value of CRIT1.

C. Numerical Integration

For those points at which the delta-function approximation is invalid, the integrals in Eqs. 10 and 11 are evaluated numerically, by using the simple trapezoidal rule. In this case, the procedure is basically as follows:

(i) Choose a set of energies $\{E_i\}$,

(ii) calculate the set $\{\bar{s}_i\} = \{\bar{s}(E_i)\}$ for each energy from Eq. 5,

(iii) calculate $\sigma(E,E_o)$ for each energy,

(iv) evaluate the integral

$$\int_E^{E_o} A_p[\Sigma(E')/f(E')]dE'$$

at each energy.

Finally, the numerical integration is performed for a set of values for the distance s. In fact, the evaluation is greatly simplified by choosing these values to coincide with the set $\{\bar{s}_i\}$.

It remains to choose the energy set $\{E_i\}$ at which the numerical calculations are to be performed. This is done as follows. Since the term T given by Eq. A-2 is by far the most rapidly varying in both 10 and 11, we impose the requirements that in traversing the energy interval ΔE, which is the interval over which the trapezoidal rule is applied at any given step, the change in the quantity U be less than or equal to some fraction FR, where FR is a small fraction of unity. This ensures that the change in the exponential term T will likewise be small over the interval ΔE. Experimentally, a value of 0.2 for FR is found satisfactory.

The change in U across ΔE is approximated by

$$\Delta U \cong \Delta\bar{s}/\sqrt{2}\ \sigma(E,E_o) \ ,$$

where $\Delta\bar{s}$ is the difference between two successive members in the set $\{\bar{s}_i\}$. It is assumed that $\sigma(E,E_o)$ remains relatively constant over the interval. We require, then,

$$\Delta\bar{s}/\sqrt{2}\ \sigma(E,E_o) < FR. \qquad (A\text{-}9)$$

Using Eq. 1, we obtain a relation between the change in distance $\Delta\bar{s}$ and the corresponding energy change ΔE:

$$\Delta E = \frac{1}{A_p} \cdot f(E) \cdot \Delta\bar{s} \ .$$

Substituting into Eq. A-9, we obtain the restriction on ΔE:

$$\Delta E < \frac{\sqrt{2}}{A_p} \cdot f(E) \cdot \sigma(E,E_o) \cdot FR. \qquad (A\text{-}10)$$

Thus, for a given energy E_i, the next energy E_{i+1} at which the calculations are performed is given by Eq. A-10, where the equality sign is chosen. Therefore, we can write

$$E_{i+1} = E_i - \Delta E.$$

D. Coulomb Excitation

If a bombarding ion comes sufficiently close to a target nucleus, a quadrupole interaction may occur in which one or both nuclei are raised to an excited state. This inelastic process is called Coulomb excitation, and the amount of energy that may be lost in a single interaction is on the order of 1 MeV.

We can easily show that this Coulomb interaction process is not significant from the standpoint of energy loss by comparing the specific energy loss due to Coulomb excitation with that due to ionization. The microscopic cross section for a Coulomb excitation to occur can be shown to be on the order of one to two times the geometric cross section given by $\eta = \pi R^2$.[52] If this quantity is multiplied by the atom density of the medium, the result is the macroscopic cross section for a Coulomb excitation. If this is then multiplied by the mean excitation energy lost per interaction, the result is the stopping power, or specific energy loss, due to Coulomb excitation.

Estimates of this stopping power are made for a few extreme cases, and the results are shown in Table XXI. Also shown are calculated values of stopping power due to ionization. In all cases, the Coulomb excitation stopping power is a negligible fraction of the total.

Table XXI. Comparison of stopping power due to Coulomb excitation and to ionization.

System	Stopping power	
	Coulomb excitation	Ionization
500-MeV/amu Ne ions in U	≈ 0.01	140
500-MeV/amu Ne ions in H_2O	≈ 0.1	280
500-MeV/amu Ne ions in Cu	≈ 0.05	191
500-MeV/amu U ions in U	≈ 0.05	11500

REFERENCES

* This work was done under the auspices of the U. S. Atomic Energy Commission.

1. L. Northcliffe, Ann. Rev. Nucl. Sci. 13, 67 (1963).

2. U. Fano, Penetration of Protons, Alpha-Particles, and Mesons, in Studies in Penetration of Charged Particles in Matter, NAS-NRC-1133, 1964.

3. R. D. Evans, The Atomic Nucleus (McGraw-Hill Book Co., New York, 1955).

4. H. Bichsel and E. A. Uehling, Phys. Rev. 119, 1670 (1960).

5. C. N. Yang, Phys. Rev. 84, 599 (1951).

6. H. W. Lewis, Phys. Rev. 85, 20 (1952).

7. Martin J. Berger and Stephen M. Seltzer, Multiple-Scattering Corrections for Proton Range Measurements, in Studies in Penetration of Charged Particles in Matter, NAS-NRC-1133, 1964.

8. F. Bloch, Z. Physik 81, 363 (1938).

9. Howard D. Maccabee, Fluctuations of Energy Loss by Heavy Charged Particles in Matter (Ph.D. Thesis), UCRL-16931, July 1966.

10. P. V. Vavilov, Zh. Experim. i Teor. Fiz. 32, 920 (1957); English translation: Soviet Phys. JETP 5, 749 (1957).

11. R. M. Sternheimer, Phys. Rev. 117, 485 (1960=

12. R. M. Sternheimer, Phys. Rev. 115, 137 (1959).

13. P. Steward and R. Wallace, Calculations of Stopping Power and Range Energy Values for any Heavy Ion in Nongaseous Media, UCRL-17314, Dec. 1966.

14. J. Lindhard and M. Scharff, Energy Dissipation by Ions in the keV Region, Phys. Rev. 124, 128 (1961).

15. J. Lindhard, M. Scharff, and H. E. Schiott, Range Concepts and Heavy Ion Ranges (Notes on Atomic Collisions, II), Kg. Danske Videnskab. Selskab, Mat.-Fys. Medd. 33, 14 (1963).

16. Walter H. Barkas and Martin J. Berger, Tables of Energy Losses and Ranges of Heavy Charged Particles, in Studies in Penetration of Charged Particles in Matter, NAS-NRC-1133, 1964.

17. J. E. Turner, Values of I and I_{adj}, in Studies in Penetration of Charged Particles in Matter, NAS-NRC-1133, 1964.

18. E. Segrè, Experimental Nuclear Physics, Vol. I (John Wiley and Sons, New York, 1953).

19. J. Blatt and V. Weisskopf, Theoretical Nuclear Physics (John Wiley and Sons, New York, 1952).

20. G. Igo, Phys. Rev. 115, 1665 (1959).

21. L. N. Cooper and E. M. Henley, Phys. Rev. 92, 801 (1953).

22. F. Bitter and H. Feshbach, Phys. Rev. 92, 837 (1953).

23. V. L. Fitch and J. Rainwater, Phys. Rev. 92, 789 (1953).

24. J. A. Wheeler, Phys. Rev. 92, 812 (1953).

25. A. L. Schawlow and C. H. Townes, Science 115, 284 (1952).

26. I. Perlman and T. J. Ypsilantis, Phys. Rev. 79, 30 (1950).

27. E. C. Pollard, Phys. Rev. 47, 611 (1935).

28. M. M. Shapiro, Phys. Rev. 90, 171 (1953).

29. D. S. Willoughby, Phys. Rev. 101, 324 (1956)

30. R. W. Williams, Phys. Rev. 98, 1387 (1955).

31. T. D. Thomas, Phys. Rev. 116, 703 (1959).

32. M. J. Longo and B. J. Moyer, Phys. Rev. 125, 701 (1962).

33. C. Zerby, Material Requirements for Shielding Against Space Radiation, ORNL-TM-552, May 1963.

34. R. Wallace, P. Steward, and C. Sondhaus, Primary and Secondary Proton Dose Rates in Spheres and Slabs of Tissue, UCRL-10980 Rev., July 1964.

35. R. Hofstadter, Ann. Rev. Nucl. Sci. 7, 231 (1957).

36. H. Bichsel, American Institute of Physics Handbook, Second Ed. (McGraw-Hill Book Co., New York, 1964), pp. 8-20.

37. Z. Molière, Naturforschung 30, 78 (1948).

38. S. A. Goudsmit and J. L. Sanderson, Phys. Rev. 57, 24 (1940).

39. S. A. Goudsmit and J. L. Sanderson, Phys. Rev. 58, 36 (1940).

40. H. A. Bethe, Phys. Rev. 89, 1256 (1953).

41. H. Overas, On Small-Angle Multiple Scattering in Confined Bodies, CERN 60-18, 1960.

42. Bruno Rossi, High Energy Particles (Prentice-Hall, Englewood Cliffs, N.J., 1956).

43. E. J. Williams, Proc. Roy. Soc. (London) A169, 591 (1939).

44. R. Mather and E. Segrè, Phys. Rev. 84, 191 (1951).

45. H. Snyder and W. T. Scott, Phys. Rev. 76, 220 (1949).

46. David Halliday, Introductory Nuclear Physics (John Wiley and Sons, New York, 1955).

47. G. M. Litton, Program BRAGG, a FORTRAN-IV Program for Calculating Bragg Curves and Flux Distributions, UCRL-17391, Feb. 1967.

48. M. J. Berger, Methods in Computational Physics, Vol. 1,(Academic Press, New York, 1963), p. 135.

49. W. M. Preston and A. M. Koehler, The Effects of Scattering on Small Proton Beams, Harvard University Report (unpublished).

50. Mudundi Raju and Graeme Welch (Lawrence Radiation Laboratory, Berkeley), Private communication.

51. M. Raju, presented at workshop Conference on Space Radiation Biology, Berkeley, California, September 1965, proceedings to be published. See also UCRL-16613 (1965).

52. J. DeBoer (Department of Physics, Rutgers University, N. Y.), private communication.

53. Tor Brustad, Piero Arriotti, and John Lyman, Experimental Setup and Dosimetry for Investigating Biological Effects of Densely Ionizing Radiations, UCRL-9454, Oct. 1960.